PORPHYRY SYSTEM FERTILITY DISCRIMINATION AND MINERALIZATION VECTORING USING IGNEOUS APATITE SUBSTITUTIONS TO DERIVE PRE-EXSOLUTION MELT MINERALIZATION COMPONENT CONCENTRATIONS

by

Jonathan T. Boswell

A thesis submitted to the faculty of
The University of Utah
in partial fulfillment of the requirements for the degree of

Master of Science

in

Geology

Department of Geology and Geophysics

The University of Utah

May 2014

THE UNIVERSITY OF UTAH GRADUATE SCHOOL

STATEMENT OF THESIS APPROVAL

The thesis of Jonathan T. Boswell

has been approved by the following supervisory committee members:

Erich U. Petersen , Chair	March, 07, 2014 Date Approved
Diego P. Fernandez , Member	March, 12, 2014 Date Approved
Barbara P. Nash , Member	March, 12, 2014 Date Approved

and by John M. Bartley, Chair of

the Department of Geology and Geophysics

and by David B. Kieda, Dean of The Graduate School.

ABSTRACT

Igneous apatite is an early magmatic phase that accepts a wide variety of elemental substitutions. These substitutions include porphyry Cu hypogene mineralization elements S and Cu, as well as other potentially mineralization related elements. These characteristics make apatite useful in understanding pre-exsolution concentrations of these elements in melts and, subsequently, useful as porphyry system/intrusive unit fertility indicators.

Apatite element substitution concentrations in pre-, syn- and late-mineralization emplaced units of the San Enrique Monolito deposit in the Los Bronces-Río Blanco porphyry district, Central Chile were assessed to evaluate the use of apatite substitutions as porphyry system/intrusive unit fertility indicators. Major, trace and rare earth element (REE) concentrations in apatite grains were determined, sulfur substitution mechanisms and controls were assessed, melt S was calculated using apatite/melt S partition coefficients and apatite S, melt S, and other elemental substitution correlations to mineralization were determined.

The ratio of S to Na substitution indicates S in analyzed apatite grains is incorporated by the coupled exchange $S^{6+} + Na^{+} \Leftrightarrow P^{5+} + Ca^{2+}$ and systematic fluctuations in Cl vs. Mn, Fe and light rare earth elements (LREE) suggest a change in apatite structure associated with concomitant increases in these elements. Neither S

exchange nor crystal structure, however, display a preferential control on S uptake. This is interpreted to indicate S concentrations are wholly a function of S availability in melt.

Apatite S and melt S are low in premineralization emplaced units, elevated in syn and late-mineralization units and highest in units emplaced contemporaneously with the height of mineralization. Apatite Cu correlates similarly. Apatite Mg was detected only in grains from synmineralization emplaced units, possibly substantiating mafic magma input and underplating as Cu source models for porphyry mineralization.

Concentrations of apatite S and melt S above 750 ppm and 200 ppm, respectively, are proposed as fertility indicators. However, because of the cumulative uncertainty associated with melt S calculations, it is proposed that apatite S is a more robust discriminant than melt S. Apatite Cu above 700 ppm and apatite Mg above 300 ppm are also proposed as mineralization potential indicators.

TABLE OF CONTENTS

LIST OF TABLES

LIST OF FIGURES

ACKNOWLEDGEMENTS

This project was supported by a grant from Anglo American (UK). Sample preparation and QEMSCAN work was also funded in part by the Society of Economic Geologist Student Research Grant Program.

I gratefully acknowledge Dr. Erich U. Petersen, Dr. Dave P. Braxton, John Barr, Dr. Barbara P. Nash and Dr. Diego P. Fernandez for their reviews and guidance. I also thank Dr. Diego P. Fernandez for his assistance with LA-ICP-MS work and Dr. Henrietta E. Cathey and Dr. Erich U. Petersen for their assistance with microprobe analyses. For their assistance with sampling, I thank Evan Vela, Claudia Castillo, Carolina Nuñez and others who assisted me at Las Tórtolas. I am extremely grateful to my family, Jessica Boswell, Carter Sloots and Kennedy Sloots for their encouragement and patience.

INTRODUCTION

In fertile porphyry systems, mineralization components are exsolved from the cupolas of magma chambers during system cooling and depressurization (Sillitoe, 2010). These components separate from the magma into vapor and generally hypersaline aqueous phases and are deposited in a variety of different chemical and physical traps. This process can leave residual magmas that are coevally or later intruded or extruded over or adjacent to mineralization as dikes, plugs or volcanic piles, barren or depleted in these mineralization components; a scenario that can lead to blind deposits. The pre-exsolution concentrations of these constituents, however, are recorded within units of an intrusive system as elemental substitutions in igneous apatite (Piccoli and Candela, 1994; Streck and Dilles, 1998; Parat and Holtz, 2004), a characteristic that can be used to evaluate the mineralization potential a system possesses.

Herein, elemental substitutions in igneous apatite and melt S calculated from apatite S are evaluated for their potential as porphyry system/intrusive unit fertility indicators. This evaluation was performed by comparing substitution and calculated melt S concentrations in intrusive units to known intrusion and mineralization chronology in the high grade (3.7 billion tons >0.7% Cu) San Enrique deposit in the Los Bronces-Río Blanco Cu-Mo district located 50 km northeast of Santiago, Chile (Toro et al., 2012).

Eight units that include pre-, syn- and late-mineralization emplaced host and porphyry intrusive units were sampled from drill core from the deposit. Whole rock

geochemistry was obtained for each of the units and system evolution was evaluated using Zr/Ti vs. Nb/Y and REE trends. Age dates and mineralization/unit emplacement timing relationships were obtained from published studies (Toro et al., 2012; Deckart et al., 2012: Deckart et al., 2005; Davidson et al., 2005; Vargas et al., 1999). Apatite Ca, P, F and Cl, as well as fifteen other trace element concentrations were determined using microprobe analysis of apatite. Fourteen REE element plus boron concentrations were determined using La-ICP-MS analysis of apatite. Melt S concentrations were calculated using the methods of Porter and Titley (2004). To determine influences from extraneous controls on S substitution such as postcrystallization alteration, S concentration bias imparted by grain zonation, S substitution mechanisms or magma composition, correlations between S concentrations and apatite grain morphology, apatite grain S zonation, apatite S substitution mechanisms and rock compositions were assessed. Resulting system evolutionary trends, extraneous controls on S substitution, apatite elemental substitution correlations to mineralization related units and the application of apatite substitutions to discriminate mineralization potential are discussed.

GEOLOGIC SETTING

Regional Geology

The geologic evolution of Central Chile since the Jurassic Period has been one of subduction related arc magmatism and uplift (Pankhurst and Hervé, 2007). It was during this regime that the Andean sequence, largely of a Mesozoic and Cenozoic volcanic pile, was deposited on metamorphic and igneous complexes of the continental basement and deformed by a series of thrusting events to produce the Andes Mountains. Arc magmatism in the region reached its peak during the Miocene 20-16 Ma, at which time up to 3000 m of Farellones Formation andesite lavas (FLA), into which the San Francisco batholith pluton, host to Los Bronces-Río Blanco, were deposited (Skews and Stern, 1994). Magmatism within Central Chile began to wane between 16 and 10 Ma as the dip angle of the subducting Nazca plate began to decrease causing eastward migration of volcanism into Argentina (Skewes and Stern, 1994, 1996). The Bajo Angulo flat slab subduction segment along the Chilean subduction zone extends from ~25° S to ~33° S. At its shallowest location, ~32° S, the dip angle is ~10°, having flattened from an original angle of ~30° (Winter, 2001). Los Bronces, at ~33° S and two other world class porphyry districts, El Teniente ~ 100 km to the south of Los Bronces-Río Blanco, and Los Pelambres ~ 100 km to the north, formed at the transition between the Bajo Angulo segment and the volcanically active Southern volcanic zone section of the Chilean subduction zone (Hollings, 2005). Snagging between the down-going plate and the

overriding crust during subduction of the Juan Fernandez Ridge is thought to be the cause of the reduced subduction angle. These momentary couplings between the down going plate and crust increased compression and thrusting leading to crustal shortening, crustal thickening and rapid uplift (Toro et al., 2012).

Exhumation resulting from uplift and subsequent erosion (in the case of Los Bronces) and/or tectonic unroofing related to flat slab subduction has been attributed as an ingredient in the development of porphyry copper deposits of Central Chile and porphyries around the world. With the magma chambers at shallower depths, decompression affected rapid exsolution of metal rich volatiles (Cooke et al., 2005; Gow and Walshe, 2005; Deckart et al., 2005; Sillitoe 2010; Skewes and Stern, 1994).

Los Bronces-Río BlancoPorphyry Cu-Mo District Geology

The Los Bronces-Río Blanco copper-molybdenum district consists of a series of mineralized breccias focused along N-S trending structures in the San Francisco batholith, and FLA. Three domains characterized by relative age of mineralization, rock types and bounding structures have been defined within the district. From west to east these domains are: the Los Piches-Ortiga block, the San Manuel-El Plomo block and the Río Blanco-Los Bronces block (Fig. 1) (Toro, 2012). From block-to-block west to east, brecciation and mineral endowment youngs and intensifies, with the earliest mineralization forming in the Los Piches-Ortiga block at 14.8 Ma and the youngest most endowed portion of the district forming within the Río Blanco-Los Bronces block at 4.3 Ma. (Toro, 2012). On the district scale, typical porphyry alteration assemblages can be observed. Advanced argillic lithocap assemblages (quartz, pyrophyllite, alunite, kaolinite,

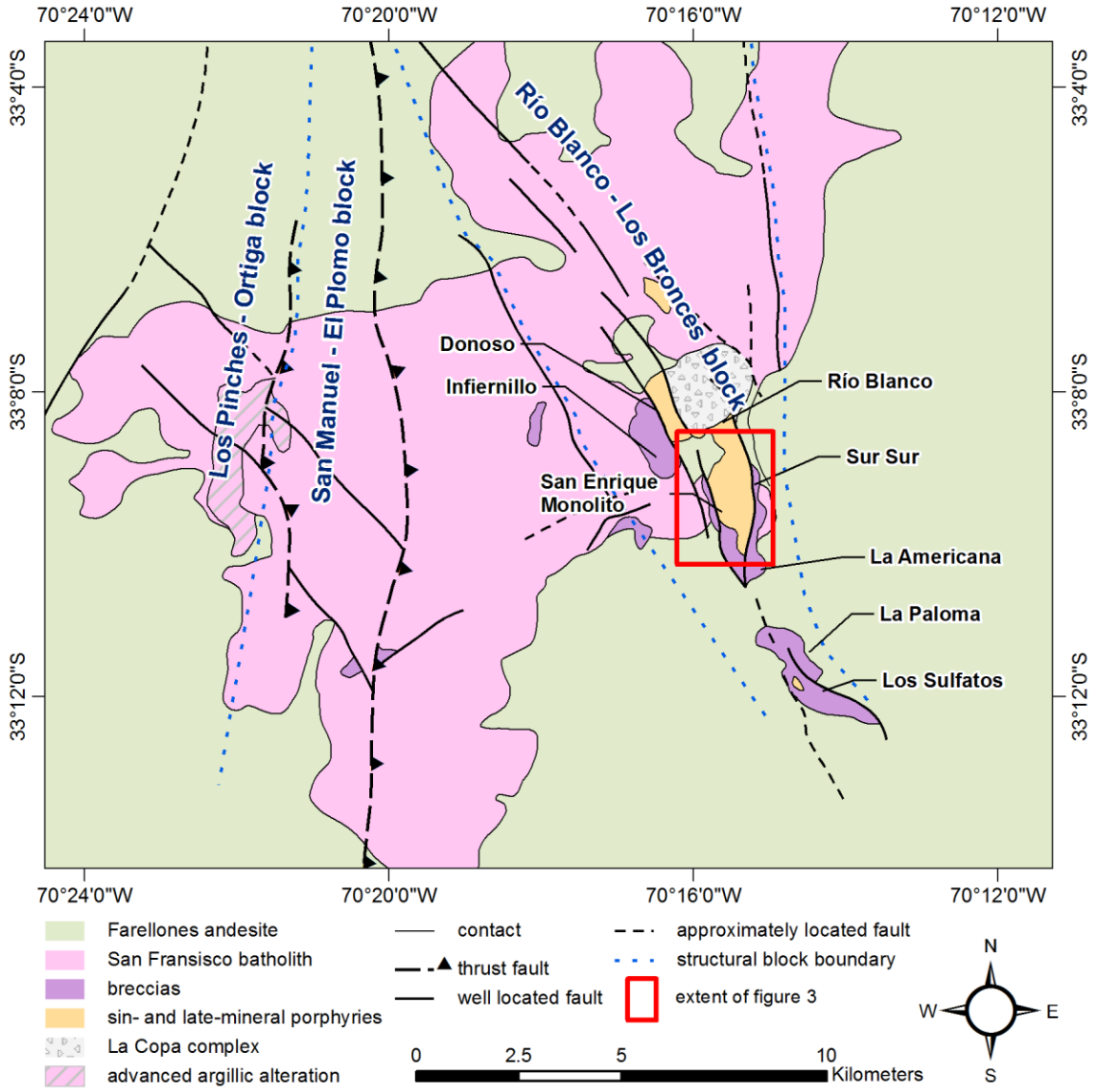

Figure 1. Structural blocks within the Los Bronces - Río Blanco Cu-Mo district. Adapted from Toro (2012).

and pyrite) in a graben within the Los Piches-Ortiga block exemplify the higher portion of the system and Cu-Mo mineralization in biotite-sulfide-anhydrite breccias and biotization of mafic minerals and interstitial K-feldspar in units of the San Francisco Batholith represent potassic alteration assemblages; the dominant alteration assemblage within the Río Blanco-Los Bronces block (Toro, 2012).

Deposits discovered within the Río Blanco-Los Bronces block include, from north to south: Los Bronces, which herein includes Donoso, Infiernillo and Río Blanco; San Enrique Monolito; Sur-Sur; La Paloma; La Americana and Los Sulfatos. These deposits extend over a northwest-southeast 1 km wide and over 6 km long trend along the eastern portion of the San Francisco Batholith. Cu-Mo mineralization forms as sulfide matrix fill in horizontally and vertically extensive breccias and as sulfide disseminations and veins in intrusive units. Late-mineralization dikes and plugs cut these breccias and late-mineralization volcanics cap these units in the northern portion of the district (Fig. 1).

The San Francisco Batholith intruded the early Miocene FLA as multistage intrusive events. Units range from quartz monzonite to diorite and are largely equigranular (Toro et. al., 2012). Units of the San Francisco Batholith in the San Enrique Monolito deposit used in this study include: the Quartz Monzonite Gruesa (QMG) which is intruded by two younger units, the Quartz Monzonite Fine-I (QMF-I) and the Quartz Monzonite Fine-II (QMF-II). Age dates for these units in the San Enrique deposit are not available, however, based on petrography and spatial distribution, the QMG is equivalent to the Biotite Sienogranite with a $^{206}Pb/^{238}U$ date of 16.4 Ma (Toro et al., 2012) and the QMF-I and QMF-II are equivalent to the Río Blanco Granodiorite with a $^{206}Pb/^{238}U$ date of 11.96 Ma and the Casada Granodiorite with a $^{206}Pb/^{238}U$ date of 8.40 Ma, respectively

(Deckart et al., 2012). Dated samples for these three units come from the Río Blanco deposit ~1 km north of the San Enrique deposit (Fig. 1).

The breccias, largely magmatic, compositionally different and containing varying but generally high grade (over 1% Cu) mineralization, cut units of the San Francisco batholith and FLA. Matrix mineral dating (Deckart et al., 2005; Toro et al., 2012) and the relationship of one breccia type forming clasts in another (Warnaars et al., 1985) indicate there were multiple episodes of brecciation and mineralization. In general, the breccias contain from 50 to 95% by volume angular clasts of units of the San Francisco batholith and FLA volcanics (Skew and Stern, 1994) and the matrices consist principally of tourmaline, biotite, rock flour, chalcopyrite, molybdenite, bornite, galena and specularite. In La Americana, Sur-Sur (Vargas et al., 1999) and San Enrique Monolito, chalcopyrite, bornite and biotite increase downward and tourmaline and specularite increase upward. In the Donoso portion of Los Bronces, copper grades alternate between high and low throughout rapidly changing shells in which one of three minerals, chalcopyrite, pyrite or specularite predominate. These shells are subvertical and roughly parallel to the breccia contact (Warnaars et al., 1985). Contacts between the host batholith and all breccias are generally sharp; however, contacts between different breccia units intertwine and are gradational (Warnaars et al., 1985).

Thermomicroscopy performed on fluid inclusion in quartz grains from breccia matrix indicate fluids that precipitated mineralization in the Donoso breccia in the Los Bronces deposit (Skewes et al., 2002) and breccias of the Sur-Sur and La Americana deposit (Vargas et al., 1999) were high saline brines. These brines contained 32-56 wt. percent NaCl equivalent, and 30 to 55 wt. percent NaCl equivalent, respectively, at

temperatures exceeding 690°C and 503°C, respectively. Isotopic ranges of +5.6 to +9.1 ‰ in ^{18}O and -51 to -80 ‰ in δD (temperature corrected) obtained from quartz and tourmaline in the matrix of the Donoso Breccia, along with the high salinities found in fluid inclusions support a magmatic fluid source model over a convecting meteoric water fluid source model (Skews et al., 2002).

Age dating suggests breccia emplacement occurred over a period as long as 10 million years. Dating of breccia matrix hornblende has produced a minimum $^{40}Ar/^{39}Ar$ plateau age as old as 14.15 Ma. for the breccia Los Machos in the Los Bronces deposit and dating of breccia matrix K-feldspar has produced a $^{40}Ar/^{39}Ar$ plateau age as young as 4.23 Ma for the magmatic breccia in the Río Blanco portion of Los Bronces (Deckart et al., 2005).

The most conformable groupings of synmineralization and late-mineralization dikes, plugs and volcanics of the Río Blanco-Los Bronces block include, from oldest to youngest, the Quartz Monzonite Porphyry (QMP), Feldspar Porphyry (FP), Don Luis Porphyry (DLP), Porphyry Observatorio (POB), and La Copa Rhyolite (LCR).

The QMP, POB and FP were intruded contemporaneous to mineralizing events as a series of quartz monzonite to monzodiorite dikes with variable mineralization (Davidson et al., 2005; Vargas et al., 1999; Toro et al., 2012). These dikes extend from Los Bronces in the north to Los Sulfatos in the south.

Ages for the QMP range from 7.7 Ma to 6.1 Ma (U-Pb) except at Sur-Sur were a U-Pb date of 5.74 Ma has been obtained (Deckart et al., 2012). Slightly younger U-Pb results for the POB indicate an age of 6.0 Ma (Toro et al., 2012) and even younger U-Pb results for the FP indicate an age range between 5.8 and 5.2 Ma (Deckart et al., 2012).

The DLP intrudes as a late-mineralization subvolcanic dacite porphyry stock that crosscuts all previously described units and mineralization, and is the hypabyssal counterpart to the extruded LCR. It contains infrequent quartz-molybdenite ± chalcopyrite veins, quartz-sericite ± anhydrite ± sulfide veins and tourmaline breccias along its perimeter indicating that the hydrothermal event responsible for mineralization had not yet terminated or was reactivated during is intrusion. The LCR forms as a dacitic ignimbrite cap in the northern portion of the block (Davidson et al., 2005), and likely once covered much of the area. U-Pb age dates for the DLP range from 5.2 to 5.0 Ma and a U-Pb age for the LCR suggests it was erupted at 4.69 Ma (Deckart et al., 2012). An overview of mineralization and intrusive events is shown in Figure 2.

Fifteen samples were selected from the FLA, QMG, QMF-I, QMF-II, QMP, POB, FP and DLP. Samples were taken from drill core along north-south and east-west cross sections through the heart of the San Enrique Monolito deposit. Cross sections and sample locations are shown in Figures 3 and 4.

Core Logging and Sample Petrography

Detailed sample mineralogy, textures, alteration and mineralization determined from core logging and petrography are provided in Table 1. In summary, the FLA is a medium-grained (0.75-2 mm) porphyritic andesite, containing mostly plagioclase phenocrysts with <5% biotite and trace amphibole and magnetite. The FLA is generally unmineralized and hydrothermal biotite replacing biotite and amphibole is the dominant alteration. The QMG unit of the San Francisco batholith is a coarse-grained (3-8 mm) equigranular monzonite containing interstitial chlorite altered biotite. The QMG contains

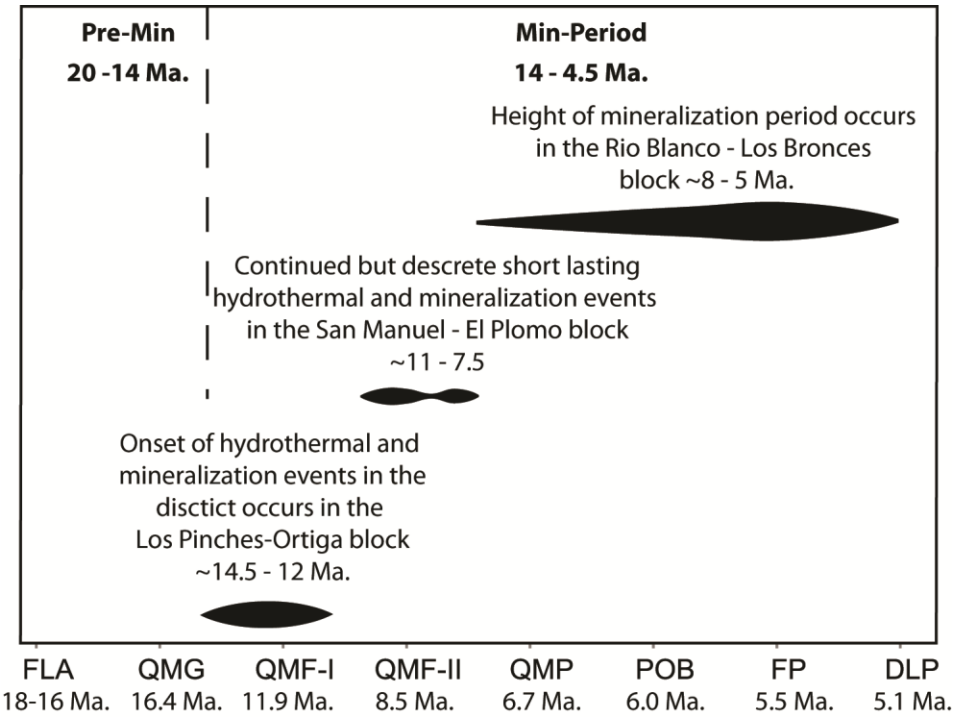

Figure 2. Hydrothermal and mineralization events are shown as horizontal lines that increase in width with increase in activity moving through time from left to right (length is not scaled to time durations but correlates with ages of unit emplacement below. Pre-Min is premineralization timespan and Min-Period is mineralization timespan. The vertical dashed line separates the two timespans. Rock units are listed along the bottom in order of emplacement timing from left to right. Mean ages of emplacement are listed underneath. Data source: Deckart et al. (2005) and Toro et al. (2012).

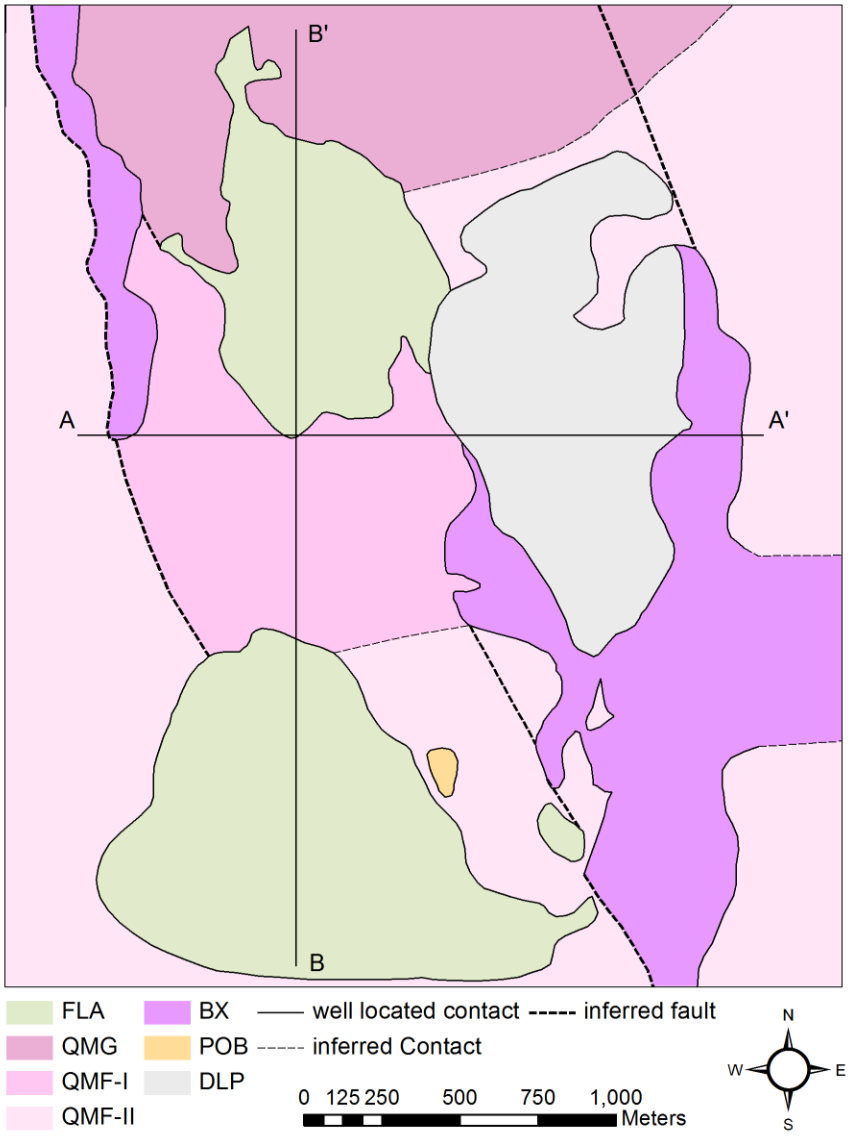

Figure 3. Surface geology of the San Enrique Monolito deposit with cross section locations indicated by lines A-A' and B-B' (map location shown in Figure 1).

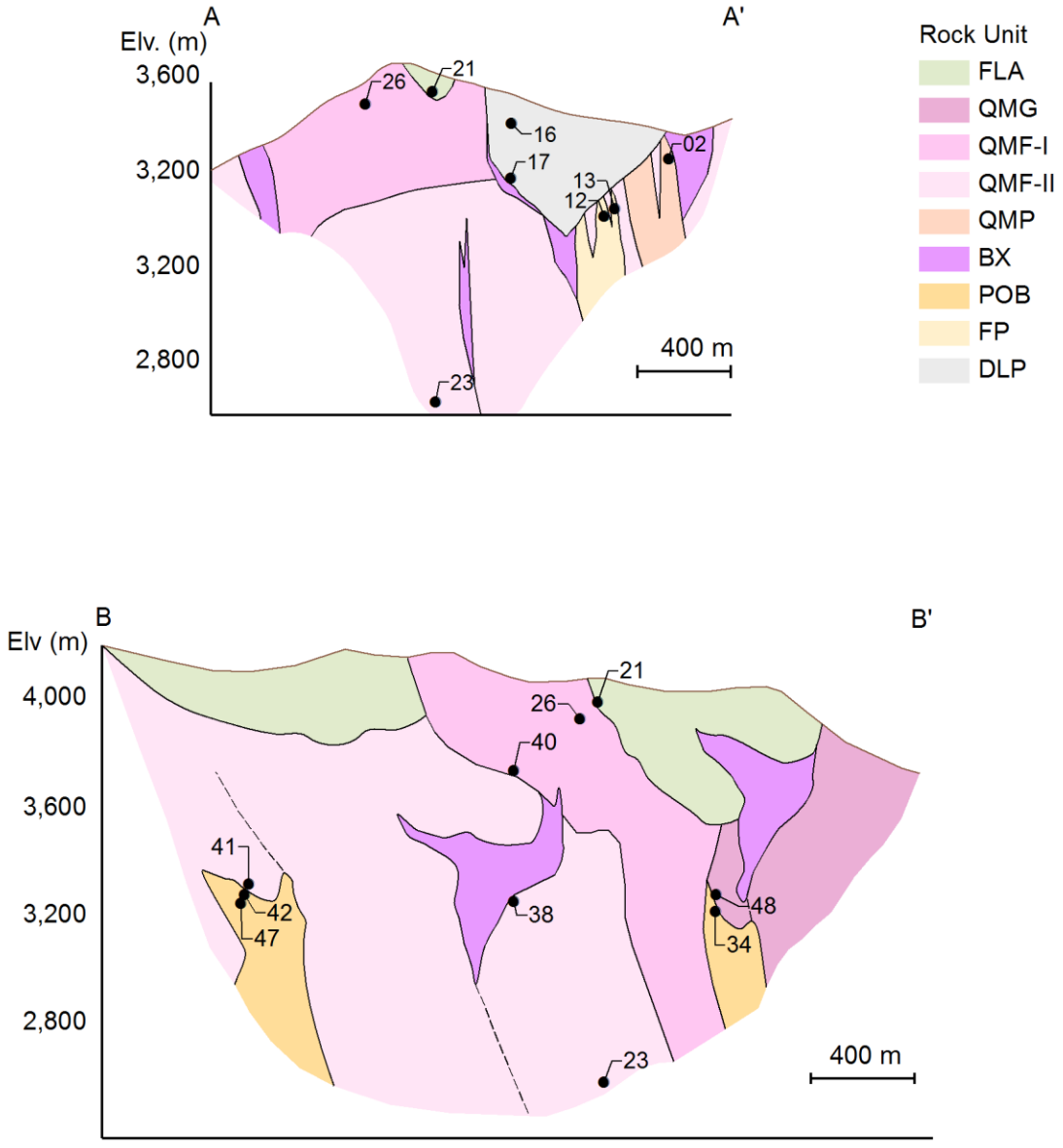

Figure 4. Cross sections through the San Enrique Monolito deposit. Black circles indicate sample locations and are labeled with sample numbers. Cross-section A-A' is west-east and cross section B-B' is south-north (cross section locations shown in Figure 3).

Table 1. Sample Descriptions.

Drill Hole ID	Depth (m)	Sample ID	Rock Unit	Composition	Textures	Mineralization	Alteration	Veins
MO123	78.65 - 78.79	21	FLA	20% phenocrysts of 95% Pl and 5% Bt and trace Am in a 80% groundmass composed of Qtz, Bt and 2% Mag	fine to medium grained (0.75-2 mm) porphyritic mostly euhedral phenocrysts with a microcrystaline allotriomorphic groundmass	veins- infrequent veins of Py	potassic alteration as Bt breaking down to hydrothermal Bt and alteration of Am to Bt, Chl alteration of Bt	Anh + Py with Qtz + Ser halo veins, Ep veinlets
MO120	719.1 - 719.4	48	QMG	70% Pl, 19% Qtz and 10% Kfs, 1% Chl altered Bt 1% and trace Mag	medium to coarse grained (3-8 mm) holocrystalline allotriomorphic	disseminations- trace Py, trace Cp, veins- Py, Cp	strong fine grained Ser alteration of feldspars, Chl alteration of Bt	Tur + Py + Cp veins, Kfs veins cut by Anh + Py with Qtz + Ser halo veins
MO123	1419 - 1419.3	23	QMF-I	58% Pl, 24% Qtz, 5% Kfs and 0.5% Mag with interstitial 7% Bt, 4% Chl and 1% Anh	fine-medium grained (1-1.5 mm) holocrystalline hypidiomorphic	veins - 1% Cp	weak Chl alteration of Bt	Cp + Qtz + Anh with Qtz Ser halo veins
MO128	73.95 - 74.25	26	QMF-I	30% phenocrysts of 85% Pl, 5% Ab rimmed Kfs, 5% Qtz, 2% Am, and 3% Chl altered Bt in a 70% medium grained groundmass of feldspar Qtz and trace Mag	porphyritic and holocrystalline with medium grained (2-4 mm) mostly euhedral phenocrysts with a fine grained (up to 1 mm) hypidiomorphic groundmass	veins - infrequent Py, veins - 0.1% specular Hem	Chl alteration of Bt	Qtz + Chl +/- Py with Ab halo veins , Hem + Py veins

Py – pyrite, Cp – chalcopyrite, Mo – molybdenite, Hem – hematite, Mag – magnetite, Chl – chlorite, Tur – tourmaline, Anh – anhydrite, Qtz – quartz, Ser – sericite, Am – Amphibole, Bt – Biotite, Kfs – K-feldspar, Ep – epidote, Ab – albite.

Table 1 Continued.

Drill Hole ID	Depth (m)	Sample ID	Rock Unit	Composition	Textures	Mineralization	Alteration	Veins
MO126	271.5 - 271.8	40	QMF-I	25% phenocrysts of 95% Pl, 5% Chl altered Am and Bt in a 75% groundmass of predominately Qtz and feldspar with 2% Mag	medium grained (2-5 mm) porphyritic phenocrysts with a microcrystaline hypidiomorphic groundmass	disseminations - blebby 1% Py and Py replacing Mag, veins- infrequent Py, veins- trace specular Hem	Chl alteration of mafic minerals	Py + Cp + Hem + Qtz with Ab halo veins
MO110	902.05 - 902.3	41	QMF-II	20% phenocrysts of 80% Pl, 10% Kfs and 10% Am altered to Chl in a 80% groundmass of predominately feldspar and Qtz with 2% Anh and 2% Mag	medium grained (2-4 mm) porphyritic mostly euhedral phenocrysts with a microcrystaline allotriomorphic groundmass	veins - >1% Cp, trace Mo, disseminations - 2% euhedral Mag	moderate Ser alteration of feldspars, Chl alteration of Am	Anh + Cp +/- Mo w Qtz Ser + Chl halo veins cutting Cp + Qtz + Ep with Chl halo cut by Qtz + Py veins
MO126	742.5 - 742.8	38	QMF-II	20% phenocrysts of 60% Pl laths, 40% Ab rimmed Kfs and trace Am in a 80% fine grained groundmass composed of predominately Qtz and feldspar with 3% Chl altered Bt, 1% Anh, 1% Am and trace Mag	fine to medium grained (1 to 2 mm) porphyritic mostly euhedral phenocrysts with a microcrystaline allotriomorphic groundmass	veins - 0.2% Py and 0.1% Cp	weak to moderate Ser alteration of feldsapars, Chloritization of mafics, minor Ep	Qtz + Py +/- Cp +/- Ep with Qtz Ser halo veins
DDH4203	17.43 - 17.73	02	QMP	20% phenocrysts of 5% Qtz 60% Pl, 33% K feldspar and 2% Chl in a groundmass of predominately feldspar and Qtz with trace Mag and Anh	medium to coarse grained (3-8 mm) porphyritic mostly euhedral phenocrysts with a by textural microcrystaline hypidiomorphic and cryptocrystalline groundmass	disseminations- 0.3 % blebby Cp and Cp replacing Mag	moderate to strong fine grained Ser alteration of feldspars, Chl alteration of mafics	Cp + Qtz + Mo with Qtz + Ser halo veins

Table 1 Continued.

Drill Hole ID	Depth (m)	Sample ID	Rock Unit	Composition	Textures	Mineralization	Alteration	Veins
MO110	939.75 - 940	47	POB	10% phenocrysts of 65% Qtz eyes, 24% feldspar and 1% Ser and silicic altered Bt in a 80% fine grained groundmass composed of predominately Qtz and feldspar	medium grained (2-4 mm) porphyritic mostly euhedral phenocrysts with a microcrystaline allotriomorphic groundmass	disseminations - blebby 2% Py and 0.7% Cp replacing mafics, veins - >1% Py, >1% Cp, trace Mo, trace specular Hem	strong fine Ser alteration of groundmass, strong course grained Sericite and silicic replacement of feldspars, rosettes of Tur filling vugs, Ser alteration and silicification of Bt	Cp + Py + Hem + Qtz + Anh veins, Cp + Py + specular Hem + Chl w Kfs halo veins, Py + Cp + Mo + Qtz + Anh veins
MO120	743.05 - 743.3	34	POB	20% phenocrysts of 89% smaller Pl laths, 10% larger Qtz eyes and 1% Chlite altered Bt in a 80% fine grained groundmass composed of predominately Qtz and Kfs, trace Mag	medium to coarse grained (3-6 mm) porphyritic subhedral angular fragments with a cryptocrystaline groundmass	disseminations - 2% Py and 0.1% Cp replacing mafics and in vugs lined with coarse grained Ser	strong fine and course gained Ser alteration of feldspars and groundmass, Chlitization of Bt	Py + Anh, Qtz + Py +/- Cp with Qtz Ser halo veins, Tur + Py + Cp with Qtz Ser halo veins
MO110	912.1 - 912.4	42	POB	10% phenocrysts of 65% Qtz eyes, 35% feldspar and 1% Bt in a fine groundmass of Qtz and feldspar	medium grained (3-5 mm) porphyritic phenocrysts with a microcrystaline allotriomorphic groundmass	disseminations - blebby 2% cy and 1% Py replacing mafics, veins - >1% Py, >1% Cp, trace Mo	strong fine grained Ser alteration of feldspar and groundmass, strong course grained Ser replacement of feldspars	Cp + Py + Hem + Qtz + Anh veins, Cp + Py + specular Hem + Chl w Kfs halo veins, Py + Cp + Mo + Qtz + Anh veins
DDH4203	344.56 - 344.8	13	FP	15% phenocrysts of Pl laths and trace Bt in a 85% fine grain groundmass of predominately Qtz and feldspar with 2% Anh and 3% partially Ser altered Bt	medium to coarse grained (3-8 mm) porphyritic mostly euhedral phenocrysts with microcrystaline allotriomorphic groundmass	disseminations - 0.4% Cp and .1% Py replacing mafics, veins - 0.5% Py, 0.1% Cp	intense Ser alteration of feldspars and Bt, Chl alteration of Bt, potassic alteration in the form of Bt breaking down to hydrothermal Bt	Qtz veins cut by Py + Qtz +/- Cp with Qtz Ser halo veins

Table 1 Continued.

Drill Hole ID	Depth (m)	Sample ID	Rock Unit	Composition	Textures	Mineralization	Alteration	Veins
DDH4203	364.4 - 364.65	12	FP	15% phenocrysts of 79% Pl laths, 5% Ab rimmed Kfs, 1% Bt and 5% Qtz eyes in a 85% fine grain groundmass composed of predominately Qtz and feldspar with 2% Anh and 3% Bt	medium grained (2-4 mm) porphyritic mostly euhedral phenocrysts with a microcrystaline allotriomorphic groundmass	disseminations - 0.4% Py and 0.2% blebby Cp, veins - 0.6% Cp and 0.4 % Py	intense patchy Ser alteration of feldspars and groundmass, especially Kfss	Kfs veins cut by Qtz + Cp + Py veins cut by Py +/- Cp + Mo with Qtz + Ser halo veins, Py +/- Cp + Qtz + Anh with Qtz + Ser halo veins
MO124	372 - 372.3	17	DLP	25% phenocrysts of 40% Pl, 30% Kfs and 30% Qtz eyes in a 75% fine grained groundmass composed of predominately Qtz and feldspar with 2% Chl altered Bt, trace Mag	medium grained (3-5 mm) porphyritic euhedral phenocrysts and subhedral angular fragments with a cryptocrystaline groundmass	veins- infrequent veins of Py and Cp, disseminatations - 0.2% specular Hem	moderate Ser alteration of Bt and feldspars, Chl alteration of Bt	Py + Hem + Chl veins, Cp + Py + specular Hem + Tur + Qtz with Qtz Ser halo veins
MO124	156.13 - 156.37	16	DLP	20% phenocrysts of 40% Pl, 30% Kfs and 30% Qtz eyes in a 80% fine grained groundmass composed of predominately Qtz and feldspar with 2% Chl altered Bt	medium to coarse grained (3-8 mm) porphyritic mostly euhedral phenocrysts with a cryptocrystaline groundmass	veins- infrequent veins of Py and Cp, disseminatations - 0.2% specular Hem	moderate Ser alteration of Bt and feldspars, Chl alteration of Bt	Py + specular Hem + Chl veins, Cp + Py + specular Hem + Tur + Qtz with Qtz Ser halo veins

trace chalcopyrite and pyrite as disseminations and in veins. Feldspars show strong sericite alteration. Samples of the QMF units are fine to medium-grained (2-5 mm), generally diorite to monzodiorite, with variable biotite, ~8% amphibole and trace to several percent magnetite. Pyrite is the main sulfide and is observed replacing magnetite. Chalcopyrite occurs mostly in veins at low abundances, generally <0.2%. Feldspars are variably sericite altered and biotite and chlorite alteration of amphibole and chlorite alteration of biotite are present. The main porphyry units, QMP, POB, FP and DLP, often referred to as late porphyries (Toro et al., 2012; Deckart et al., 2005; Warnaars et al., 1985), have ~20% up to 8 mm plagioclase and K-feldspar phenocrysts in a fine groundmass and range from dacite to rhyodacite in composition. These units are variably mineralized. The POB is the most mineralized with up to several percent of disseminated chalcopyrite, and in places, dense veining contributing up to 1% chalcopyrite and lesser pyrite. Alteration is variable but generally includes strong-intense sericitization and some silicification. Tourmaline occurs as vug fillings and is associated with chalcopyrite mineralization. Hematite is abundant in veins and as disseminations in the DLP.

APATITE

Apatite group minerals have the formula $M_{10}(ZO_4)_6X_2$. Flourapatite (FAp) is the most common igneous apatite endmember and has the general formula $Ca_{10}(PO_4)_6F_2$. In the case of chlorapatite (ClAp) or hydroxyapatite (OHAp), the X site is occupied by Cl or OH, respectively (Pan and Fleet, 2002). The ideal structure of FAp has a close packed $P6_3/m$ space group forming hexagonal symmetry (Hughes and Rakovan, 2002). In this symmetry, 6/10ths of the Ca are arranged in triangles (Ca2) perpendicular to the c-axis around a central anion. Successively stacked triangles order by a 6_3 screw operation and form the central anion channel (Bauer and Klee, 1993) (Fig. 5).

Parallel anion columns are joined via PO_4 tetrahedra and the remaining 4/10ths of Ca in Ca polytrahedra (Ca1) link these columns through bonds with their coordinating oxygen (Bauer and Klee, 1993). ClAp and OHAp endmembers deviate from this ideal structure and form with a $P2_1/b$ space group and monoclinic symmetry. This structure is caused by ordering of adjacent anion channels. Ordering of adjacent anion channels is caused by the required offset of the Cl or OH anion from the z = ¼ and ¾ minor planes necessary to accommodate these larger anions (Hughes and Rakovan, 2002) (Fig. 5).

Trace element substitutions in apatite commonly occur as coupled substitutions in the M and Z sites. Coupled substitutions allow for charge balance and provide space accommodation for substituting elements of different valances or atomic radii. Of significance, is that couplings make substitutions resistant to postcrystallization alteration

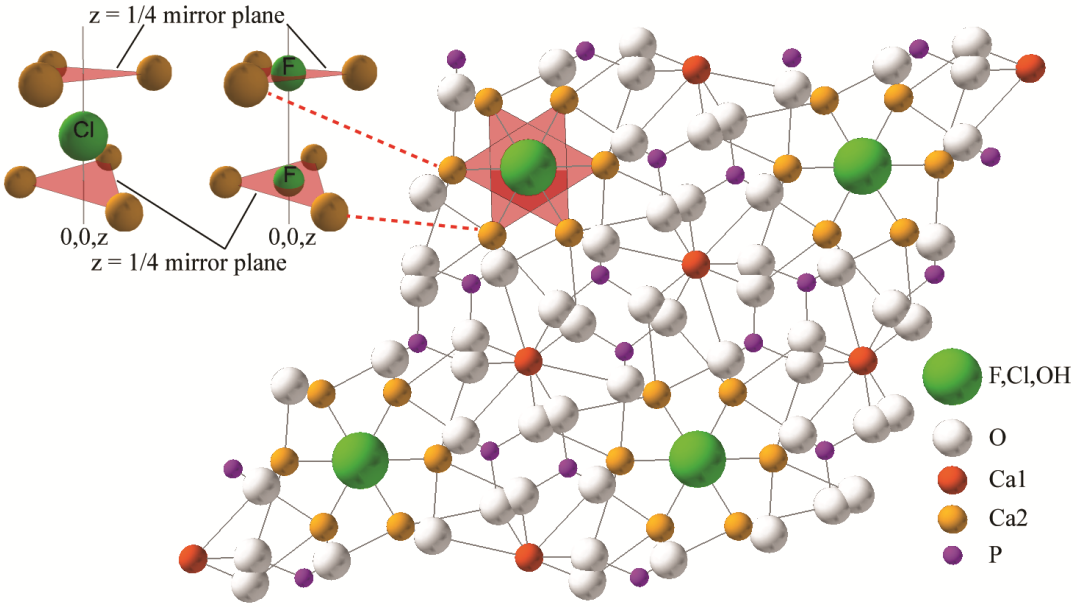

Figure 5. The atomic arrangement of apatite projected on (001). Phosphorous is purple, O is white, F,Cl, or OH is green and Ca1 and Ca2 are dark orange and light orange, respectively. Red triangles represent successive mirror planes moving down the anion channel. In the upper left hand corner is a depiction of an inverted anion channel for fluorapatite (right) and chlorapatite (left). The mirror planes z=3/4 and z=1/4 are shown with Cl and F atom positions indicated. Adapted from Hughes and Rakovan (2002).
and in turn make apatite particularly useful in understanding early magma compositions

(Porter and Titley, 2004). Recognized substitutions in the M and Z sites, in both natural and synthetic apatite include: M (substituting for Ca^{2+}) = Na, Mg, Sr, Ba, Sr, Cu, Pb, Ce, Y and Z (substituting for P in PO_4^{3-}) = Na, La, Ce, As, Si, S, V, B (Pan and Fleet, 2002; Hughes and Rakovan, 2002).

ANALYTICAL METHODS

Samples were collected from drill core exhibiting the least alteration and influence from veining. Samples were sent to ACME labs, Vancouver for whole rock geochemistry analysis. In situ apatite grains in core samples prepared as polished plugs were analyzed at the University of Utah microprobe and ICP-MS facilities for trace element and rare earth element concentrations.

Whole Rock Geochemistry

Major element oxide, trace element, rare earth and metal concentrations for each of the 16 samples were analyzed. Samples were prepared using lithium metaborate/tetraborate fusion and dilute nitric acid digestion and analyzed by ICP-AES for major oxides, Ba, Ni and Sc. For rare earth and refractory elements, samples were prepared using lithium metaborate/tetraborate fusion and nitric acid digestion and analyzed by ICP-MS. Mo, Cu, Pb, Zn, Ni, As, Cd, Sb, Bi, Ag and Tl concentrations were determined using a multi-acid digestion and ICP-MS.

Apatite Trace Element Geochemistry

An average of five apatite grains from each sample were analyzed on a Cameca model SX-50 electron microprobe equipped with four wavelength-dispersive X-ray spectrometers. Grains within rock matrix and located away from veins were chosen to

minimalize influence from alteration. For each grain, an average of three spot analyses were performed to determine Ca, P, F, Cl, Na, Mg, K, Ti, V, Mn, Fe, Cu, Sr, Ba, Ce, As, Si, S and Al concentrations. A 5 μm diameter beam, 15 kV voltage and 30 nA beam current were used to provide high spatial resolution and limit migration of lighter elements during analysis. The crystals, lines, slopes, standards and count times are provided in Appendix A. The detection limit was estimated at 300 ppm.

The three spots were located along a traverse across the grain, or in a fashion so that change in concentrations from core to rim could be evaluated (Appendix B). These analyses were attributed as core or rim based on their location. Zonation of S was evaluated using the following seven categories: decreasing rim to rim, core high irregular, rim high irregular, core high concentric, rim high concentric, high asymmetric plateau (indicating a core and one rim high with one rim low), low asymmetric plateau (indicating a core and one rim low with one rim high) and no zonation (Appendix F). Only grains with three or more spots having above detection levels (>300 ppm) and at least one of the three above 500 ppm were included for evaluation. Distinction of one category from another was based on a difference in value of greater or less than an estimated 1 sigma (est.1σ). The est.1σ was extrapolated as a best fit line for combined residuals of all elements determined for analyses of the Fap apatite standard analyzed as an unknown.

Grains were noted to be embayed and to have varying crystal morphologies indicating possible resorption or postcrystallization alteration. To assess possible effects on S concentrations from such postcrystallization processes, morphologies were characterized using six categories: euhedral, euhedral/corners embayed, subhedral,

subhedral/embayed, anhedral and anhedral/embayed and these morphologies were evaluated for correlation to S concentration depletion or enhancement.

Apatite Rare Earth Element (REE) Geochemistry

An average of four apatite grains from each sample, excluding sample 34, were analyzed on an Agilent 7500ce, quadrapole inductively coupled plasma mass spectrometer (ICP-MS) attached to an Analyte 193 photon laser. Analytes included La, Ce, Pr, Nd, Sm, Eu, Gd, Tb, Dy, Ho, Er, Yd, Lu and Hf. Boron was also analyzed. The results for Ho and Er were unrealistically high and low, respectively, and were not further considered. All grains were ablated using a laser spot size of 9.7 μm, repeat rate of 5 Hz and output of 45% of maximum. Grains in samples 12, 17, 13 and 41 were ablated using a scan speed of 5 μm/s and all other grains were ablated using a scan speed of 3 μm/s. Of the two scan speeds, 3 μm/s produced the best signal to noise ratio. The 610 NIST glass was used as a standard reference material, and Ca within the 610 glass and Ca determined in grains using EMPA was used as an internal standard to correct for matrix effects and changes in laser ablation yield. Analysis of the 610 glass was performed before every third grain to allow for drift correction. Aluminum counts were used to discriminate between apatite grain and matrix.

Calculation of Melt S Concentrations

Calculation of melt S concentrations was performed using the methods of Porter and Titley (2004). This method involves two steps.

First, the apatite saturation temperature (AST) is determined using the AST

equation of Piccoli and Candela (1994) modeled after the experimental findings of Harrison and Watson (1984). Harrison and Watson (1984) found that apatite crystallization is a function of temperature and instantaneous melt SiO_2 and P_2O_5 concentrations in paraluminous melts, and that H_2O and pressure are not major contributors at H_2O concentrations between 0 and 10 wt. % and SiO_2 between 45 and 75 wt. %. Their findings were formulated into a partition coefficient that Piccoli and Candela (1994) recast as Equation 1 where AST is the apatite saturation temperature in C°, C_{SiO2}^{l} is the whole rock concentration of SiO_2 in wt. %, C_{P2O5}^{lo} is the whole rock concentration of P_2O_5 in wt. % and X is the crystallinity of the melt.

$$AST = \frac{264000 * C_{SiO\text{-}2}^{l} - 4800}{12.4 \times C_{SiO\text{-}2}^{l} - \ln\left(\frac{C_{P2O5}^{lo}}{1 - X/100}\right) - 3.97} \quad (1)$$

In the method of Porter and Titley (2004), the AST equation is reformed into Equation 2 where ($C_{SiO\text{-}2}^{x}$) is wt. % SiO_2 of the melt given the crystallinity (x) of the melt. This equation is used in an iterative process to converge on an instantaneous wt. % SiO_2 and wt. % P_2O_5 and thus a final AST.

$$AST = \frac{264000 * C_{SiO\text{-}2}^{x} - 4800}{12.4 \times C_{SiO\text{-}2}^{l} - \ln\left(\frac{C_{P2O5}^{lo}}{1 - X/100}\right) - 3.97} \quad (2)$$

The iterative process is as follows: First, the whole rock SiO_2 and P_2O_5 content is used to determine an initial AST by Equation 1. This AST is then used to estimate first

iteration crystallization limit using the data from Whitney (1988) and a new melt SiO_2 concentration is calculated by mathematically removing early crystalizing phases. Using the calculated melt SiO_2, the AST is recalculated using Equation 2 and a lower crystallization limit is produced. The process is repeated until percent crystallization and resulting SiO_2, P_2O_5 and ASTs converge. This AST is taken as the instantaneous melt SiO_2 and P_2O_5 corrected temperature for apatite saturation.

Second, melt S is calculated using the converged AST and partition coefficient equations for anhydrite undersaturated conditions (AUC) (Equation 3) and anhydrite saturated conditions (ASC) (Equation 4). Equation 3 is the linier regression of the experimentally derived AUC $K_D^{ap/melt}$ data of Parat and Holtz (2004). Equation 4 is the linier regression of the best fit ASC $K_D^{ap/melt}$ data of Streck and Dilles (1998). In each equation $K_D^{ap/m}$ is the S partition coefficient between apatite (ap) and the melt (m) and T is temperature in K°.

$$K_D^{ap/m} = 11700\ e^{(-0.0057T)}, \tag{3}$$

$$K_D^{ap/m} = 912845\ e^{(-0.0103T)} \tag{4}$$

RESULTS

Whole Rock Geochemistry

Strong alteration of units within the San Enrique deposit make determination of composition or evaluation of the evolution of system from major element geochemistry unreliable. However, based on Zr/Ti and Nb/Y ratios after Pearce (1996), lithologies follow a progression from less evolved, lower intermediate subalkaline composition for the FLA to a more alkaline, but still lower intermediate composition for the QMF. Two magma compositions with differing alkali content are indicated for the QMF. Samples 26, 40 and 23 (QMF-I) cluster at subalkaline lower intermediate compositions and samples 38 and 41 (QMF-II) cluster at alkali lower intermediate compositions. Upper intermediate compositions are indicated for the synmineralization and late-mineralization porphyries. The late-mineralization porphyries have the most evolved compositions (Fig. 6, Tables 2 and 3). The composition indicated for the QMG, however, does not fall in this trend. The QMG is the oldest unit of the San Francisco Batholith but has more evolved alkali metal and silica content relative to other San Francisco Batholith units.

Chondrite normalized heavy rare earth elements (HREE) for all units are depleted compared to light rare earth elements (LREE). Heavy rare earth element depletion progresses from less depleted for less evolved units, starting with the FLA, to more depleted for more evolved units, ending with the DLP (Fig. 7). The QMG, however, is generally more HREE depletion than other units of the San Francisco Batholith.

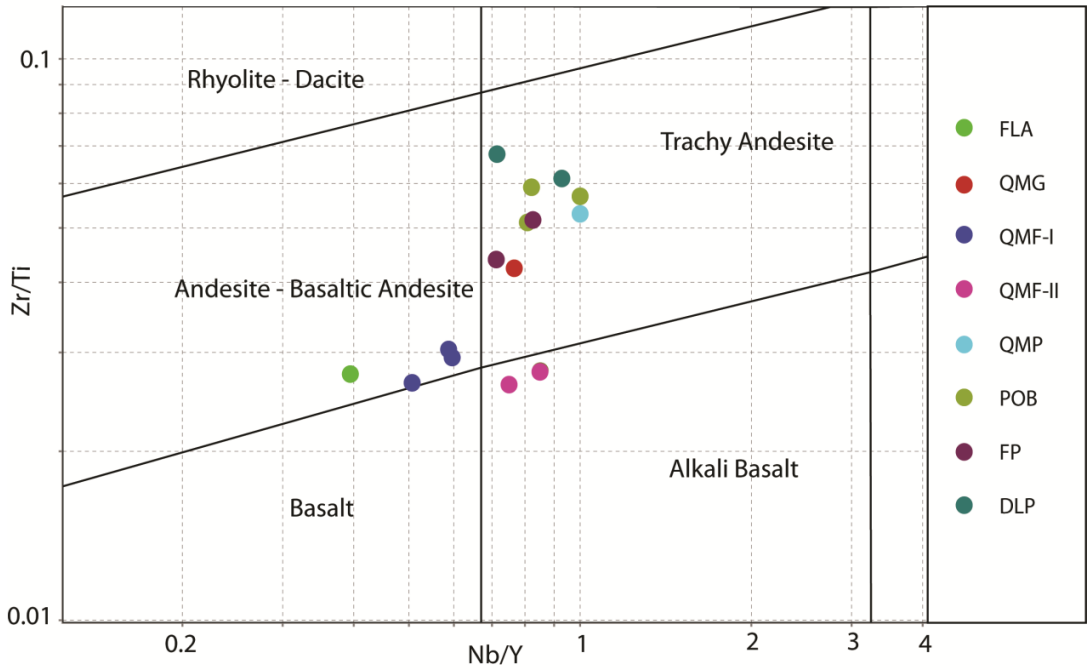

Figure 6. Whole rock Zr/Ti vs. Nb/Y plot.

Table 2. Select Whole Rock Major Element Chemistry.

Rock Unit		**FLA**	**QMG**	**QMF-I**	**QMF-II**	**QMP**	**POB**	**FP**	**DLP**
Sample ID	**LOD**	**21**	**48**	**26**	**41**	**02**	**42**	**13**	**17**
SiO_2	0.01	57.7	66.42	60.17	60.36	67.64	67.63	64.57	69.41
Al_2O_3	0.01	16.55	15.01	18.31	16.78	16	14.57	16.4	15.96
Fe_2O_3	0.04	7.62	3.97	4.85	5.07	2.07	3.15	1.75	2.28
CaO	0.01	4.86	1.09	5.14	3.19	1.44	0.61	2.61	0.6
Na_2O	0.01	3.73	2.35	4.91	5.48	5.05	0.6	5.84	4.61
K_2O	0.01	2.92	5.36	2.17	2.05	4.48	7.67	3.15	5.1
TiO_2	0.01	0.92	0.45	0.74	0.6	0.28	0.23	0.44	0.23
MgO	0.01	3.46	1.85	2.12	2.05	0.57	0.69	1.29	0.63
Cr_2O_3	0.002	0.01	0.002	nd	0.003	nd	nd	nd	nd
P_2O_5	0.01	0.25	0.12	0.22	0.19	0.12	0.1	0.19	0.09
MnO	0.01	0.21	0.07	0.08	0.04	0.02	0.02	0.02	0.02
Total C	0.01	0.13	0.2	0.02	0.23	0.18	0.06	0.09	0.06
Total S	0.01	0.03	0.26	0.03	0.54	0.39	1.38	0.93	0.03
LOI	--	1.5	3.1	1.1	3.9	1.9	3.5	3.2	0.9
Total	0.01	99.76	99.76	99.78	99.75	99.59	98.75	99.47	99.81

LOD – limit of detection, nd – not detected, concentrations in wt. %.

Table 3. Select Whole Rock Trace Element Chemistry.

Rock Unit		FLA	QMG	QMF-I	QMF-II	QMP	POB	FP	DLP
Sample ID	**LOD**	**21**	**48**	**26**	**41**	**02**	**42**	**13**	**17**
Rb	0.1	76.7	135.1	47.2	79.2	99.4	179.5	82.9	131.5
Cs	0.1	1.8	1.8	1.1	1.8	1.6	1.3	1.2	2
Sr	0.5	487.2	232.8	812.3	553.3	435.6	155.8	617.7	367.7
Ba	1	670	823	488	354	697	884	572	1017
Sc	1	15	5	6	7	2	2	4	2
Y	0.1	14.7	4.7	7.5	4.7	2.7	2.6	6.6	2.8
Zr	0.1	151.4	114.3	117.6	100.2	88.9	70.5	115.8	84.6
Nb	0.1	5.8	3.6	3.8	4	2.7	2.1	4.7	2.6
Ga	0.5	16.4	12.8	17.5	19.1	15.8	17.7	20.9	17.8
Sn	1	1	nd	nd	1	1	3	2	nd
La	0.1	18.3	10.8	15.6	16.2	13.6	18	15.2	14.3
Ce	0.1	40.6	25	35.3	32	25.6	34.9	30.2	25
Pr	0.02	4.81	2.83	4.18	3.9	2.83	3.81	3.61	2.62
Nd	0.3	19	12.3	15.5	17.1	10.3	14.8	13.3	11.5
Sm	0.05	3.96	1.84	2.87	2.81	1.64	2.3	2.47	1.57
Eu	0.02	0.97	0.73	0.87	0.74	0.43	0.42	0.73	0.52
Gd	0.05	3.38	1.39	2.1	1.91	1.12	1.33	1.82	1.17
Tb	0.01	0.51	0.2	0.28	0.22	0.13	0.13	0.24	0.13
Dy	0.05	2.95	0.76	1.55	1.01	0.53	0.52	1.11	0.52
Ho	0.02	0.53	0.18	0.26	0.18	0.1	0.07	0.24	0.1
Er	0.03	1.43	0.43	0.63	0.43	0.24	0.18	0.7	0.24
Tm	0.01	0.22	0.07	0.1	0.07	0.04	0.03	0.11	0.03
Yb	0.05	1.41	0.45	0.42	0.44	0.32	0.22	0.53	0.19
Lu	0.01	0.23	0.07	0.1	0.07	0.04	0.03	0.09	0.03
Hf	0.1	4.6	3.7	3.4	2.7	2.8	2.3	3	2.7
Th	0.2	10.9	9.7	4.3	3.8	4.1	3.8	3.7	4.4
V	8	138	44	93	101	28	29	66	39
Ni	0.1	34.4	10.4	10.1	14.1	3.1	2.3	3.7	2.6
Co	0.2	20.5	1.4	12.8	6.8	3.3	4	2.9	1.3
Mo	0.1	1.1	0.2	1.5	0.8	23.9	35	19.9	0.9
Cu	0.1	13.1	603.3	80.3	692.8	2242.6	8643.2	3032.9	122.7
Pb	0.1	10	10.9	9	8.4	6.3	12.6	5.3	12.8
Zn	1	144	109	76	71	34	45	39	49
As	1	14	4	21	5	2	2	2	4
Sb	0.1	2.4	1.9	1.2	0.8	0.4	0.4	0.4	0.8
Bi	0.1	0.2	nd	nd	nd	0.3	1.6	0.1	0.6
Ag	0.1	nd	0.3	nd	0.2	0.6	3.3	1.1	0.1
Cd	0.1	nd	nd	nd	nd	nd	nd	nd	nd

LOD – limit of detection, nd – not detected, concentrations in ppm.

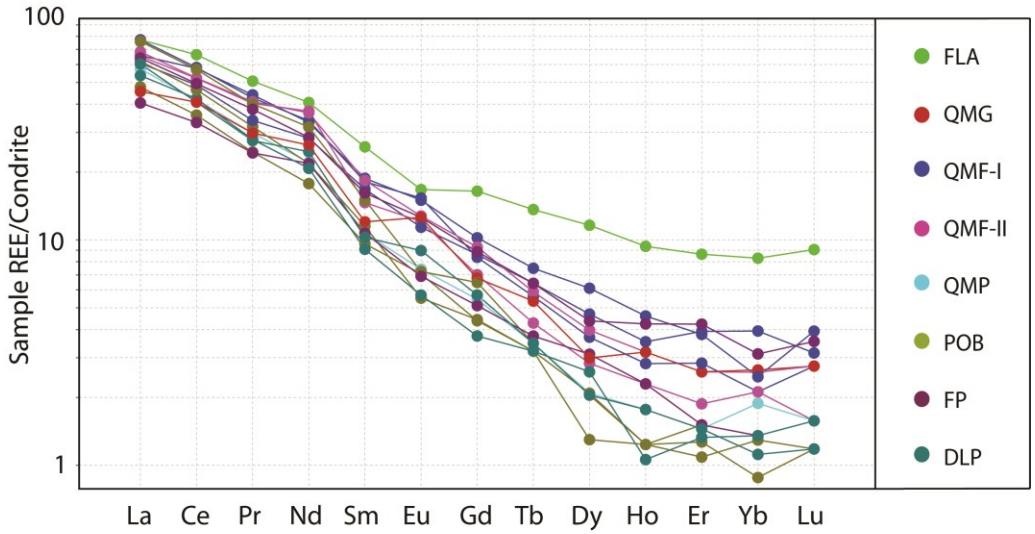

Figure 7. Sample/chondrite normalized REE trends using normative values. Adapted from McDonough and Sun (1989).

Apatite Grain Morphology and Zonation

Anhedral-embayed (37% of analyses) (Fig. 8a) and euhedral grains (33% of analyses) (Fig. 8b) are the most abundant morphologies noted for analyzed grains. The next most abundant morphology is subhedral/embayed accounting for 18% of analyzed grains. Grains with subhedral and euhedral/corners embayed account for less than 12% combined.

With the exception of three analyses from euhedral grains, with S over 2600 ppm, analysis from euhedral grains, subhedral grains and anhedral grains span equivalent ranges (Fig. 9). High S concentrations in the POB and FP units come mainly from anhedral/embayed grains (maroon squares), but low S concentrations in the FLA, QMF-I, QMP and POB also come from anhedral/embayed grains. High S concentrations from the QMF-I and DLP come mostly from euhedral not-embayed (purple circles) and subhedral not embayed (pink circles) grains. However, grains with these morphologies provide an

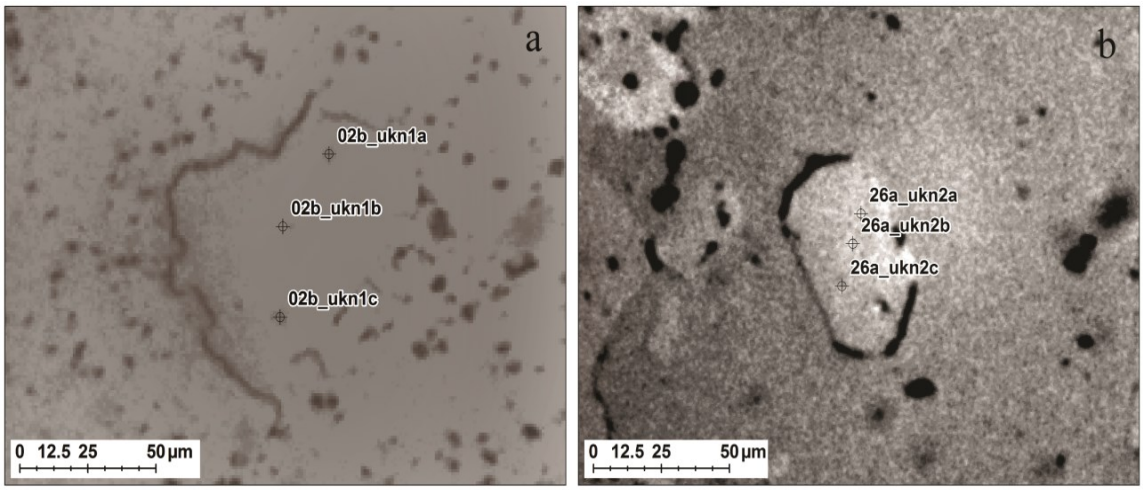

Figure 8. Visible light images of in situ aptite grains and microprobe analysis locations. (a) Anhedral embayed apatite grain. (b) Euhedral apatite grain.

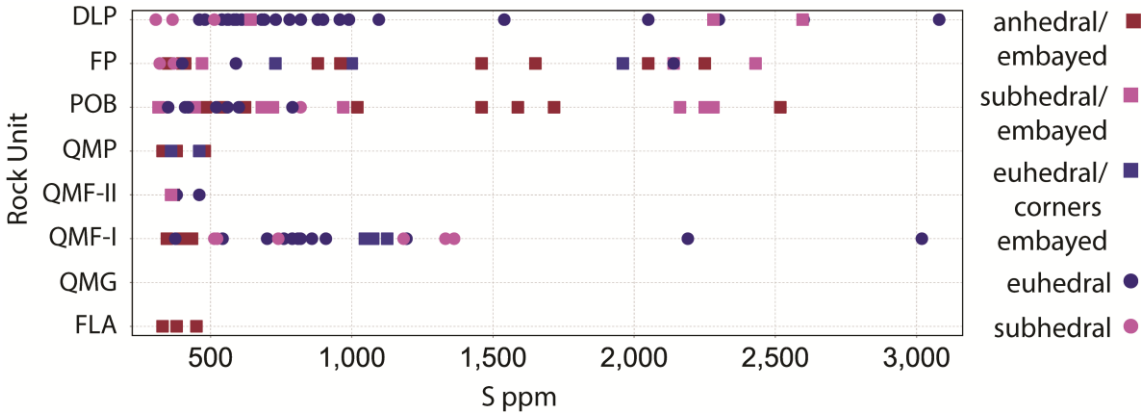

Figure 9. A plot of rock units and S concentrations in apatite grains showing grain morphology relationships to S concentration and rock unit. Anhedral (maroon), subhedral (pink), euhedral (purple), embayed (squares), not embayed (circles).

equivalent number of low concentration analyses in the POB, FP and DLP units as well.

Zonation patterns for all elements, as well as apatite grain microprobe analysis maps, are in Appendices B and C, respectively. In summary, 31 grains met S zonation evaluation criteria. The most common grain zonations are low asymmetric plateau (23%), core high irregular (19%), rim to rim (19%), high asymmetric plateau (13%) and rim high irregular (13%). Of much lower abundance are core high concentric (6%), rim high concentric (3%) and no zonation patterns (3%).

Apatite Composition

Atoms per formula unit are based on 16 cation M + Z site occupancy per formula unit (select analyses, Table 4; all analyses, Appendix E). Concentrations are given as measured (select analyses, Table 5 and 6; all analyses, Appendix C). Limits of detection and relative standard error for LA-ICP-MS analyses are provided in Table 7 (all analyses, Appendix D). One hundred ninety two analyses from 71 apatite grains are included. All but three analyses produced compositional ranges typical of FAp. Concentrations of Ca, P, F and Cl range from 40.63 to 38.13%, 18.84 to 17.04%, 3.97 to 3.27% and 2.08% to below detection, respectively. The remaining three analyses, all from one grain in sample QMF-II 38, produced below detection concentrations of F, and from 0.18 to 0.11 % Cl. Fluorine in 12 of 192 analyses is above 1estσ of stoichiometric 2 atom X site capacity for pure FAp (2.02 to as high as 2.10 atoms, or 4% above 1estσ). This overabundance of F is attributed to F migration as a function of time dependent exposure to the electron beam during analysis (Stromer et al., 1993).

Table 4. Atoms per Formula Unit in Select Analyses of Apatite Grains.

Rock Unit	FLA	QMG	QMF-I	QMF-I	QMF-II	QMF-II	QMP	POB	POB	FP	FP	DLP
Sample ID	21	48	26	40	38	41	02	47	34	13	12	16
Grain ID	21d_07	48a_21	26a_ukn 4	40d_ukn 2	38d_ukn 2	41b_ukn 1	02b_ukn 1	47c_ukn 3	34a_15	13a_33	12a_ukn 2	16a_ukn6
Anal. Location	Rim	Rim	Core	Core	Core	Rim	Rim	Rim	Core	Rim	Rim	Core
Ca	9.971	10.038	9.823	9.983	10.012	9.913	10.103	9.839	10.021	9.852	10.002	9.915
Sr	nd	0.010	nd	0.006	nd	0.004	0.006	0.012	0.011	nd	0.007	0.011
Ba	0.003	nd	nd	nd	nd	nd	nd	nd	nd	nd	nd	nd
Na	nd	nd	0.061	nd	nd	0.022	nd	0.042	nd	0.024	0.051	0.022
K	nd	nd	0.033	nd	nd	nd	nd	nd	nd	0.008	0.017	0.012
Mg	nd	nd	nd	nd	nd	nd	nd	nd	nd	nd	0.021	nd
Ti	nd	nd	nd	nd	0.007	nd	nd	nd	nd	nd	nd	nd
Mn	0.016	0.026	0.010	0.030	0.008	0.032	0.036	0.024	0.013	0.027	0.019	nd
Fe	0.021	0.049	0.007	0.037	0.015	0.090	0.022	0.042	0.029	0.037	0.052	0.014
Cu	nd	0.008	nd	nd	nd	nd	0.005	0.007	nd	nd	nd	0.013
P	5.937	5.835	5.904	5.932	5.954	5.898	5.801	5.935	5.838	6.019	5.716	5.923
S	0.010	nd	0.069	nd	nd	0.011	0.011	0.049	0.032	0.010	0.052	0.034
B	0.004	0.004	nd	0.003	na	na	0.004	0.005	na	nd	0.005	0.009
Si	0.017	0.014	0.051	nd	nd	nd	nd	0.031	0.032	nd	0.029	0.025
As	nd	nd	nd	nd	nd	0.013	nd	nd	nd	nd	nd	nd
V	nd	nd	nd	nd	nd	nd	nd	nd	nd	nd	nd	nd
F	1.97	2.01	1.92	1.99	2.00	1.96	2.01	1.91	1.92	1.95	1.96	2.00
Cl	0.27	0.07	0.48	0.06	0.04	0.16	0.07	0.07	0.04	0.08	0.06	0.07
O	23.81	23.71	23.79	23.86	23.92	23.79	23.67	24.01	23.89	24.01	23.65	23.92

nd = not detected, na = not analyzed.

Table 4 Continued.

Rock Unit	**FLA**	**QMG**	**QMF-I**	**QMF-I**	**QMF-II**	**QMF-II**	**QMP**	**POB**	**POB**	**FP**	**FP**	**DLP**
Sample ID	**21**	**48**	**26**	**40**	**38**	**41**	**02**	**47**	**34**	**13**	**12**	**16**
Grain ID	**21d_07**	**48a_21**	**26a_ukn4**	**40d_ukn2**	**38d_ukn2**	**41b_ukn1**	**02b_ukn1**	**47c_ukn3**	**34a_15**	**13a_33**	**12a_ukn2**	**16a_ukn6**
Location	**Rim**	**Rim**	**Core**	**Core**	**Core**	**Rim**	**Rim**	**Rim**	**Core**	**Rim**	**Rim**	**Core**
La	0.003	0.001	0.007	0.001	na	na	0.002	0.003	na	0.003	0.005	0.005
Ce	0.008	0.005	0.019	0.003	0.005	0.016	0.005	0.006	0.025	0.007	0.010	0.009
Pr	0.0011	0.0008	0.0025	0.0004	na	na	0.0007	0.0007	na	0.0014	0.0015	0. 0011
Nd	0.0047	0.0038	0.0102	0.0018	na	na	0.0033	0.0025	na	0.0061	0.0070	0.0045
Sm	0.0011	0.0011	0.0017	0.0005	na	na	0.0009	0.0005	na	0.0019	0.0016	0.0007
Eu	0.0001	0.0003	0.0003	0.0002	na	na	0.0003	0.0001	na	0.0003	0.0002	0.0002
Gd	0.0009	0.0013	0.0012	0.0004	na	na	0.0009	0.0004	na	0.0014	0.0013	0.0006
Tb	0.0001	0.0002	0.0001	0.0001	na	na	0.0001	0.0001	na	0.0002	0.0002	0.0001
Dy	0.0005	0.0014	0.0005	0.0003	na	na	0.0007	0.0003	na	0.0010	0.0009	0.0002
Yb	0.0002	0.0005	0.0002	0.0001	na	na	0.0002	0.0001	na	0.0005	0.0003	0.0001
Lu	0.0000	0.0001	0.0000	0.0000	na	na	0.0000	0.0000	na	0.0001	0.0001	0.0000
Hf	0.0001	nd	nd	0.0000	na	na	0.0000	nd	na	nd	nd	0.0001
Total Charge (+)	49.92	49.56	50.06	49.81	49.88	49.75	49.47	50.05	49.73	50.10	49.40	49.97
Total Charge (-)	-49.87	-49.51	-49.98	-49.78	-49.87	-49.70	-49.42	-50.01	-49.73	-50.04	-49.32	-49.90
Charge Difference	0.06	0.05	0.08	0.03	0.00	0.05	0.05	0.05	0.00	0.06	0.08	0.07

Table 5. Elemental Concentrations from Select Microprobe Analyses of Apatite Grains.

Rock Unit	**FLA**	**QMG**	**QMF-I**	**QMF-I**	**QMF-II**	**QMF-II**	**QMP**	**POB**	**POB**	**FP**	**FP**	**DLP**
Sample ID	**21**	**48**	**26**	**40**	**38**	**41**	**02**	**47**	**34**	**13**	**12**	**16**
Grain ID	**21d_07**	**48a_21**	**26a_ukn4**	**40d_ukn2**	**38d_ukn2**	**41b_ukn1**	**02b_ukn1**	**47c_ukn3**	**34a_15**	**13a_33**	**12a_ukn2**	**16a_ukn6**
Location	**Rim**	**Rim**	**Core**	**Core**	**Rim**	**Rim**	**Rim**	**Rim**	**Rim**	**Rim**	**Rim**	**Rim**
wt. %												
Ca	39.28	39.74	39.12	40.09	40.62	39.47	39.42	39.71	40.11	39.51	39.31	39.54
P	18.07	17.85	17.71	18.41	18.45	18.15	17.49	18.51	18.15	18.30	17.36	18.03
F	3.69	3.77	3.71	3.79	3.83	3.70	3.72	3.65	3.69	3.68	3.65	3.84
Cl	0.93	0.25	1.64	0.21	0.12	0.55	0.24	0.26	0.09	0.30	0.21	0.19
O	37.24	37.26	36.54	38.12	38.39	37.50	36.69	38.15	37.87	37.78	36.52	37.40
ppm												
Sr	nd	840	668	486	638	340	470	1032	nd	nd	570	678
Ba	400	nd	nd	nd	nd	nd	nd	nd	480	nd	nd	nd
Na	nd	nd	1651	nd	nd	507	nd	972	nd	497	1150	458
K	nd	nd	1387	nd	nd	nd	nd	nd	nd	nd	650	637
Mg	nd	nd	nd	nd	nd	nd	nd	nd	nd	nd	490	nd
Ti	nd	nd	nd	nd	nd	nd	nd	nd	nd	nd	nd	nd
Mn	860	1400	800	1660	nd	1750	1910	1340	310	2170	1040	950
Fe	1160	2700	410	2080	1150	5010	1170	2360	510	2490	2840	1000
Cu	nd	500	nd	nd	nd	nd	310	470	nd	370	nd	nd
S	330	nd	3019	nd	nd	360	330	1588	nd	370	1650	898
Si	470	380	1240	nd	nd	nd	nd	878	nd	nd	810	1020
As	nd	nd	nd	nd	nd	1000	nd	nd	nd	nd	nd	nd
V	nd	nd	nd	nd	nd	nd	nd	nd	nd	nd	nd	nd

LOD = 300 ppm.

Table 6. Average Elemental Concentrations of Select Apatite Grains Determined Through LA-ICP-MS Analysis.

Rock Unit	**FLA**	**QMG**	**QMF-I**	**QMF-I**	**QMF-II**	**QMF-II**	**QMP**	**POB**	**POB**	**FP**	**FP**	**DLP**
Sample ID	**21**	**48**	**26**	**40**	**38**	**41**	**02**	**47**	**34**	**13**	**12**	**16**
Grain ID	**21d_07**	**48a_21**	**26a_ukn4**	**40d_ukn2**	**38d_ukn2**	**41b_ukn1**	**02b_ukn1**	**47c_ukn3**	**34a_15**	**13a_33**	**12a_ukn2**	**16a_ukn6**
Location	**Rim**	**Rim**	**Core**	**Core**	**Rim**	**Rim**	**Rim**	**Rim**	**Rim**	**Rim**	**Rim**	**Rim**
ppm												
La	407	160	911	152	na	na	211	480	na	346	616	680
Ce	1060	715	2683	441	10	2180	615	872	520	995	1408	1262
Pr	154	113	354	59	na	na	95	97	na	193	208	157
Nd	665	537	1457	255	na	na	465	361	na	872	992	643
Sm	157	170	261	69	na	na	137	71	na	287	230	111
Eu	15	40	38	24	na	na	41	17	na	49	35	35
Gd	139	201	192	67	na	na	139	61	na	214	205	89
Tb	17	38	22	10	na	na	17	12	na	30	28	9
Dy	88	223	80	48	na	na	108	45	na	163	146	36
Yb	30	79	29	16	na	na	36	21	na	83	59	15
Lu	5	10	5	4	na	na	4	4	na	17	9	4
Hf	12	nd	nd	8	na	na	8	nd	na	nd	nd	19
B	45	41	nd	36	na	na	41	50	na	nd	51	93

nd = not detected, na = not analyzed. See Table 7 for relative standard error and limits of detection. Ce values determined through LA-ICP-MS unless not analyzed, in which case, reported Ce values were determined through microprobe analysis.

Table 7**.** Relative Standard Error and Limits of Detection LA-ICP-MS Analysis of Select Apatite Grains.

Grain ID	**21d_07**	**48a_21**	**26a_ukn4**	**40d_ukn2**	**38d_ukn2**	**41b_ukn1**	**02b_ukn1**	**47c_ukn3**	**34a_15**	**13a_33**	**12a_ukn2**	**16a_ukn6**
1σ (ppm)												
La	23.3	7.7	88.1	6.5	na	na	12.7	27.1	na	34.0	32.9	38.4
Ce	72.5	64.3	646.7	17.5	na	na	42.5	58.9	na	71.0	59.1	119.5
Pr	12.3	10.6	98.4	2.8	na	na	5.9	7.0	na	15.7	9.3	21.8
Nd	56.9	62.2	331.5	11.4	na	na	37.1	25.0	na	53.1	62.0	95.0
Sm	16.9	20.7	72.0	3.5	na	na	16.7	8.3	na	28.3	19.0	23.2
Eu	0.9	5.0	8.4	1.3	na	na	4.2	2.6	na	6.4	3.7	7.2
Gd	11.5	23.6	40.5	4.8	na	na	14.0	8.0	na	19.8	17.9	14.0
Tb	1.7	4.9	5.4	0.6	na	na	1.7	2.6	na	3.0	2.4	1.5
Dy	7.6	26.8	15.5	2.6	na	na	10.9	6.0	na	16.1	14.7	5.3
Yb	2.1	6.1	4.4	0.9	na	na	2.6	3.0	na	0.6	5.8	1.9
Lu	0.4	0.6	0.8	0.5	na	na	0.2	0.4	na	nd	0.8	0.5
Hf	nd	nd	nd	nd	na	na	nd	nd	na	nd	nd	nd
B	7.6	5.1	nd	3.9	na	na	3.2	4.4	na	nd	nd	14.3
LOD (ppm)												
La	4	4	7	4	na	na	3	4	na	19	8	5
Ce	4	5	3	3	na	na	2	4	na	17	6	2
Pr	4	4	3	4	na	na	3	3	na	14	4	3
Nd	25	23	20	23	na	na	15	16	na	78	28	29
Sm	36	22	29	19	na	na	23	21	na	124	40	20
Eu	9	5	6	5	na	na	4	4	na	21	9	5
Gd	30	30	28	27	na	na	18	19	na	83	34	17
Tb	4	4	4	3	na	na	2	4	na	13	4	3
Dy	16	14	15	15	na	na	13	10	na	53	22	11
Yb	13	13	10	7	na	na	11	7	na	67	20	10
Lu	3	3	2	3	na	na	2	2	na	14	4	2
Hf	11	10	9	7	na	na	7	7	na	47	15	6
B	34	35	66	29	na	na	34	44	na	103	50	28

nd = not detected, na = not analyzed, σ = relative standard error.

Elemental Substitution in Apatite

Of all elements, Cl, Na, Mg, K, Ti, V, Mn, Fe, Cu, Sr, Ba, As, Si, S, La, Ce, Pr, Nd, Sm, Eu, Gd, Tb, Dy, Ho, Er, Yd, Lu and Hf, substitution is greatest for Cl, Fe, S, Na, Si and Mn with highs of 0.600 atoms (2.08 wt. %), 0.151 atoms (8,310 ppm), 0.098 atoms (3080 ppm), 0.084 atoms (1900 ppm), 0.073 atoms (2000 ppm) and 0.070 atoms (3,790 ppm), respectively. These elements are above detection in 98%, 94%, 58%, 42%, 66% and 96% of analyses, respectively. All other elements are less than 50% as abundant with the exception of K with a high of 0.049 atoms (1941 ppm) and above detection concentrations in 23% of analyses, and Cu with a high of 0.054 atoms (3410 ppm) and above detection concentrations in 31% of analyses.

REEs in Apatite

REE abundances in apatite grains are roughly 1.5 orders of magnitude higher than their counterparts in whole rock analyses. The most abundant REE is Ce with concentrations as high as 0.028 atoms (3858 ppm). Lanthanum is the next most abundant with concentrations as high as 0.010 atoms (1537 ppm).

With the exception of the QMG and QMF-II units, which show less depletion of HREEs relative to LREE, mean chondrite normalized REE patterns for apatite in rock units show equivalent relative HREEs vs. LREE trends as whole rock analyses for these units. One difference in apatite REE trends is prominent negative Eu anomalies for all units except the QMG (Fig. 10). The negative Eu anomalies are a likely indicator that, at the time of apatite crystallization, Eu had been strongly fractionated into earlier crystalizing plagioclase (Chu et al., 2009).

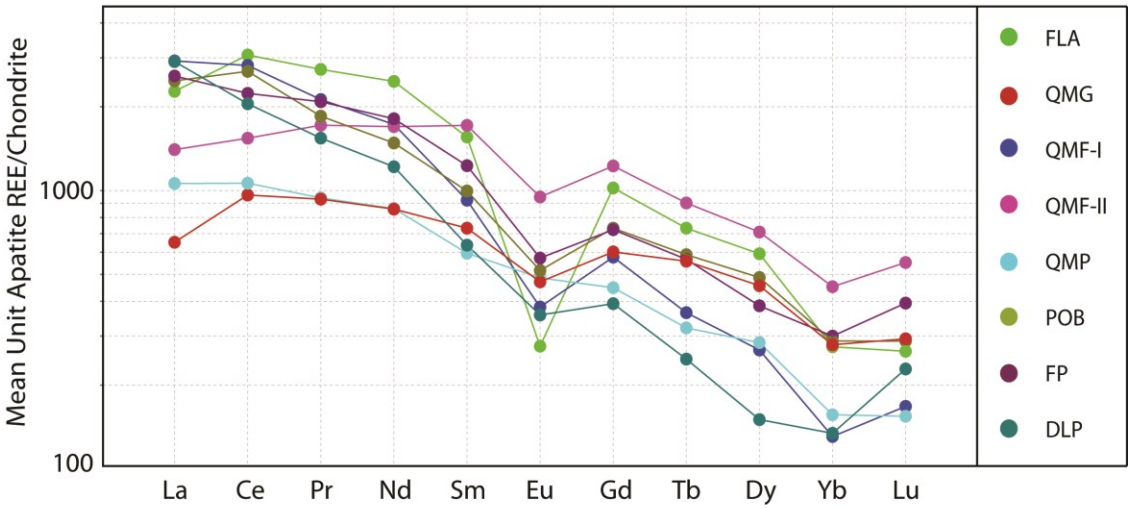

Figure 10. Mean rock unit apatite/chondrite normalized REE concentrations using normative values from McDonough and Sun (1989).

Sulfur and Other Mineralization Related Substitutions

Percentages and ratios of analyses of apatite with detectable concentrations of S in each unit as well as mean S in apatite for each unit are provided in Table 8. Other element substitutions in apatite with higher concentrations in mineralization contemporaneous units include Mg and Cu. Six analyses from the POB and three from the FP have concentrations of Mg from 330 to 650 ppm and 340 to 490 ppm, respectively, and one other analysis in sample QMF-I 40 has 720 ppm Mg. All units have apatite with detectable concentrations of Cu. However, Cu peaks in the QMF-I, POB, and DLP units (Table 9).

Melt S Concentrations

All samples converged on single ASTs. The resulting crystallinities and ASTs ranged between 13 and 21 % crystals in the melt and 930 and 970 °C, respectively (Table 10). Minimum and maximum calculated S concentrations at AUC and ASC are min; 27 ppm, max; 300 ppm and min; 87 ppm, max; 1100 ppm, respectively. The mean of calculated melt S for analyses of each unit at AUC and ASC are provided in Table 11.

Table 8. Analyses Above Detection and Mean S in Apatite for Each Rock Unit.

Rock Unit	% of Analyses Above Detection	Above Detection/All Analyses Ratio	Mean S (ppm)
FLA	21	3/14	387
QMG	0	0/15	nd
QMF-I	62	24/39	960
QMF-II	14	4/28	393
QMP	36	5/14	402
POB	86	25/29	948
FP	91	21/23	1108
DLP	97	29/30	1037

nd – not detected.

Table 9. Mean and Maximum Cu in Apatite for Each Rock Unit.

Rock Unit	Mean Cu (ppm)	Maximum Cu (ppm)
FLA	510	690
QMG	610	910
QMF-I	920	3410
QMF-II	500	750
QMP	490	710
POB	710	2070
FP	540	890
DLP	620	1030

Table 10. Calculated Melt Crystallinity and Rock Unit ASTs.

Rock Unit	% Crystals	AST (°C)
FLA	17	930
QMG	14	940
QMF-I	14	940
QMF-II	15	940
QMP	13	950
POB	19	950
FP	16	970
DLP	17	970

Table 11. Calculated Mean Melt S for Anhydrite Undersaturated and Saturated Conditions.

Rock Unit	Mean Melt S (ppm) for AUC Parat and Holtz (2004)	Mean Melt S (ppm) for ASC Streck and Dilles (1998)
FLA	30	100
QMG	nd	nd
QMF-I	80	280
QMF-II	30	100
QMP	35	130
POB	90	330
FP	110	420
DLP	100	390

nd - not detected.

DISCUSSION

System Evolution

Unit composition evolution trends correlate well with HREE depletion trends. The overall unit composition progression, indicated by Ti/Zr to Nb/Y and HREE depletion, is consistent with fractional crystallization and typical magma evolution in intermediate-felsic systems (White, 2013).

Both Ti/Zr to Nb/Y and HREE depletion for the QMG, the oldest unit of the San Francisco Batholith, however, indicate a more evolved magma for this unit than the younger units of the San Francisco Batholith. The more evolved composition for the QMG, and return to less evolved compositions for QMF I and QMF II, suggest that magmas responsible for generation of QMF units, and possibly all subsequent units, may have been sourced from a chamber that saw recharge and magma mixing with magma of a more mafic affinity. While this scenario is only suggested by these evolutionary trends, detection of Mg only in apatite from the QMF-I and other synmineralization units supports this hypothisis. Additionally, this scenario is consistent with Cu source models that propose mafic magma underplating (Core, 2004) or mafic magma input (Keith et al., 1997; Hattori and Keith, 2001) as significant contributors of Cu in porphyry systems.

Morphology and Zonation

Analyses with high S concentrations in the POB and FP units are dominantly from anhedral/embayed grains, and analyses with high S concentrations from the DLP and QMF-I units are dominantly from euhedral or subhedral not embayed grains. Analyses with low S concentrations in the POB and FP units' are dominantly from euhedral and subhedral grains and low S concentrations in all units, with the exception of the QMF-II and DLP, come from anhedral/embayed grains and subhedral/embayed grains. This distribution provides no clear-cut correlation between S and morphology. Two possible causes are postulated for grain embayments and anhedral habits: 1) embayments and/or anhedral habits are caused by oscillation above and below the liquidus during crystal growth which allowed portions of the grain to be re-assimilated back into the melt, or 2) embayments are caused by postcrystallization alteration. In either case, the lack of correlation between S concentration and grain morphology is taken to indicate that these causes do not preferentially affect S concentrations in these grains.

The combined occurrence of grains with core high irregular and concentric zonation patterns (26%) is greater than the combined grains with rim high irregular or concentric zonation patterns (16%); the combined number of grains with uneven distribution i.e., rim to rim, low asymmetric plateau, high asymmetric plateau or no zonation (55%) far exceed either rim high or core high zonation patterns. This is contrary to the theory of Streck and Dilles (1998) that proposes that core high to rim low zonation is common in igneous apatite. Assuming that grains analyzed in this study are zoned core high to rim low, the predominance of asymmetrically zoned and rim to rim zoned grains

can be taken to indicate that zonation patterns of these apatite grains are a function of orientation of the grain with respect to the surface of the sample plug. Select evaluation of grains that are mounted with the c axis perpendicular to the plug surface, however, shows that asymmetric zonation is predominant for these grains as well, albeit the asymmetry is high asymmetric plateau zonation. This substantiates that the core is higher than one out of the two rims. Given the lack of dominant core to rim or rim to core high-low zonation and the predominance of uneven distributions, a mean of all analyses from a unit is taken to be adequately representative of S substitution in apatite for that unit.

Sulfur Substitution Mechanisms

A strong correlation (Pearson correlation coefficient of 0.84) exists between S and Na (Fig. 11a). Increases in S occur with an increase of Na at a ratio of nearly 1:1. This correlation, and the requisite for a charge balanced exchange, indicates the main S substitution mechanism includes a coupled substitution by the exchange $S^{6+} + Na^{+} \Leftrightarrow P^{5+} + Ca^{2+}$. Lack of change in correlation and slope for lower intermediate FLA, QMF-I and QMF-II units (Fig. 11b) and more evolved QMP, POB, FP and DLP units (Fig. 11c), as well as the same relative ranges in S for both groups indicate coupling and sulfur uptake is independent of bulk melt composition (within the range of rock compositions for units in this study).

Crystal System Change and Apatite S

In general, Cl concentrations in apatite trend from higher concentrations for rock units with lower intermediate subalkaline compositions to lower concentrations for more

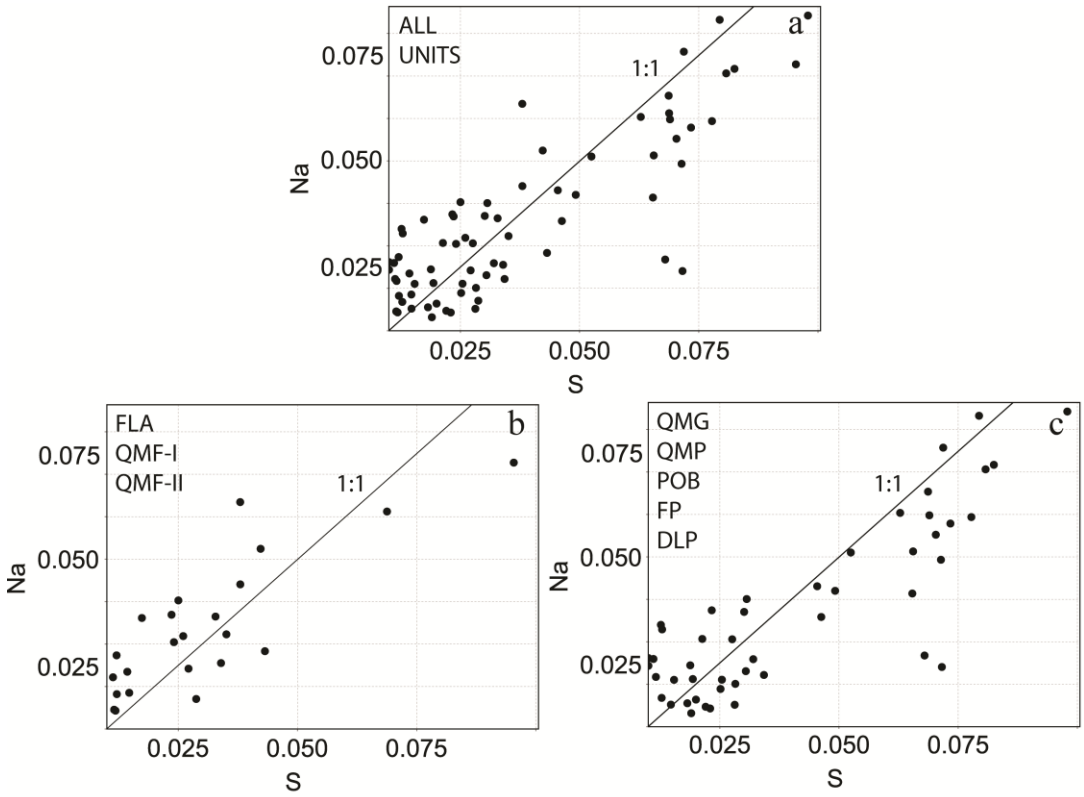

Figure 11. Plots of atoms of Na vs. S in analyzed apatite grains in rock unit samples. (a) Atoms of Na vs. S for all units. (b) Atoms Na vs. S for subalkaline lower intermediate units. (c) Atoms Na vs. S for upper intermediate units. Black circles in all figures represent individual analyses. Solid black line represents 1:1 slope.

evolved rock compositions. Ten out of thirteen analyses from four grains in sample QMF-I 26, and three analyses from one grain in sample FLA 21 have Cl concentrations that are 50% to 340% greater than analyses with the next highest Cl concentrations. Contrary to what was expected, increases in Cl have poor correlation to decreases in F. Instead, Cl peaks at 1.95 atoms (3.58 wt. %) F (Fig. 12a). The sums of F and Cl for these analyses exceed the expected X site maximum of 2.0 atoms by up to 25%.

An evaluation of the analytical methods indicates that this is not due to analytical error or migration of F and Cl. The following three points indicate that F and Cl results are both accurate and precise. First, average concentrations for the F and Cl standards, Fap and Tug, ran as unknowns were within 640 ppm ($1\sigma \pm 156$ ppm) and 400 ppm ($1\sigma \pm 372$ ppm), respectively, of published concentrations for these standards. Second, increases in Cl correlate with increases in LREEs (Fig. 13a and b). The correlating increase in LREEs analyzed using a different method indicates bulk crystal chemistry changes instead of microprobe induced data artifacts. Lastly, overages above stoichiometric X site occupancy for the highest F concentration analyses were 4 %. It is assumed that the anion channel is nearly filled with F at these concentrations, and that a completely filled channel would produce the greatest level of overage due to F migration. Stoichiometric overages for analyses with high Cl, however, are as much as 25%. This discrepancy indicates a mechanism other than F migration for nonstoichiometric behavior.

Crystal structure and crystal chemistry studies by Mackie and Young (1974), Hughes and Rakovan (2002), and Fleet et al. (2000), indicate that crystal chemistry and crystal structure may be the cause of nonstoichiometric behavior of halogens in apatite. In

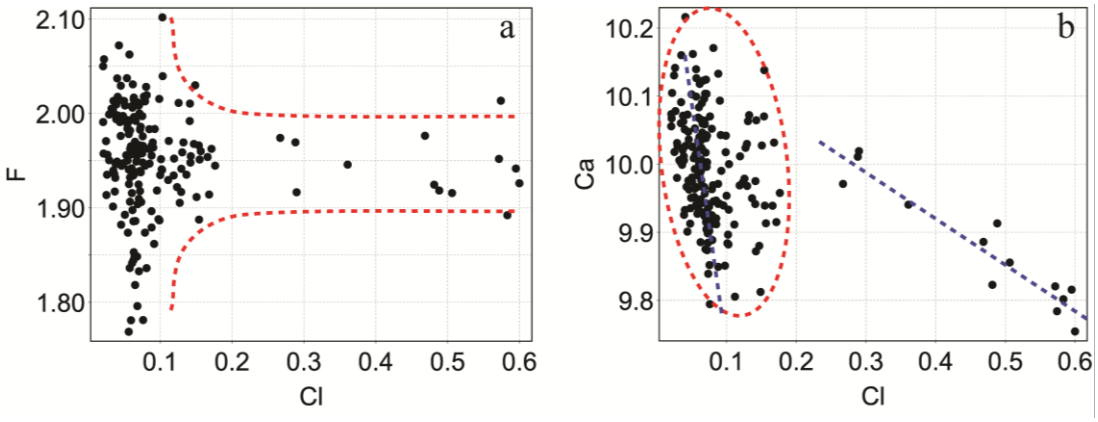

Figure 12. Plots showing correlation between atoms F and Ca vs. Cl. in analyzed apatite grains in rock unit samples. (a) Atoms F vs. Cl for all analyses. Red hashed lines delineate peak of Cl at ~1.95 atoms F. (b) Atoms Ca vs. Cl for all analyses. Red-hashed oval and blue line within indicates population and trend below 0.17 atoms Cl with weak correlation to decreases in Ca. Hashed blue line on right indicates strong correlation to decreasing Ca for population above 0.17 atoms Cl.

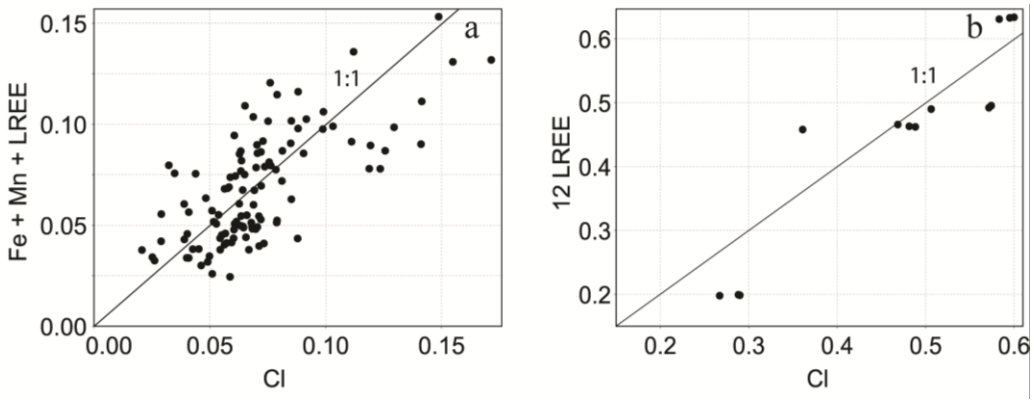

Figure 13. Plots showing correlations between atoms of Ca substitution elements and Cl in apatite. (a) Atoms Fe + Mn + LREE vs. Cl. (b) Atoms LREE X 12 vs. Cl. Solid black lines in both figures represent 1:1 slope.

a study by Mackie and Young (1974), both X-ray and chemical analysis showed excess of halogens in synthesized Cl-F apatite. X-ray results place the excess halogen in the anion column. Mackie and Young proposed that this scenario is possible given 1) a packing sequence that allows for an extra halogen (for their composition, this would require an extra halogen in every 5th unit cell), and 2) charge compensation. Furthermore, they proposed that these requirements could be met by substitution of Ca^{2+} by an ion of higher valence and/or replacement of PO^{3-}_4 by ions of low valence. Hughes and Rakovan (2002) found that these requirements are met for ternary (F, Cl, OH) apatite solid solution by a Markovian sequence of "$Cl_{A,below\ plane}$–(~2.95 Å)–$Cl_{B,below\ plane}$–(~2.95 Å)– $OH_{below\ plane}$–(~3.08 Å)– $F_{on\ plane}$–(~3.08 Å)– $OH_{\ above\ plane}$–(~2.95 Å)–$Cl_{B,above\ plane}$–(~2.95 Å)–$Cl_{A,above\ plane}$". In this instance, a 0.6 Å shift of the Cl anion toward the Ca2 plane allows for an extra Cl anion. In a study of REE substitutions in synthetic apatite Fleet et al. (2000), demonstrated that Na and REE substitution for Ca cause a shift of the Cl anion towards the Ca2 plane and in the process, reduce ordering of adjacent anion channels. The reduction of ordering results in a shift from a P63/m space group with hexagonal symmetry to a P21/b space group with monoclinic symmetry.

Out of the apatite base elements Ca, P and F, increases in apatite Cl herein correlate best with decreases in Ca. These increases correlate differently, however, for two populations of Cl concentrations. Those below ~0.17 atoms correlate weakly with a steep negative slope and those above ~0.17 atoms correlate strongly with a slope of -0.66 (Fig. 12b). Inversely, increases in Cl have a moderate positive correlation to Ca site substitution elements Fe + Mn + LREE for Cl below ~0.17 atoms and LREE for Cl above ~0.17 atoms. Increases in Fe + Mn + LREE atoms cluster along a 1:1 ratio with increases

in Cl for Cl less than ~0.17 and increases in LREE correlate to increases in Cl at a ratio of 12:1 for Cl greater than ~0.17 (Fig.13a and b, respectively).

The negative correlation of Ca to Cl and positive correlation of LREE at high Cl are consistant with the hypothesis of Mackie and Young (1974) and results of Fleet et al. (2000) and implicate substitution as a reason for nonstoichiometric behavior of halogens in apatite. Buildup of substituting element concentrations with concomitant increase in Cl up to ~0.17 atoms, with a subsequent sharp drop and progressive build up again from ~0.17 to the Cl high of 0.60 atoms is interpreted to be a result of differences between hexagonal and monoclinic structures (Fig. 14a, b and c).

No evidence for influence on sulfur substitution by crystal system changes could be determined. Sulfur highs are noted to peak in each population of Cl highs (Fig 15a). However, S does not have a linear relationship to increase in Cl as does Fe, Mn or LREEs (Fig 14a, 14b and 15a). Instead, S has symmetric increase about ~0.08 atoms Cl and 0.47 atoms Cl (Fig. 15). This lack of correlation indicates that S concentrations are not constrained by Cl substitution. The fact that S spans the same range of concentrations in each indicated crystal system population also suggests that crystal system changes do not disproportionately affect S uptake into apatite.

Melt S Calculations

Calculation of the ASTs is based on the following assumptions: First, melt H_2O was estimated based on relative hydrous mineral content. It is assumed that these estimates are representative and in relative proportion. Second, the crystallization model R-4 of Whitney (1988) is for water undersaturated granitic compositions. However, in

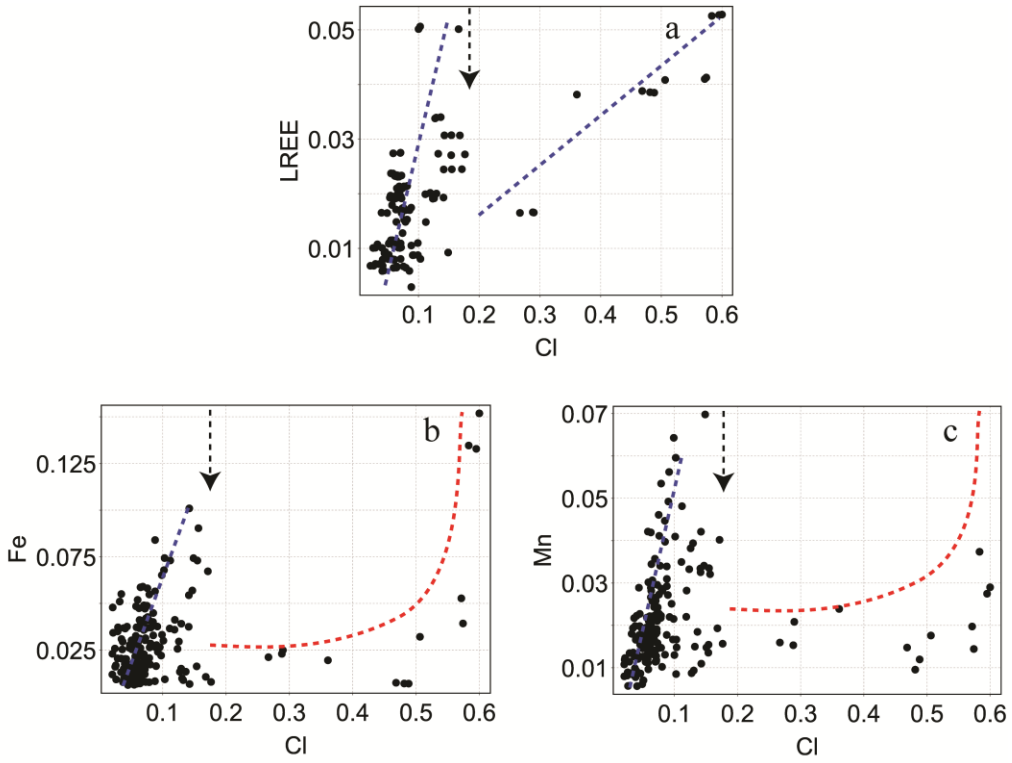

Figure 14. Plots showing bimodal correlations between atoms of LREE, Fe and Mn vs. Cl in apatite. (a) Atoms LREE vs. Cl for all analyses. Blue hashed lines indicate trends for each population (one below ~0.17 atoms Cl and one above). (b) Atoms Fe vs. Cl. (c) Atoms Mn vs. Cl. Blue lines in b and c indicate trends for Cl below ~0.17 atoms. Red lines in b and c indicate lack of linear correlation, but overall increase with increase Cl. Arrows in a-c point out change in trends indicating possible crystal system change.

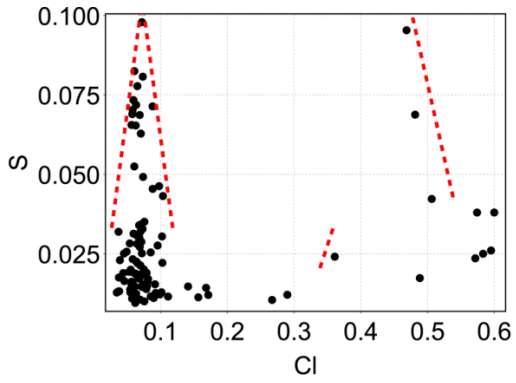

Figure 15. Plot showing symmetric (noncorrelative) nature of atoms S vs. Cl in apatite. Red hashed lines indicate a symmetrical peak of S about ~0.08 atoms Cl and a potential symmetrical peak about 0.47 atoms Cl.

the absence of crystallization models for intermediate compositions, the use of Whitney's model herein assumes that early crystallization of intermediate melts can be represented using the same model. Third, in the AST equations herein, instantaneous P_2O_5 is expressed as a function of the percent crystallization of the melt. This calculation is based on the assumption that apatite is the only P-bearing phase.

Calculation of melt S is based on the assumption that S partitioning is not affected by melt composition, and S partitioning is not affected by crystal structure.

Each assumption imparts cumulative uncertainty. However, some of these uncertainties are constrained. Parat and Holtz (2004) noted possible effects on S partitioning by melt Ca, though, their S partitioning equation was found valid for melt Ca concentrations between 0.1 and 0.36 wt %. Equivalently high apatite S concentrations in units with different bulk compositions herein indicate that bulk melt composition did not preferentially affect S concentration, supporting Parat and Holtz (2004) findings. Apatite grains with proposed crystal structure differences also have equivalently high apatite S concentrations. This lack of difference limits the possibility of a relationship between S increase and crystal structure.

The assumptions subject to the largest likely degree of uncertainty are assumed H_2O content and assumed crystallization model. Decrease in H_2O imparts an increase in crystallinity that culminates in an increase in AST and melt S that can be as high as 500 ppm per 10 degrees. A model with reduced or enhanced crystallization could bias melt S results by several hundred ppm.

In spite of the inherent uncertainties, resulting melt S concentrations produced using the ASC data of Streck and Dilles (1998) are in good agreement with melt S

determined by melt inclusion analysis from rocks of similar composition (Carroll and Rutherford, 1987). Resulting average melt S concentration herein range between 100 and 420 ppm, and melt S concentrations estimated from melt inclusions in the El Chichon trachyandesite from Mount St. Helens by Carroll and Rutherford are between 200 and 300 ppm. Melt S values calculated using the AUC data of Parat and Holtz (2004), conversely, range between 30 and 110 ppm; values that are unrealistically low. Given the more realistic melt S range calculated using the data of Streck and Dilles, these values are taken to be most representative and are used hereafter.

Melt S and Apatite S Correlation to Mineralization

Calculated melt and apatite S lows are associated with premineralization emplaced units and increases in melt and apatite S are associated with synmineralization emplaced units (Fig. 16a and b, respectively). The FLA and QMG units, units known to have intruded before the earliest dated mineralization, have the lowest mean melt and apatite S. The oldest unit with elevated melt and apatite S is the QMF-I, intruded at ~11.96 Ma. Considering that mineralization youngs eastward, this timing correlates with the earliest known mineralization in the district occuring in Los Piches-Ortiga block at ~14 Ma. While melt and apatite S for the QMF-I and QMP units are low, elevated mean melt and apatite S are elevated for every other unit that intruded during the height of mineralization, ~8.2 to ~4.3 Ma. The highest mean melt and apatite S for all units occurs in the FP, which was intruded at ~5.5 Ma.

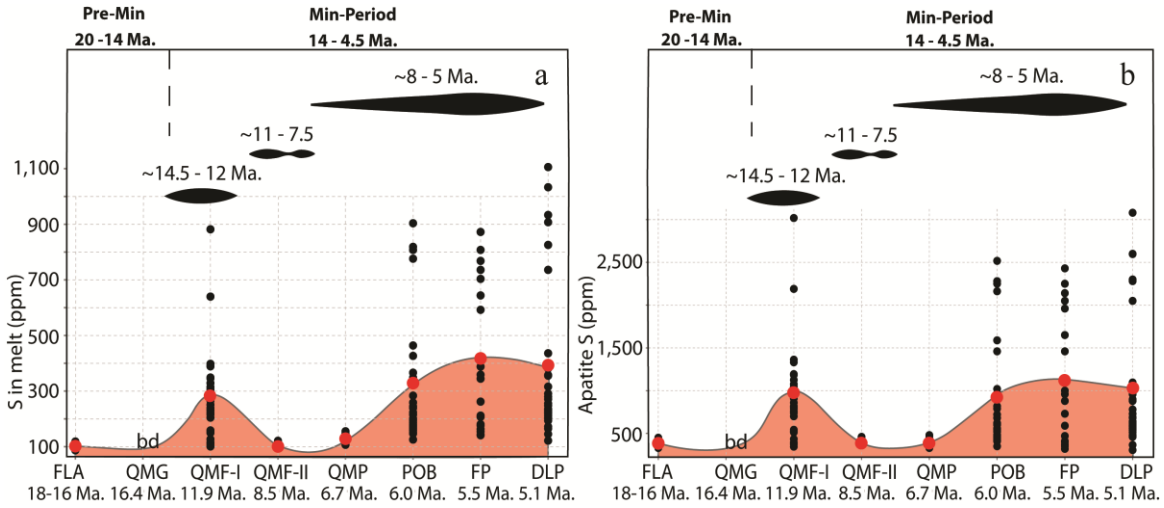

Figure 16. Diagrams showing the association between melt and apatite S, unit emplacement and mineralization timespans. (a) Melt S vs. rock unit emplacement and mineralization timespans. (b) Apatite S vs. rock unit emplacement and mineralization timespans. Black circles are individual analyses. Red circles are mean S concentrations for each rock unit. The pink field indicates change in S concentrations through time interpolated from mean S concentrations. Pre-Min is premineralization timespan and Min-Period is mineralization timespan. Dashed line separates these time periods. Thickening of the horizontal black lines indicate periods of mineralization. bd = below detection.

Other Elemental Substitution Correlation to Mineralization

Correlations between apatite REEs and mineralization were not definitive. However, of the trace elements, increases in Mg and Cu substitutions correlate well; with increases in both Mg and Cu displaying an association with synmineralization emplaced units (Fig. 17a and b). Copper was detected in apatite grains from all units and highest in apatite from the QMF-I, POB and DLP units.

Mg was detected only in apatite grains from mineralization related units, QMF-I, POB and FP. This substitution is possible evidence for recharge of the source magma chamber by mafic magma, which is in turn supportive evidence for mafic magma input Cu source models (Core, 2004; Keith et al., 1997; Hattori and Keith, 2001).

Melt S and Apatite S as Fertility Indicators

Based on the associations between melt and apatite S lows and premineralization emplaced units, baselines calculated as 3σ above the highest mean melt S and apatite S from the premineralization units can be used for mineralization potential discrimination. Using a value of half the detection limit for nondetection results in the QMG, these baselines (rounded to the nearest 50) are 200 ppm for melt S and 750 ppm for apatite S (Fig. 18). Based on the associations between melt and apatite S highs and synmineralization emplaced units, highest melt and apatite S concentrations above the baselines can be used to vector to units with the greatest mineralization association potential.

Both melt and apatite S herein prove to be reasonable mineralization potential indicators. However, due to the higher degree of cumulative uncertainty associated with

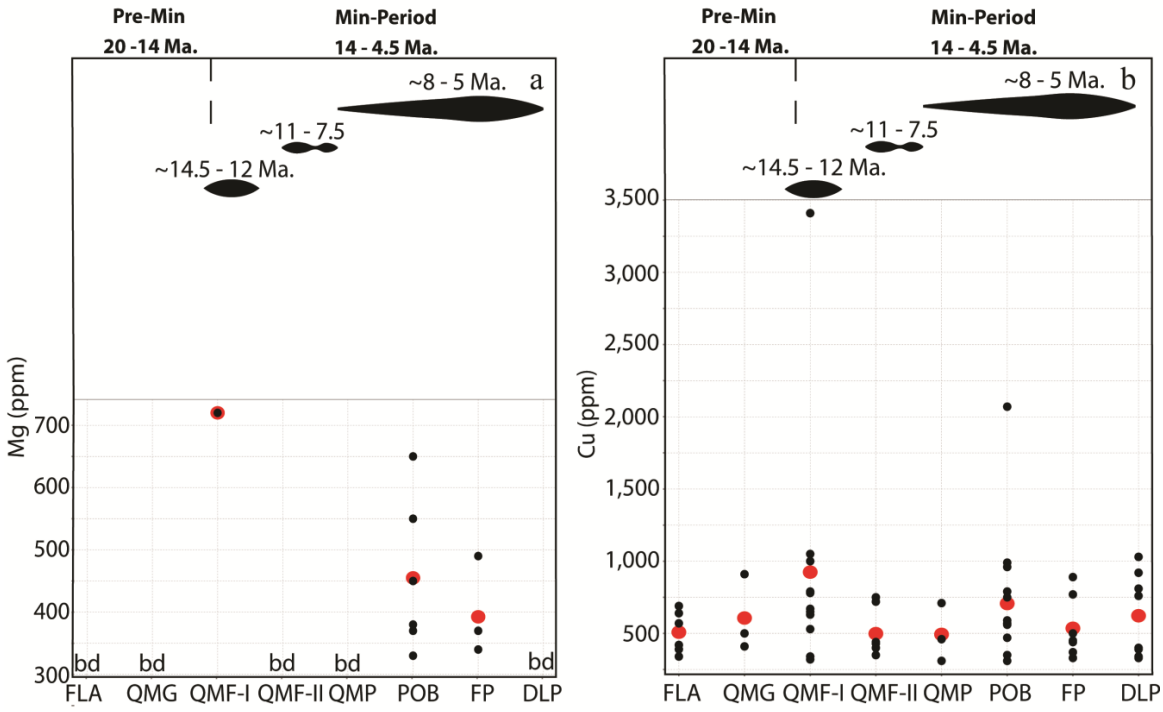

Figure 17. Diagrams showing the association between apatite Mg and Cu, unit emplacement and mineralization timespans. (a) Apatite Mg vs. rock unit emplacement and mineralization timespans. (b) Apatite Cu vs. rock unit emplacement and mineralization timespans. Black circles are concentrations for individual analyses. Red circles are mean concentrations for each rock unit. Pre-Min is premineralization timespan and Min-Period is mineralization timespan. Dashed line separates these time periods. Thickening of the horizontal black lines indicate periods of mineralization. bd= below detection.

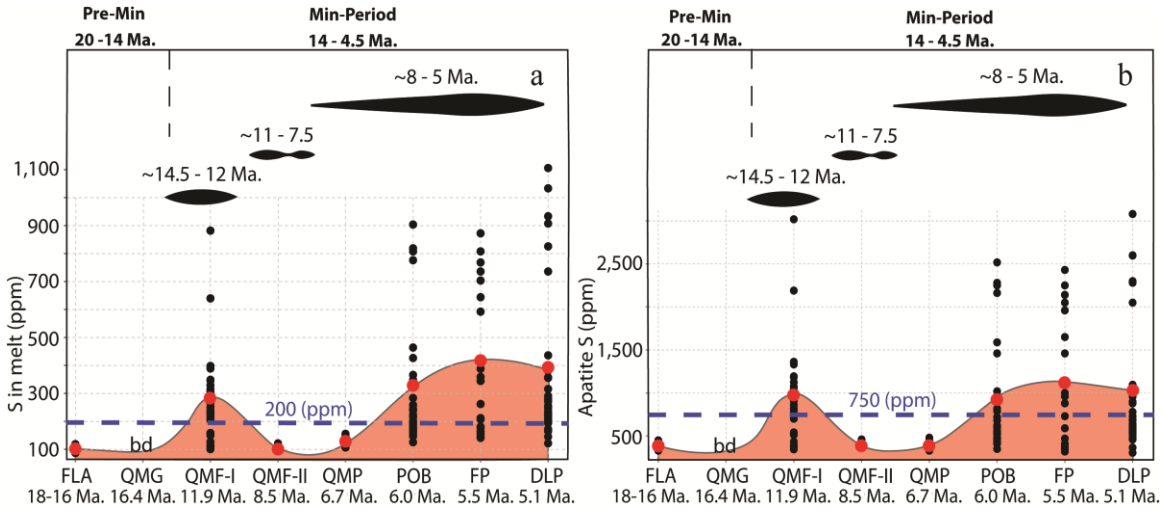

Figure 18. Diagrams showing mineralization indicator discrimination baselines and the association between melt and apatite S, unit emplacement and mineralization timespans. (a) Melt S vs. rock unit emplacement and mineralization timespans. (b) Apatite S vs. rock unit emplacement and mineralization timespans. Black circles are individual analyses. Red circles are mean S concentrations for each rock unit. The pink field indicates change in S concentrations through time interpolated from mean S concentrations. Pre-Min is premineralization timespan and Min-Period is mineralization timespan. Dashed line separates these time periods. Thickening of the horizontal black lines indicate periods of mineralization. Horizontal blue lines indicate 3σ baselines for melt S and apatite S. bd= below detection.

melt S calculations, and the good correlation between apatite S and mineralization, apatite S is proposed as a more robust measure of mineralization potential.

Apatite Mg and Cu as Fertility Indicators

The associations between detectable apatite Mg and synmineralization emplaced units suggest that apatite Mg above 300 ppm can be used as a minealization potential indicator. Considering the noted mafic magma input Cu source models (Core, 2004; Keith et al., 1997; Hattori and Keith, 2001), detectable apatite Mg may also be a significant indicator of a systems potential to produced Cu porphyry systems with similar genetic characteristics to the Los Bronces District.

Apatite Cu ranges from several hundred to several thousand ppm and associations between increases in apatite Cu and synmineralization emplaced units indicate that an apatite Cu baseline of 700 ppm could be used as a mineralization potential discriminant. The concentrations determined herein, however, are pointedly higher than apatite Cu results (tens to hundred ppm range) of other studies reviewed in the literature (Piccoli and Candela, 2002; Belousava et al., 2002; Banks, 1982). This disparity could indicate these concentrations are unique and have significant implications for fertility discrimination of other large tonnage/high grade systems. It is noted, however, that only a small number of studies analyze for, or at least publish Cu findings, giving need for additional data from other deposits to test this hypothesis.

Apatite Substitutions as Fertility Indicators in Other Systems

Frei (1996) proposed S in apatite above ~1000 ppm as an exploration tool for porphyry Cu systems based on his study of a porphyry Cu system of the Serbomacedonian Massif, Northern Greece. However, calculating a baseline using the methods herein for the data of Frei (1996) (Table 12) produces a baseline of 700 ppm for premineralization units. Average apatite S for units concurrently emplaced during mineralization is well above this baseline at 1646 ppm.

Mineralization and unit emplacement relationships for the data of Imai (2004) (Table 13) from porphyry Cu systems of the Western Luzon arc, Philippines are less well constrained. However, Miocene intrusive units that are noted as not associated to mineralization, excluding the mean apatite S value for sample 11111, which is an outlier from normal distribution of other Miocene intrusive unit mean apatite values indicating it does not belong in this population (Fig. 19), produce a baseline of 750 ppm. Apatite S for mineralization related shallow intrusions and units associated with porphyry Cu deposits also lie well above this baseline at 1330 ppm and 883 ppm, respectively. Given the agreement between the baseline and mean apatite S established herein and baselines and mean apatite S calculated in the same manner for the data of Frei (1996) and Imai (2004), apatite S above 750 ppm is proposed as a fertility indicator that can be used to evaluate other porphyry Cu-Mo systems.

Table 12. Mean Apatite S for Intrusive Units of the Serbomacedonian Massif, Northern Greece. Adapted from Frei (1996).

Sample ID	Rock Unit	Age (Ma)	Rock Unit Mean apatite S (ppm)
Units emplaced during premineralization timespan			
JE-15	granite	53.3 ± 0.3	580
ASPCHO-I	granodiorite	27.9 ± 1.2	429
ST-1A	(monzo)diorite	26.9 ± 2	575
Units emplaced during mineralization timespan			
JER-3	porphyritic syenite	22 ± 6	2233
SK-G1	porphyritic syenite	19 ± 2	1375
VA-6	monzonite	18 ± 2	1224
VATHI	monzonite	17 ± 2	1533
TS-12	porphyritic trachite	N/A (Part of Tertiary intrusive suite)	1866
	Mean for all units emplaced during mineralization timespan:		**1646**

N/A = age not available.

Table 13. Mean Apatite S for Intrusive Units from the Porphyry Cu Systems of the Western Luzon Arc, Philippines. Adapted from Imai (2004).

Sample ID	Rock Unit	Number of analyses	Rock Unit Mean apatite S (ppm)
Miocene intrusive rocks			
11111	porphyritic quartz diorite	22	*801
21111	porphyritic quartz diorite	37	280
20412	quartz diorite	83	120
741-27	quartz diorite	85	200
7404	quartz diorite	98	521
9404	quartz diorite	58	601
13407	quartz diorite	71	401
Late Miocene-Pliocene-Pleistocene shallow intrusions related to mineralization			
03328B	dacite porphyry	27	2083
6410	andesite porphyry	13	2003
10407B	dacite porphyry	71	801
3416	andesite porphyry	52	1642
01416B	porphyritic quartz diorite	9	120
	Mean for all shallow intrusion units related to mineralization:		**1330**

* Not included in mean for all Miocene intrusive apatite S or S + 3σ calculation.

Table 13 Continued.

Sample ID	Rock Unit	Number of analyses	Rock Unit Mean apatite S (ppm)
Intrusive rocks associated with porphyry Cu deposits			
81-26 2015-2152	quartz diorite porphyry (alt)	44	641
041114/4	dacite porphyry	81	801
051115/5	dacite porphyry	129	721
11209	dacite porphyry	100	761
01413A	porphyritic quartz diorite	57	801
2414	quartz diorite porphyry	29	841
11412	quartz diorite porphyry (alt)	46	280
5401	andesite porphyry	73	961
11405	andesite porphyry	68	1202
4401	andesite porphyry	75	1001
06405A	andesite porphyry (alt)	61	1001
15331	andesite porphyry (alt)	46	1162
8401	quartz diorite porphyry	59	1041
8331	quartz diorite porphyry (alt)	84	1041
11331	quartz diorite porphyry (alt)	86	1122
4410	porphyritic quartz diorite	32	801
34Q-1	porphyritic quartz diorite (alt)	38	881
CLF1-4	andesite porphyry	41	1162

Table 13 Continued.

Sample ID	Rock Unit	Number of analyses	Rock Unit Mean apatite S (ppm)
Intrusive rocks associated with porphyry Cu deposits			
2402	andesite porphyry	51	1081
X6403	andesite porphyry (alt)	96	1202
8402	quartz diorite porphyry	51	921
CLF1-10	porphyritic quartz diorite	44	881
CLF1-12	porphyritic quartz diorite	49	601
BIN-3	andesite porphyry	24	1362
WH9	quartz diorite porphyry	31	841
WH8	porphyritic quartz diorite	29	401
WH6	porphyritic quartz diorite	33	601
X3415	andesite poprhyry	50	481
1417	andesite porphyry (alt)	51	721
1415	porphyritic quartz diorite	51	761
11220	quartz diorite porphyry	45	360
031103A	quartz diorite	40	200
11107	dacite porphyry	106	681
CT2-13	quartz diorite porphyry	40	801
BT58-1	quartz diorite	77	561
	Mean for all intrusive units associated with porphyry Cu deposits:		**883**

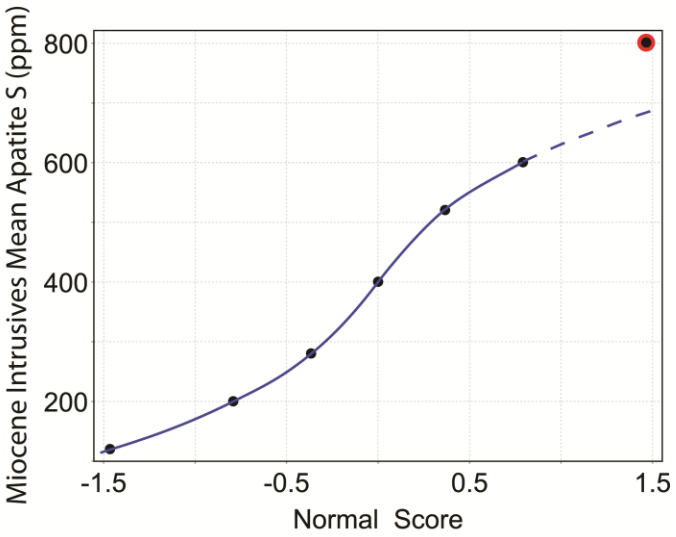

Figure 19. Normal distribution of mean apatite S for Miocene intrusive units. Black circles are mean apatite S for each unit. Blue line delineates normal behavior (dashed line is projected normal behavior). Red halo around black circle in upper right hand corner denotes outlier, sample 11111.

CONCLUSIONS

- No associations between S concentrations and apatite grain morphology, grain zonation, S substitution mechanism or crystal structure is evident, indicating that S concentrations are more wholly a function of S availability in melt.
- Equivalent ranges of S in both lower intermediate subalkaline and upper intermediate rocks indicate bulk melt composition does not disproportionately affect S uptake into apatite.
- Apatite S and melt S are low for premineralization units, elevated for syn- and late-mineralization units and highest for units emplaced at the height of mineralization. Apatite Cu has a similar distribution and apatite Mg was detected only in grains from mineralization related units.
- The agreement between the apatite S baseline (750 ppm) established herein and the aptitite S baselines calculated in the same manner for the data of Frei (1996) (700 ppm) and Imai (2004) (750 ppm) indicate the baseline herein can be applied to other porphyry systems.

The following are proposed for using apatite substitutions as porphyry system/intrusive unit fertility indicators: First, mean concentrations of melt and apatite S S above 3σ of premineralization unit concentrations (200 ppm and 750 ppm, respectively) can be used as fertility indicators in porphyry Cu-Mo systems. Second, highest melt and apatite S concentrations above 200 ppm and 750 ppm, respectively, can

be used to vector to units that had the greatest potential to produce mineralizing fluids. Third, apatite S is a more robust discriminant than melt S. Fourth, Mg above 300 ppm can be used as a mineralization potential discriminant and potentially used to discriminate systems with similar genetics to the Los Bronces District. Lastly, apatite Cu above 700 ppm may be useful in exploration for porphyry Cu deposits with similar mineralization endowement potential as San Enrique Monolito.

APPENDIX A

MICROPROBE ANALYTICAL ROUTINE

This appendix contains input variables used for setup of microprobe analyses (Table 14). Electron microprobe analyses were performed on a Cameca model SX-50 electron microprobe equipped with four wavelength-dispersive X-ray spectrometers at the University of Utah electron microprobe facilities.

Table 14. Microprobe Analysis Declare.

Spectrometer	Crystal	Element	Line	BG Offset	Slope	Peak	BG (+)	BG (–)	Std
1	TAP	F	Ka	0, -1700	1	20	0	20	Fap
1	TAP	Na	Ka	± 1000		20	10	10	Albi
1	TAP	Mg	Ka	+1100, 0	1.29	20	20	0	Crdi
1	TAP	As	La	+2000, 0	1.2	20	20	0	Gaar
1	TAP	Al	Ka	+1000, 0	1.25	20	20	0	San
1	TAP	Si	Ka	± 600		20	20	20	Albi
2	LIF	Ce	La	± 600		25	20	20	Mona
2	LIF	V	Ka	± 500		25	20	20	Yvo4
2	LIF	Mn	Ka	0, -500	0.98	25	0	15	Rhod
2	LIF	Fe	Ka	0, +500*	1.03	25	0	20	Hema
2	LIF	Cu	Ka	± 500		25	20	20	Cu2o
3	PET	S	Ka	± 700		20	20	20	Cele
3	PET	P	Ka	+400, -300		10	5	5	Fap
3	PET	Cl	Ka	± 300		30	15	15	Tug
3	PET	Sr	La	+400, -600		20	20	20	Cele
3	PET	K	Ka	0, -600	0.92	20	0	20	San
4	PET	Ti	Ka	+800, 0	0.97	25	20	0	Tio2
4	PET	Ca	Ka	± 500		15	10	10	Fap
4	PET	Ba	La	± 400		30	15	15	Bari

BG – background, Std – Standard, BG (+) BG (-) and peak are count times in seconds.

APPENDIX B

APATITE GRAIN MICROPROBE ANALYSIS MAPS

This appendix contains maps of each apatite grain with locations of microprobe spot analyses (circle and crosshairs) within each grain (Figure 20). Each spot analysis was performed using 5 μm diameter beam. Analyses and grain IDs are annotated for each spot. Analysis identification is annotated as a letter at the end of the label and the Grain ID comprises the remainder of each annotation.

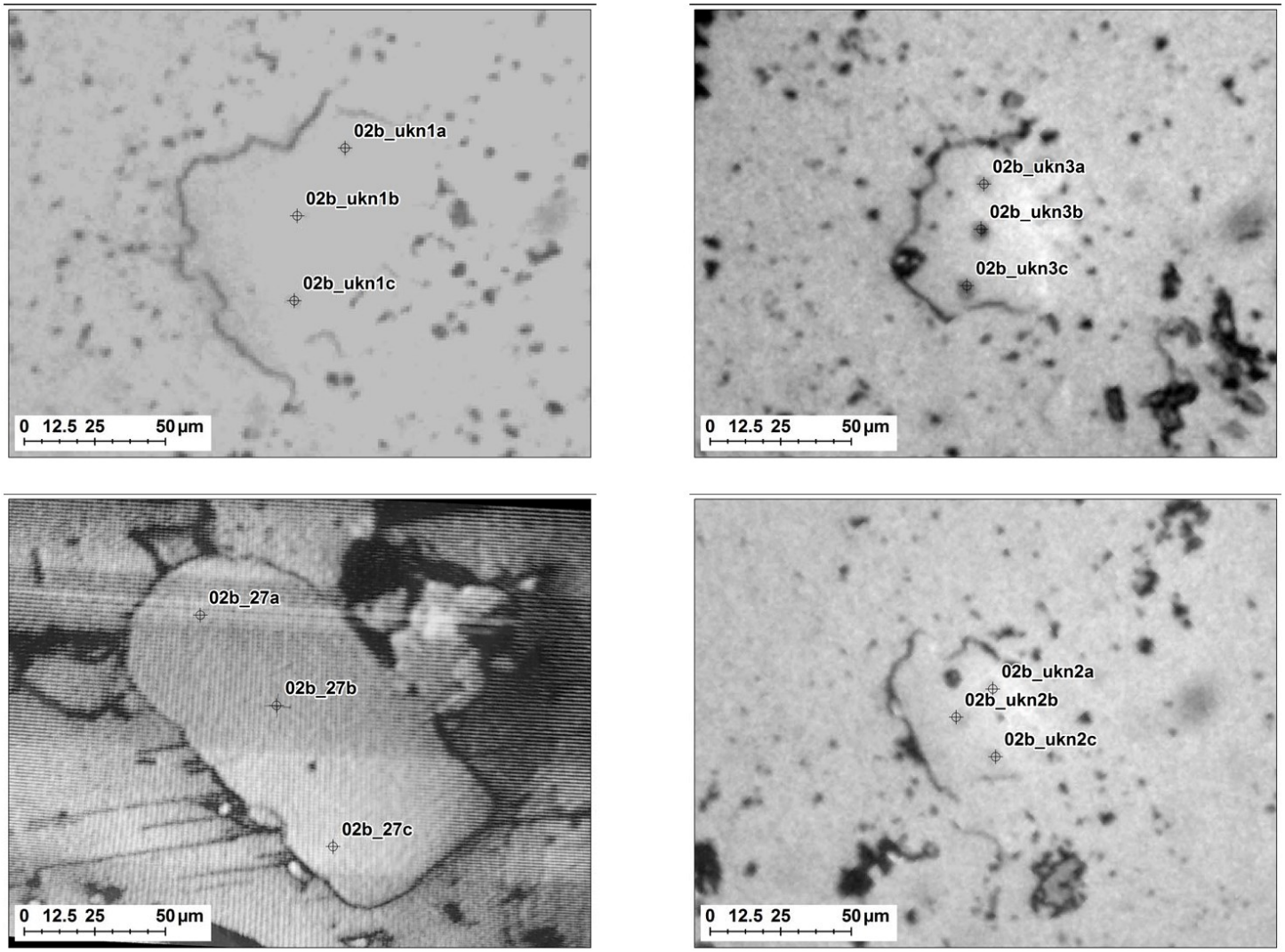

Figure 20. Maps of microprobe analysis locations in individual apatite grains. Locations are depicted by circle and crosshair and labeled with analysis ID.

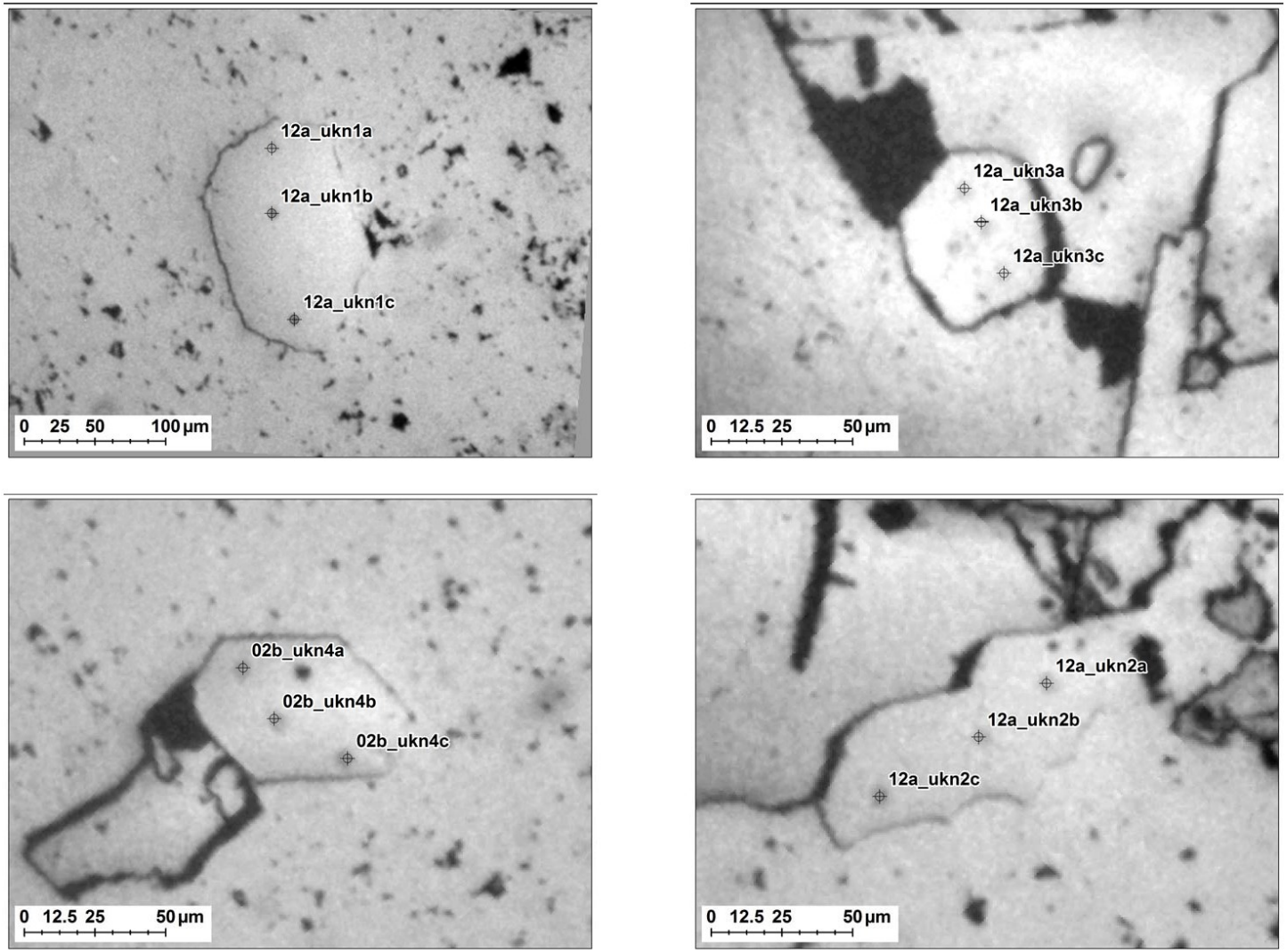

Figure 20 Continued.

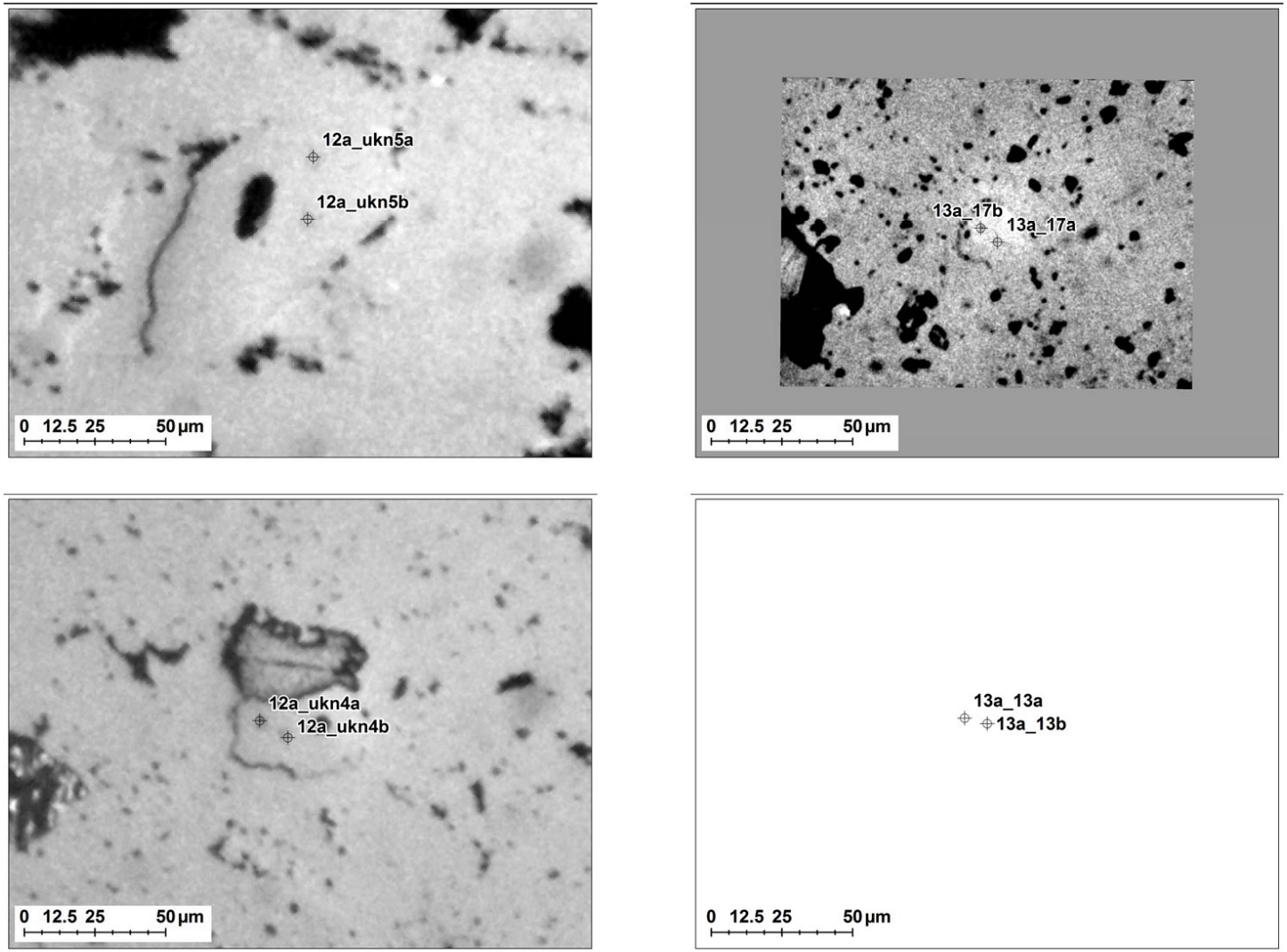

Figure 20 Continued.

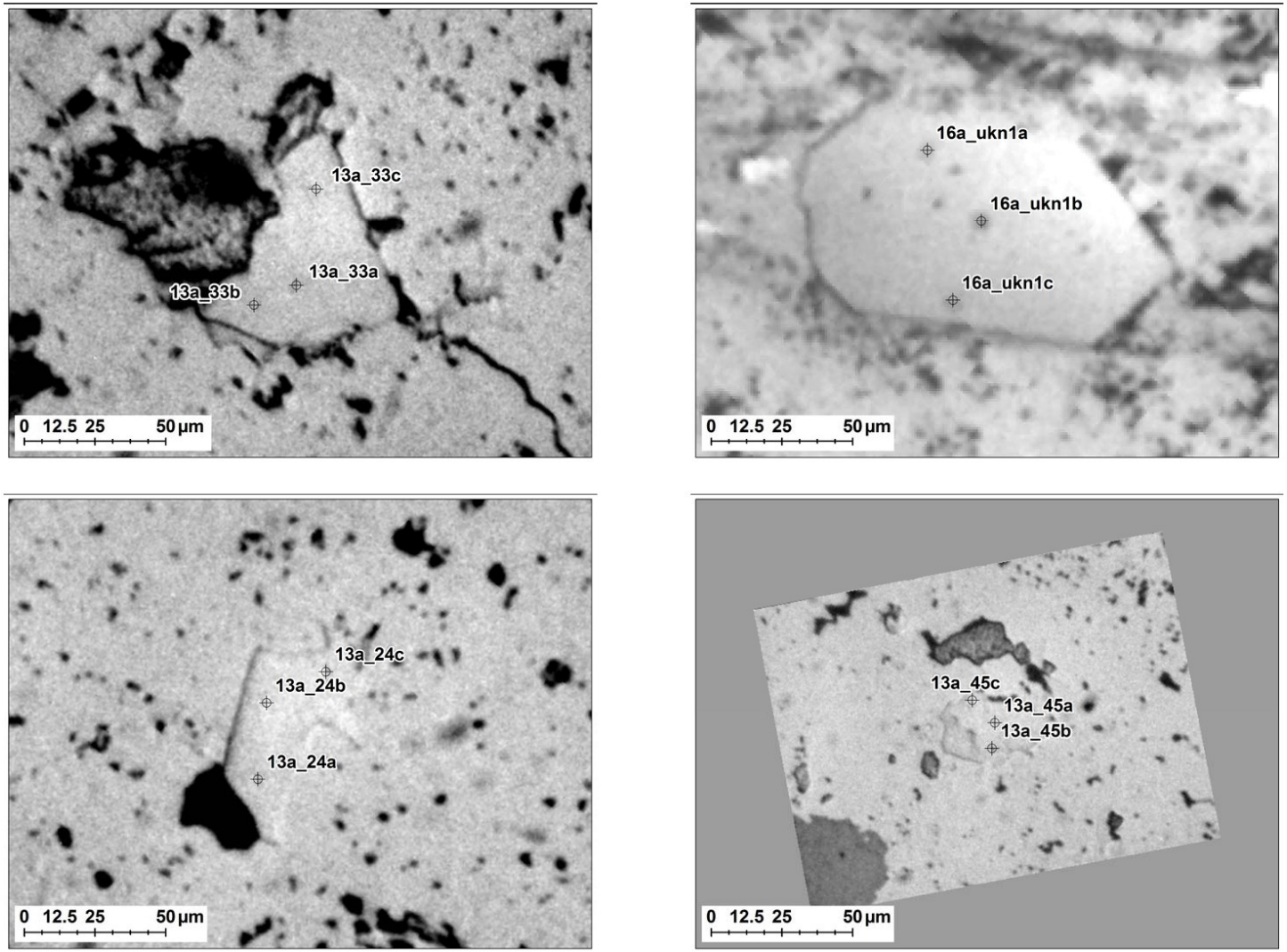

Figure 20 Continued.

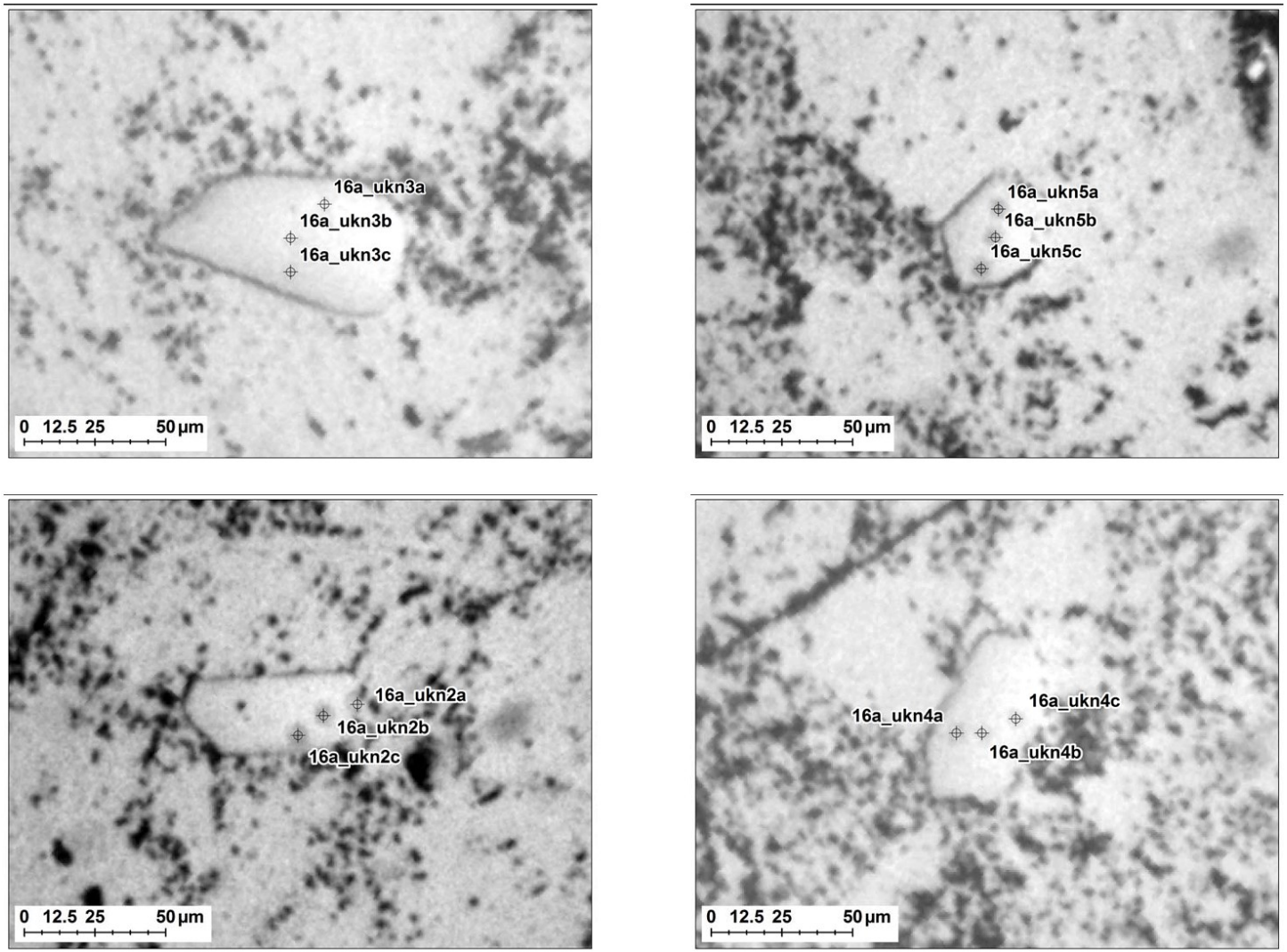

Figure 20 Continued.

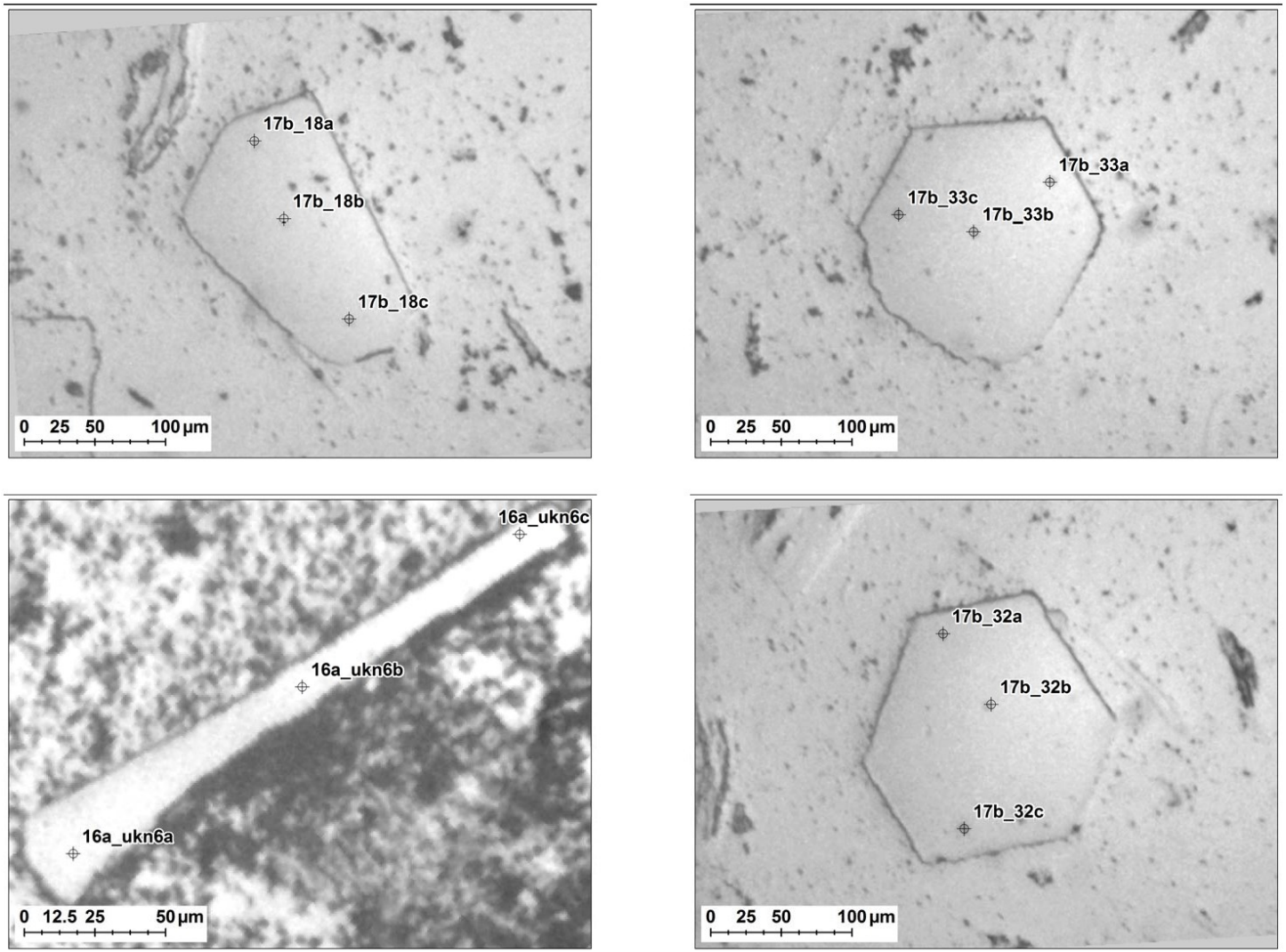

Figure 20 Continued.

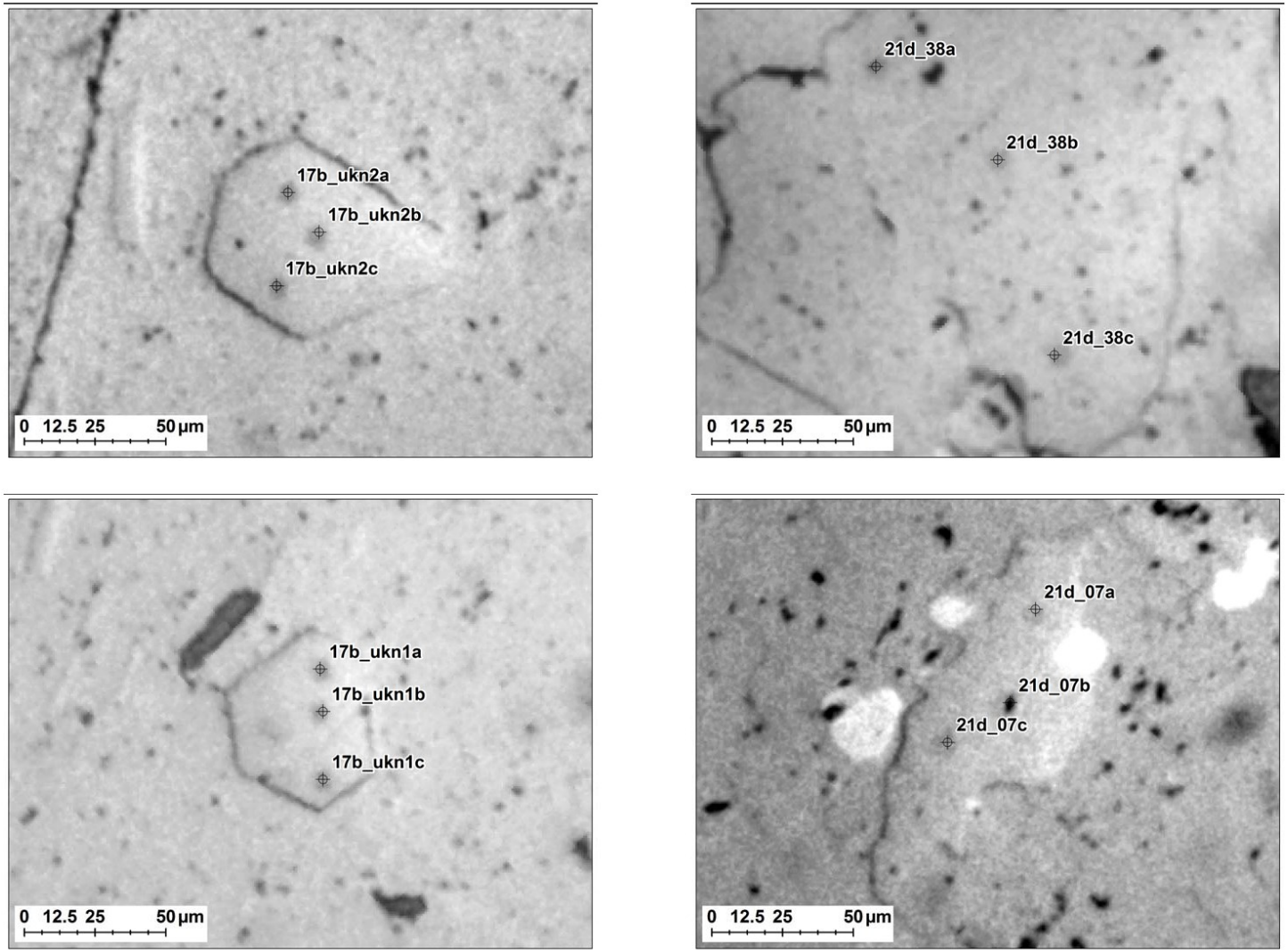

Figure 20 Continued.

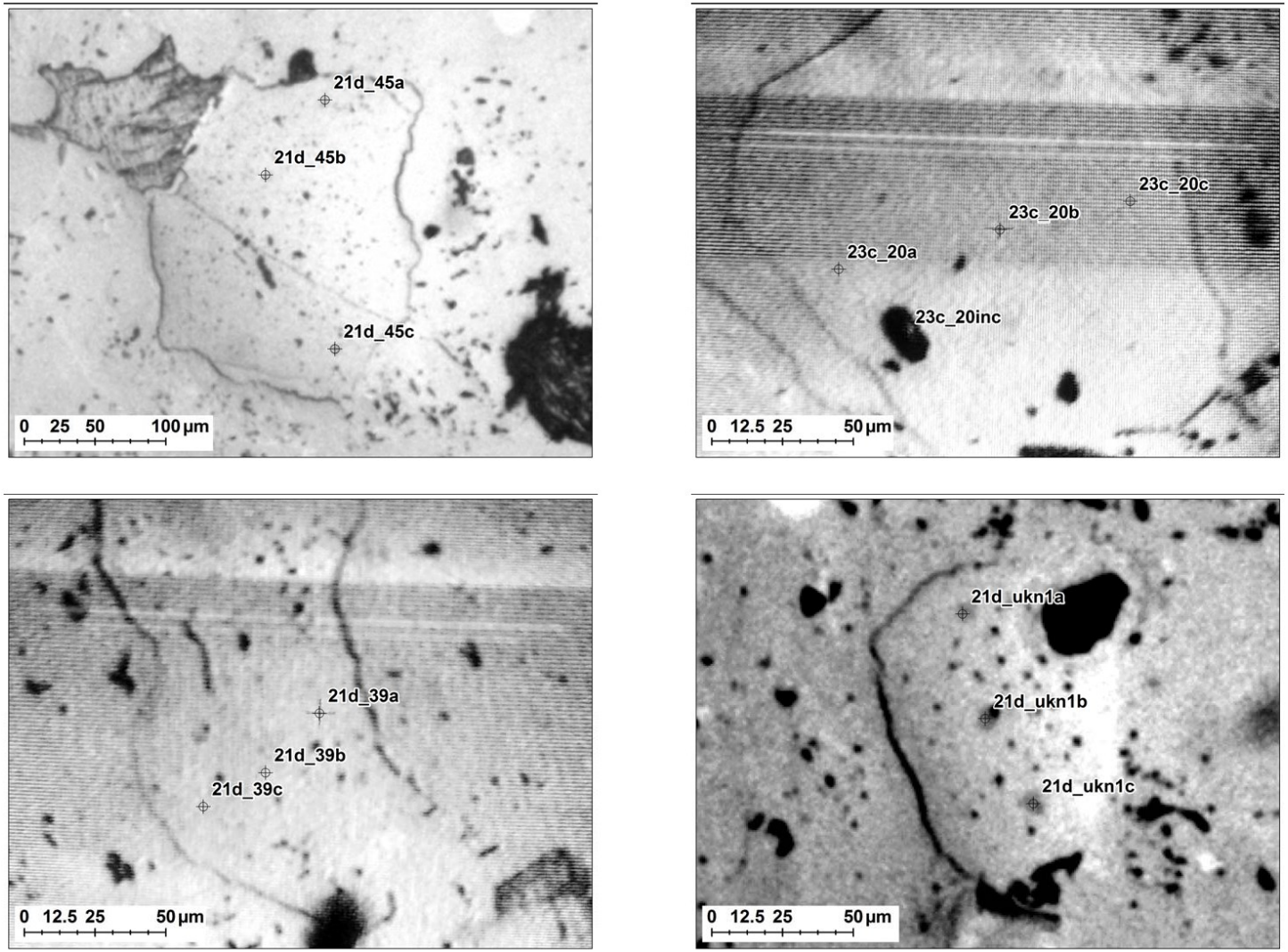

Figure 20 Continued.

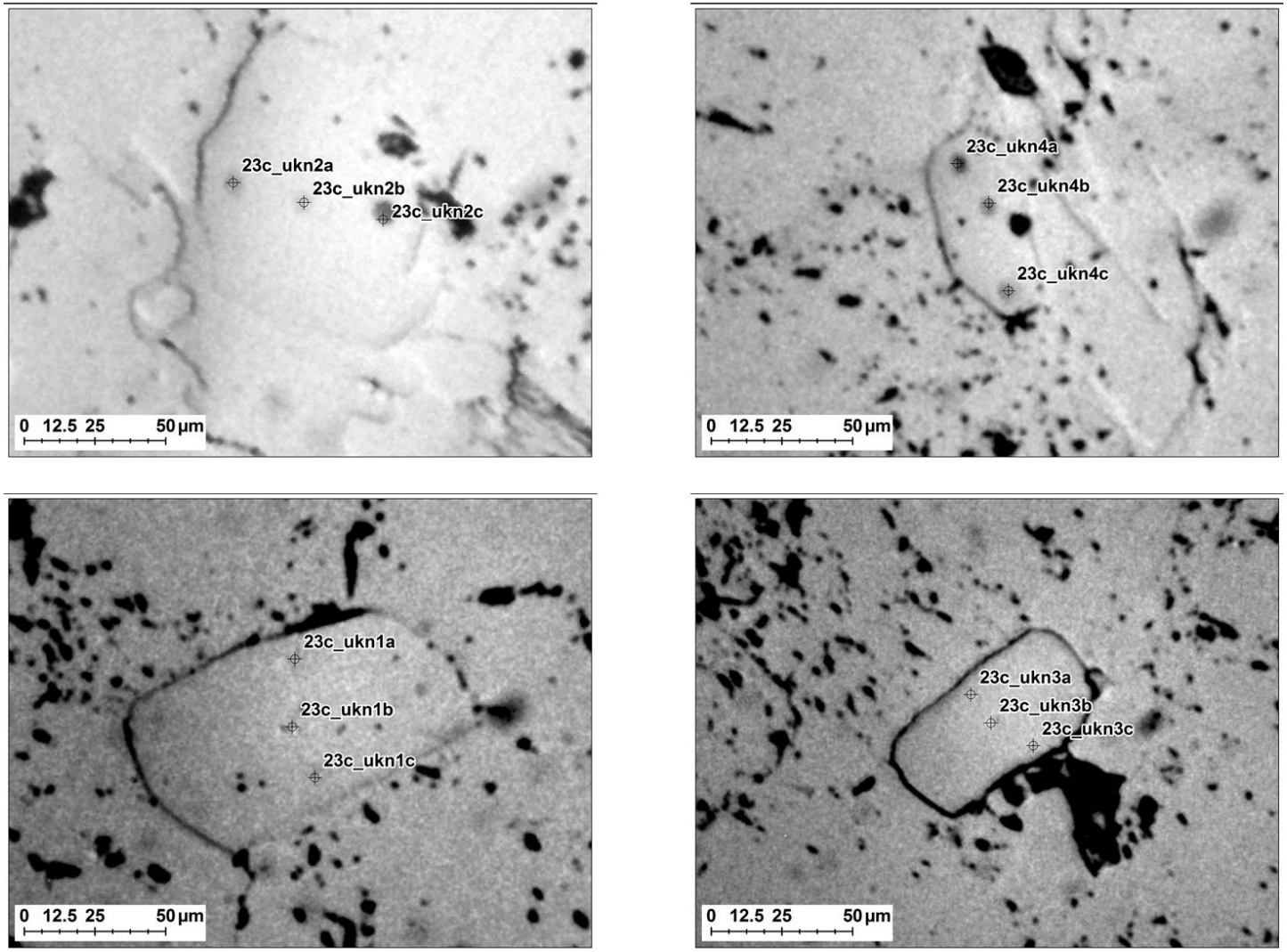

Figure 20 Continued.

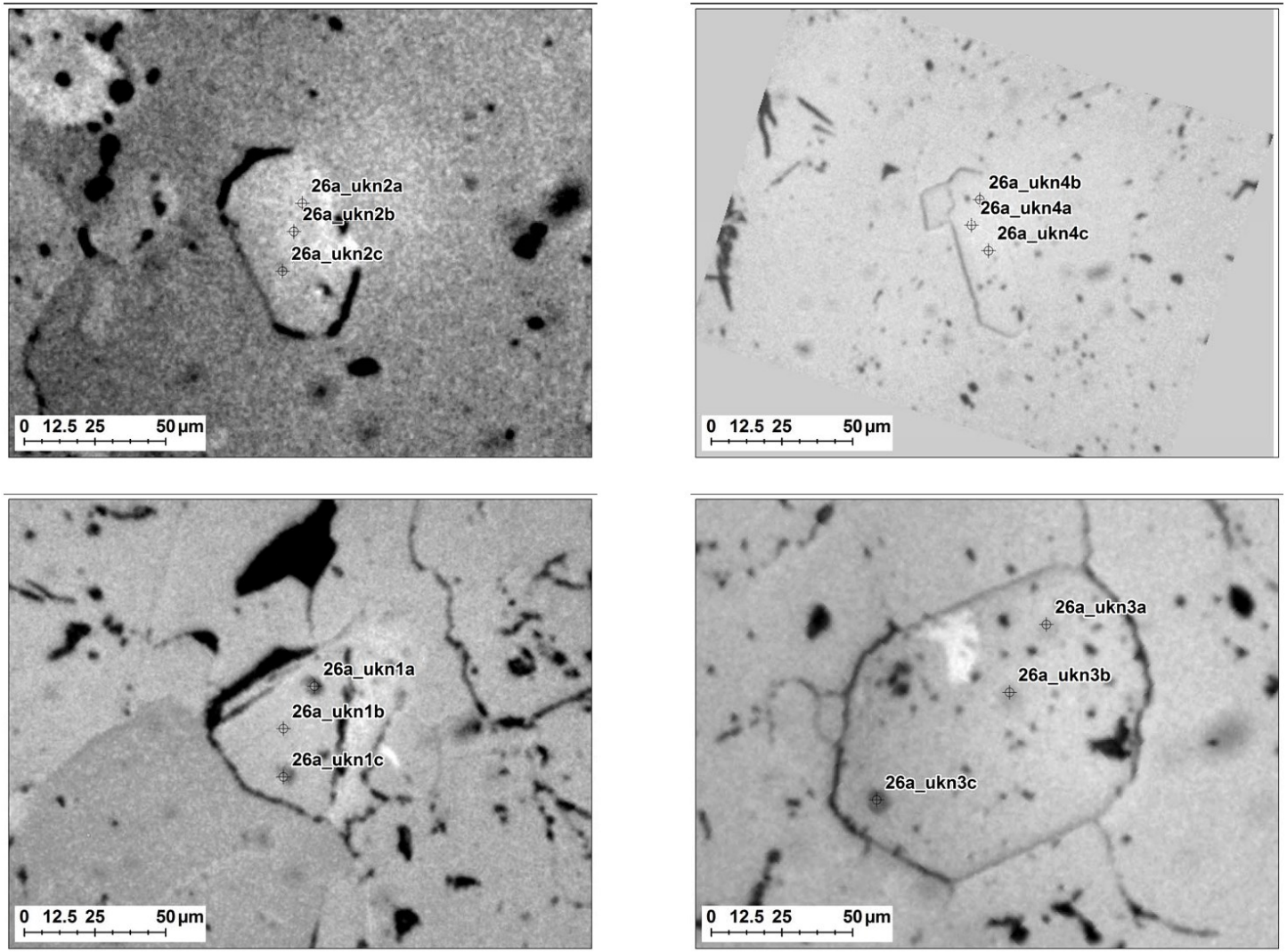

Figure 20 Continued.

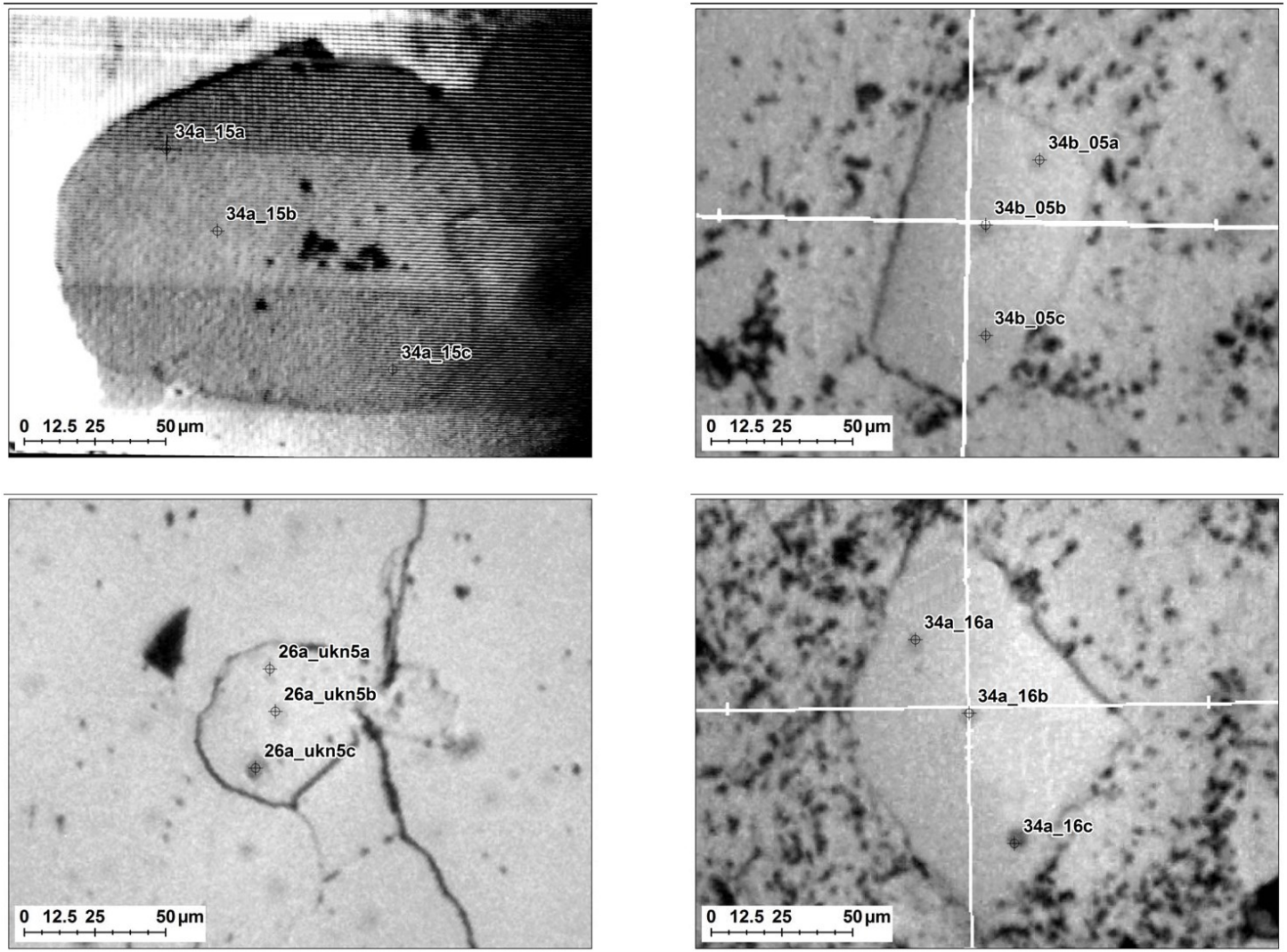

Figure 20 Continued.

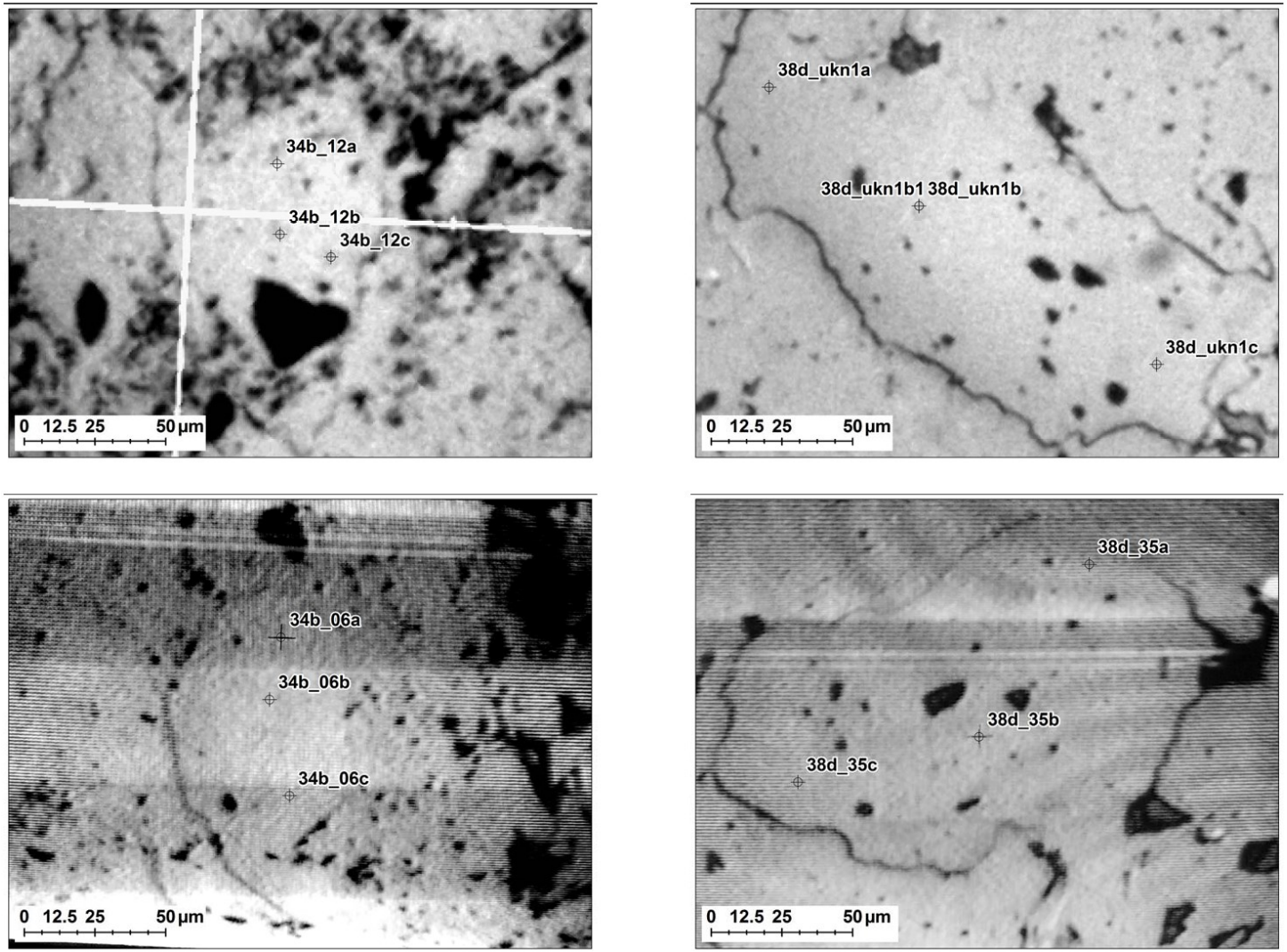

Figure 20 Continued.

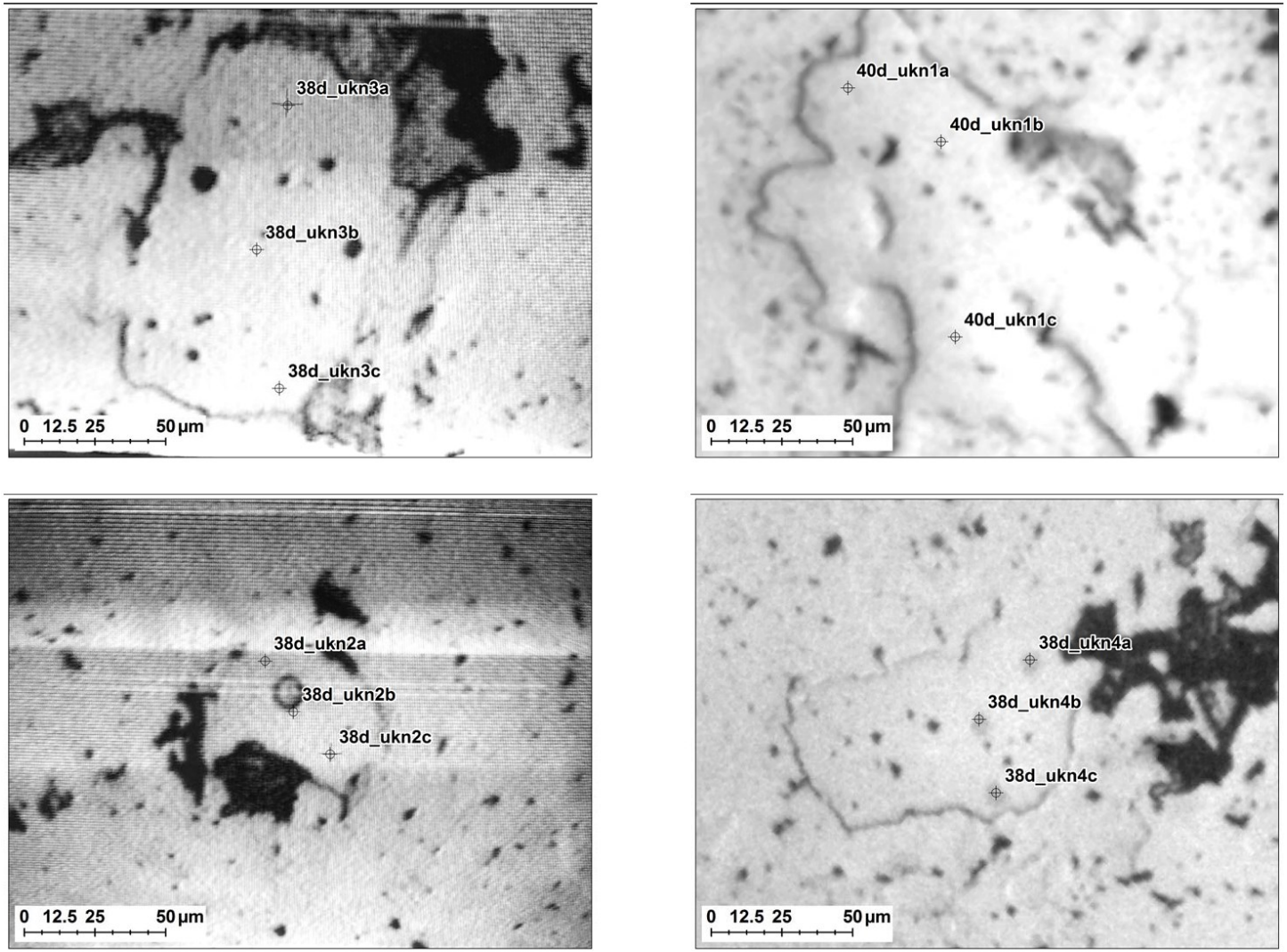

Figure 20 Continued.

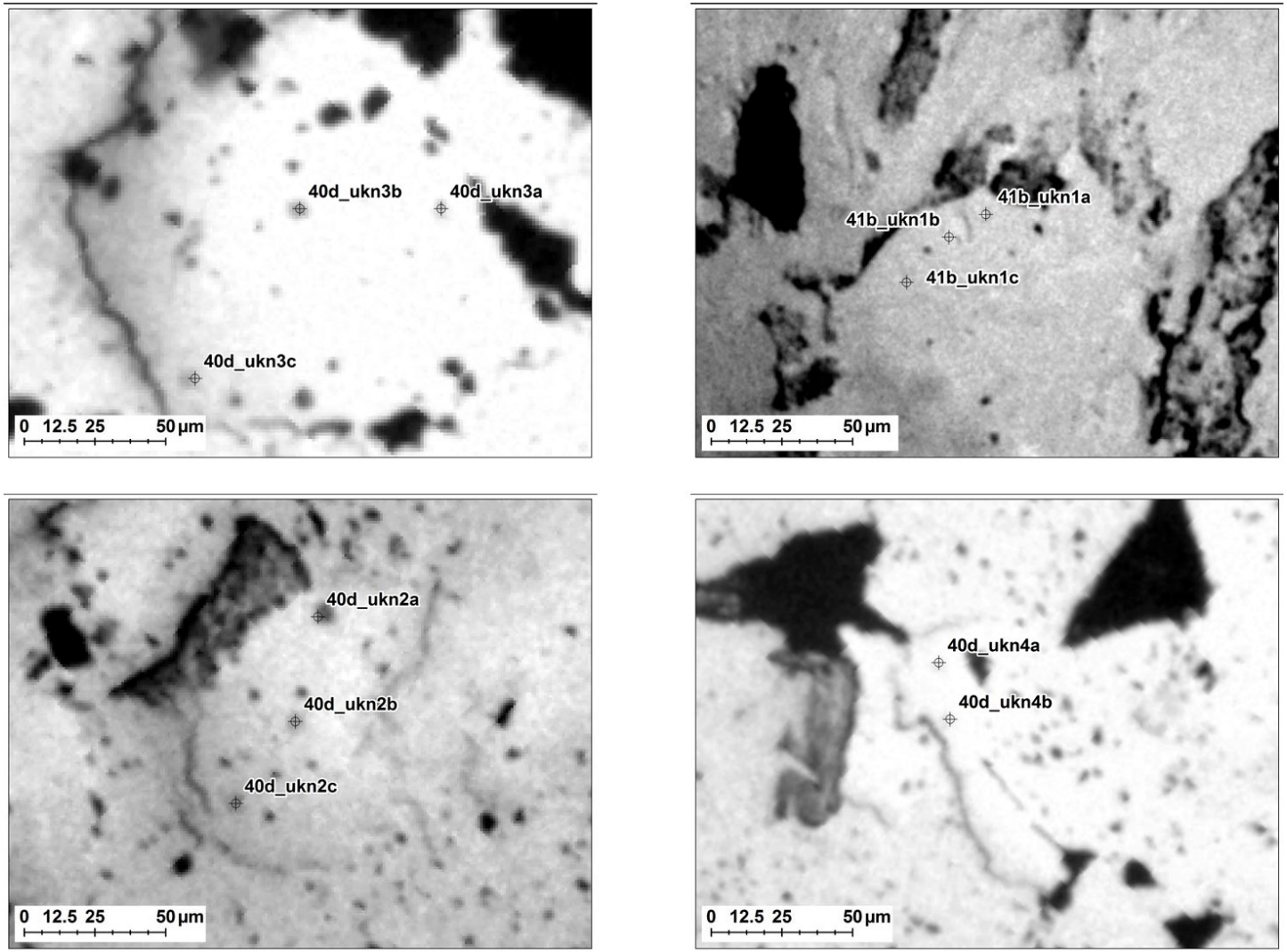

Figure 20 Continued.

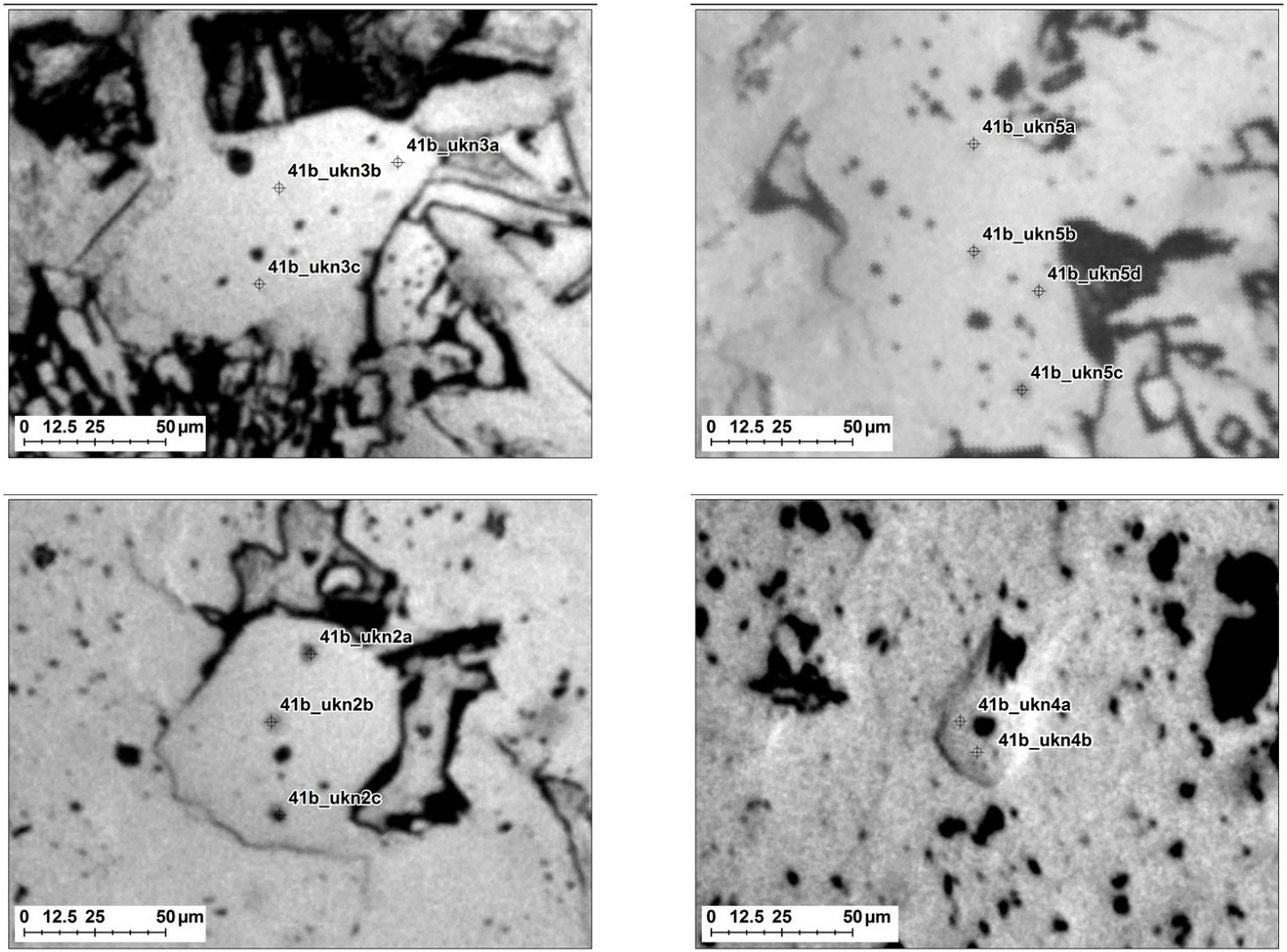

Figure 20 Continued.

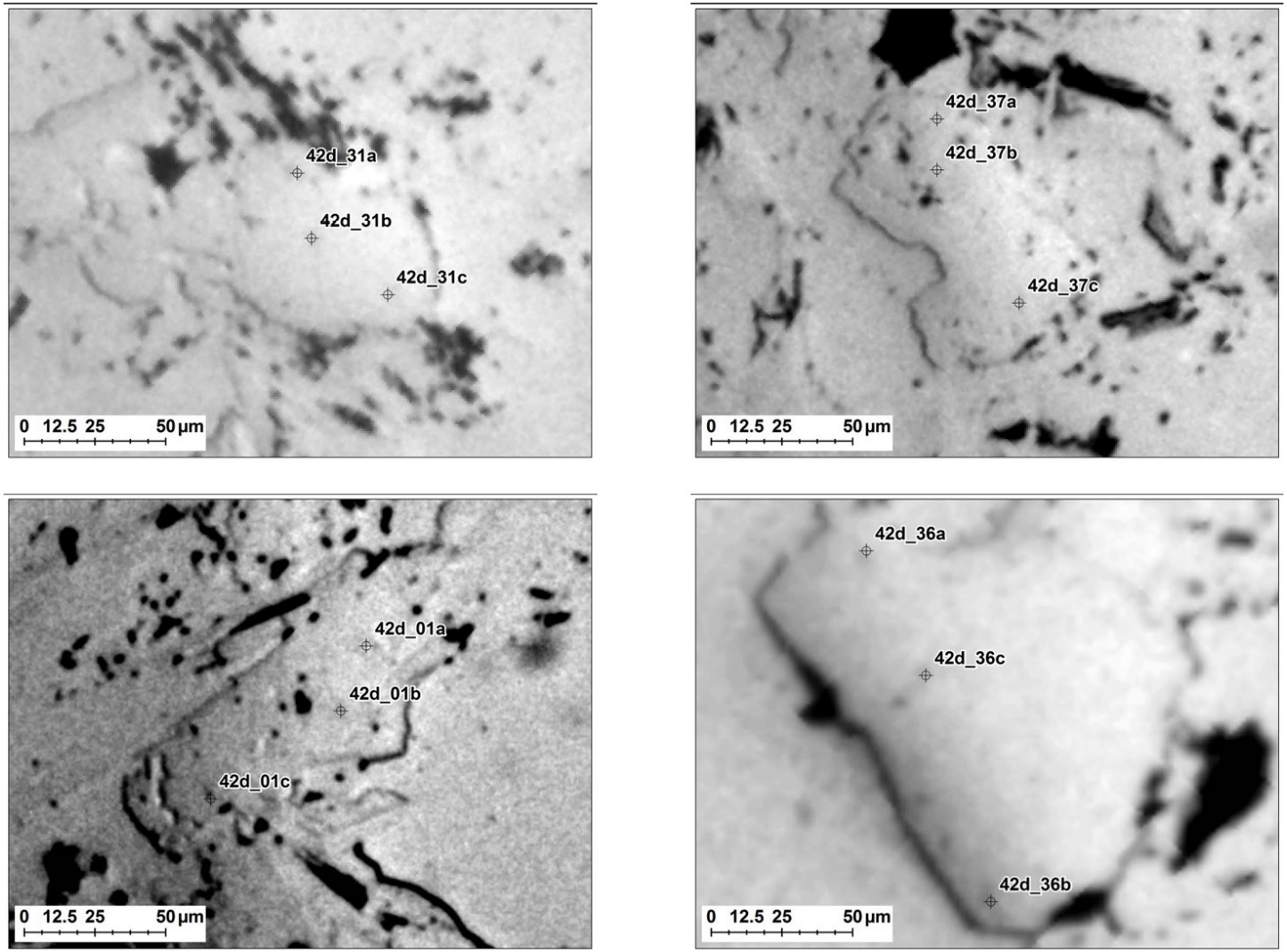

Figure 20 Continued.

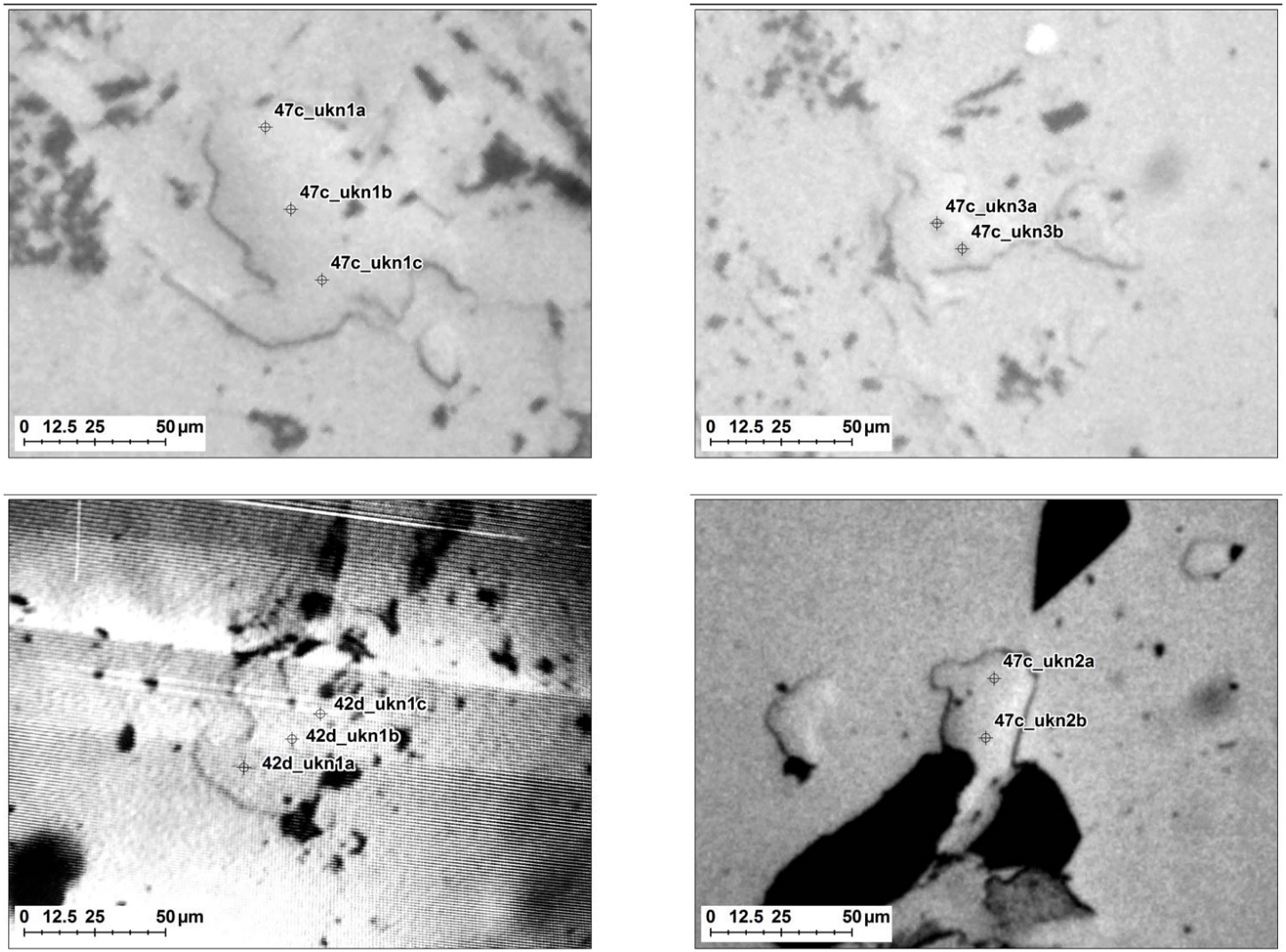

Figure 20 Continued.

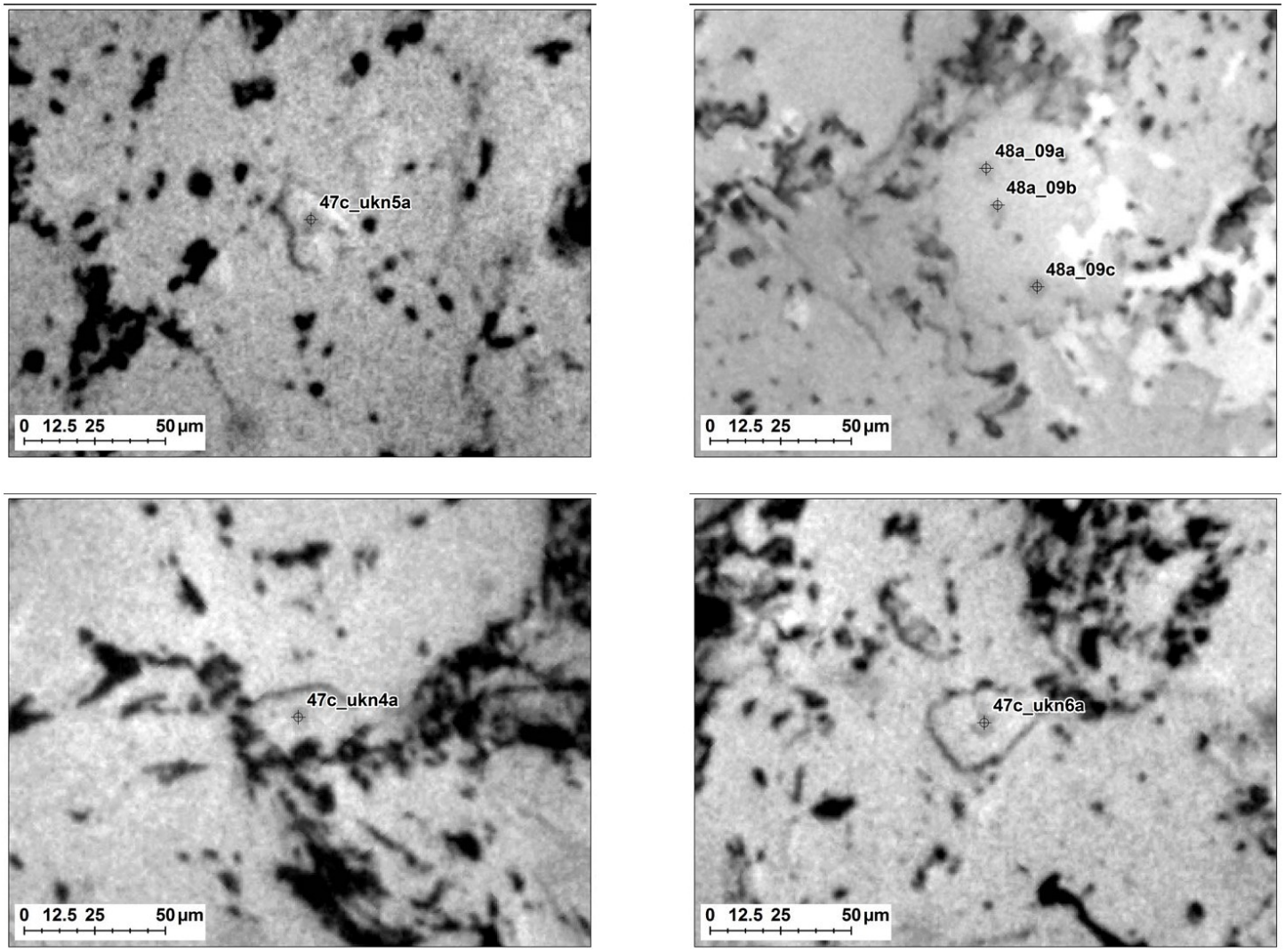

Figure 20 Continued.

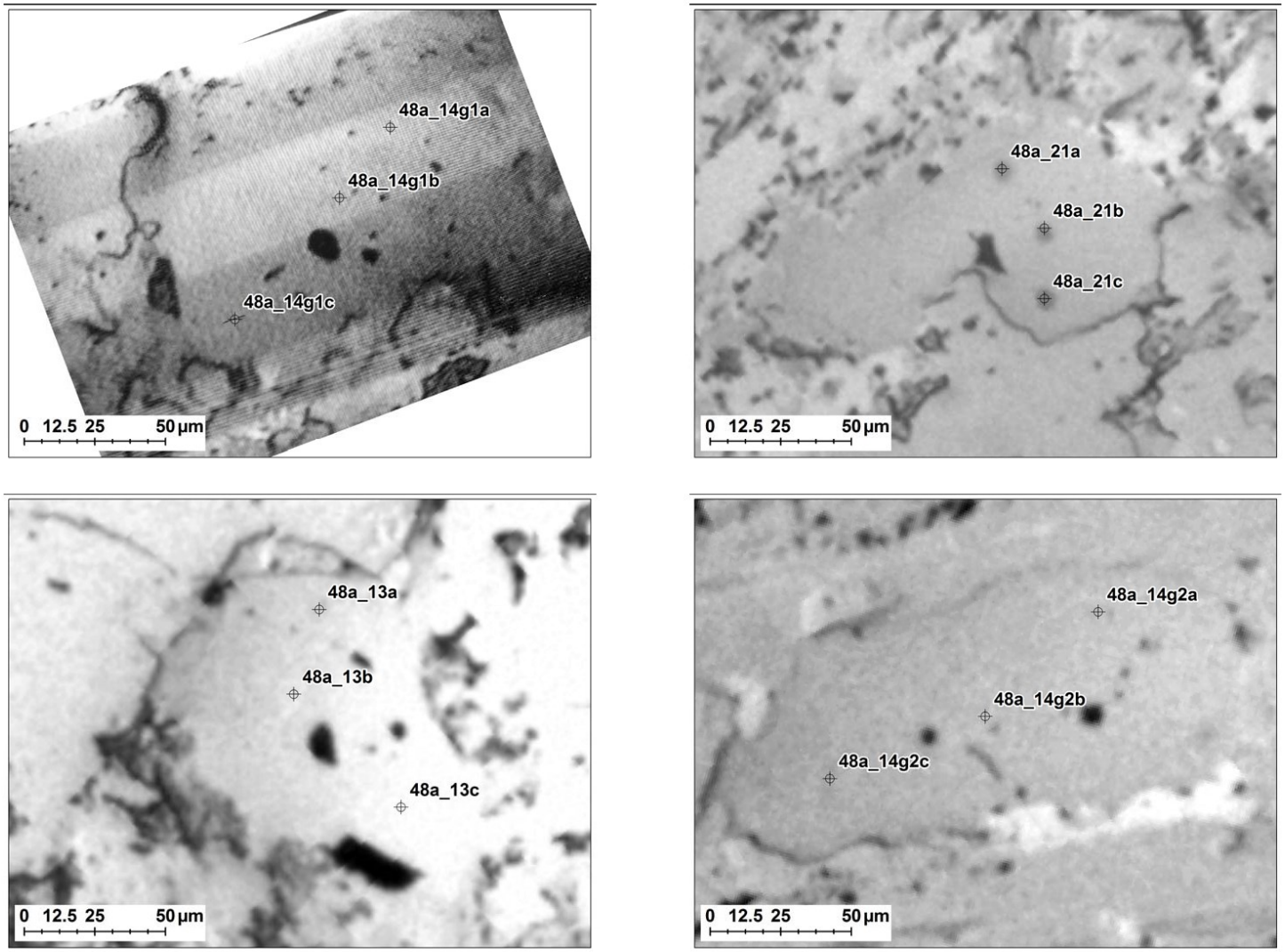

Figure 20 Continued.

APPENDIX C

APATITE COMPOSITIONS

This appendix contains aptite analysis compositions as measured using electron microprobe analysis (Table 15) and LA-ICP-MS (Table 16)

Table 15. Elemental Concentrations from Microprobe Analyses of Apatite Grains.

Rock Unit	**FLA**	**FLA**	**FLA**	**FLA**	**FLA**	**FLA**	**FLA**	**FLA**	**FLA**	**FLA**	**FLA**	**FLA**	**FLA**	**FLA**	**FLA**
Sample ID	**21**	**21**	**21**	**21**	**21**	**21**	**21**	**21**	**21**	**21**	**21**	**21**	**21**	**21**	**21**
Grain ID	**21d_07**	**21d_ukn1**	**21d_07**	**21d_45**	**21d_ukn1**	**21d_39**	**21d_ukn1**	**21d_38**	**21d_45**	**21d_38**	**21d_07**	**21d_38**	**21d_39**	**21d_45**
Location	**Rim**	**Rim**	**Core**	**Rim**	**Rim**	**Rim**	**Core**	**Rim**	**Rim**	**Rim**	**Rim**	**Core**	**Core**	**Core**
wt. %															
Ca	39.28	39.65	39.15	39.58	39.27	39.32	39.00	38.95	39.46	39.36	39.32	39.51	39.16	39.83
P	18.07	17.71	17.88	17.74	17.49	17.66	17.91	17.80	17.71	17.80	17.75	17.84	17.79	17.50
F	3.69	3.67	3.65	3.64	3.64	3.63	3.61	3.59	3.57	3.57	3.57	3.56	3.54	3.51
Cl	0.93	0.54	1.00	0.50	0.46	0.45	0.61	0.47	0.59	0.45	1.01	0.44	0.52	0.54
O	37.24	37.02	36.95	37.05	36.62	36.86	37.03	36.91	36.98	37.08	36.88	37.20	36.99	36.89
ppm															
Sr	nd	nd	nd	nd	nd	619	526	588	351	nd	578	nd	629	nd
Ba	400	nd	nd	nd	nd	nd	nd	nd	nd	nd	nd	nd	nd	nd
Na	nd	nd	nd	nd	nd	nd	nd	nd	530	nd	410	nd	nd	310
K	nd	nd	370	nd	nd	nd	nd	nd	nd	nd	nd	nd	nd	nd
Mg	nd	nd	nd	nd	nd	nd	nd	nd	nd	nd	nd	nd	nd	nd
Ti	nd	nd	nd	nd	nd	nd	nd	nd	nd	nd	nd	nd	nd	nd
Mn	860	730	820	590	800	500	840	990	1040	nd	1120	470	790	830
Fe	1160	890	1250	370	480	530	430	730	580	820	1360	730	nd	nd
Cu	nd	nd	nd	340	640	nd	nd	390	nd	420	nd	690	570	nd
S	330	nd	nd	nd	nd	nd	nd	nd	450	nd	380	nd	nd	nd
Si	470	610	nd	950	880	1020	610	2000	880	1020	480	1200	820	790
As	nd	nd	nd	nd	nd	360	580	310	nd	nd	410	nd	nd	nd
V	nd	nd	nd	nd	nd	nd	340	nd	nd	nd	nd	nd	nd	nd

LOD – 300 ppm, nd – not detected.

Table 15 Continued.

Rock Unit	QMG	QMG	QMG	QMG	QMG	QMG	QMG	QMG	QMG	QMG	QMG	QMG	QMG	QMG
Sample ID	48	48	48	48	48	48	48	48	48	48	48	48	48	48
Grain ID	48a_14g1	48a_14g2	48a_13	48a_21	48a_14g1	48a_21	48a_14g2	48a_21	48a_09	48a_14g1	48a_13	48a_09	48a_09	48a_14g2
Location	Rim	Rim	Rim	Core	Rim	Rim	Rim	Rim	Rim	Core	Rim	Core	Rim	Core
wt. %														
Ca	40.23	39.70	40.16	39.68	40.16	39.74	40.18	39.42	39.64	40.32	39.81	39.76	40.15	39.89
P	17.99	17.91	18.33	18.05	17.65	17.85	17.35	17.71	18.02	17.98	17.36	18.00	17.89	17.68
F	3.88	3.83	3.81	3.79	3.77	3.77	3.76	3.76	3.74	3.72	3.70	3.66	3.66	3.61
Cl	0.08	0.07	0.11	0.22	0.12	0.25	0.14	0.34	0.14	0.09	0.18	0.10	0.12	0.09
O	37.63	37.34	38.06	37.49	37.20	37.26	36.82	36.94	37.48	37.72	36.70	37.54	37.55	37.20
ppm														
Sr	na	nd	nd	nd	na	840	450	nd	nd	na	nd	nd	nd	470
Ba	nd	nd	nd	nd	nd	nd	nd	nd	nd	nd	nd	nd	nd	390
Na	nd	nd	nd	nd	nd	nd	nd	nd	nd	nd	770	nd	nd	nd
K	nd	nd	nd	nd	nd	nd	nd	nd	nd	nd	nd	nd	nd	nd
Mg	nd	nd	nd	nd	nd	nd	nd	nd	nd	nd	nd	nd	nd	nd
Ti	nd	nd	nd	320	nd	nd	nd	1030	1430	nd	nd	nd	430	nd
Mn	670	430	990	1530	450	1400	710	1160	900	nd	830	730	740	480
Fe	1900	1260	2850	2090	1700	2700	2000	3570	2030	1430	1380	1930	3050	920
Cu	nd	nd	nd	nd	nd	500	nd	410	nd	nd	nd	910	nd	nd
S	nd	nd	nd	nd	nd	nd	nd	nd	nd	nd	nd	nd	nd	nd
Si	nd	nd	nd	308	380	380	339	369	359	nd	369	410	nd	nd
As	nd	nd	nd	nd	nd	nd	nd	820	nd	nd	nd	nd	nd	nd
V	nd	340	nd	nd	nd	nd	nd	nd	nd	nd	nd	nd	nd	nd

Table 15 Continued.

Rock Unit	**QMG**	**QMF-I**	**QMF-I**	**QMF-I**	**QMF-I**	**QMF-I**	**QMF-I**	**QMF-I**	**QMF-I**	**QMF-I**	**QMF-I**	**QMF-I**	**QMF-I**
Sample ID	**48**	**40**	**40**	**23**	**23**	**40**	**23**	**40**	**40**	**40**	**23**	**40**	**40**
Grain ID	**48a_13**	**40d_ukn1**	**40d_ukn1**	**23c_ukn2**	**23c_20**	**40d_ukn3**	**23c_20**	**40d_ukn3**	**40d_ukn4**	**40d_ukn2**	**23c_ukn2**	**40d_ukn4**	**40d_ukn1**
Location	**Core**	**Rim**	**Rim**	**Rim**	**Rim**	**Rim**	**Core**	**Rim**	**Rim**	**Core**	**Core**	**Rim**	**Core**
wt. %													
Ca	39.80	39.73	40.07	39.36	39.92	39.77	39.45	38.89	39.67	40.09	39.64	39.51	39.95
P	18.06	18.41	18.72	18.17	18.37	18.63	17.80	18.34	18.39	18.41	18.16	18.44	18.46
F	3.56	3.92	3.90	3.86	3.85	3.84	3.81	3.81	3.81	3.79	3.79	3.78	3.78
Cl	0.18	0.15	0.14	0.20	0.29	0.16	0.36	0.52	0.23	0.21	0.22	0.27	0.30
O	37.66	37.94	38.49	37.50	37.96	38.27	37.04	37.48	37.92	38.12	37.62	37.92	38.12
ppm													
Sr	800	830	628	nd	638	516	648	nd	689	486	nd	952	1286
Ba	nd	nd	nd	nd	nd	nd	nd	nd	nd	nd	nd	nd	nd
Na	nd	nd	nd	nd	nd	nd	641	nd	nd	nd	nd	nd	nd
K	nd	nd	nd	nd	nd	nd	nd	nd	nd	nd	nd	nd	nd
Mg	nd	nd	nd	nd	nd	nd	nd	720	nd	nd	nd	nd	nd
Ti	nd	nd	nd	nd	nd	nd	nd	nd	nd	nd	nd	nd	nd
Mn	880	660	1230	1020	560	1590	800	3790	1620	1660	1110	2520	2460
Fe	1670	1120	990	600	960	2100	510	4100	1730	2080	990	2710	2240
Cu	nd	nd	530	630	nd	nd	nd	nd	670	nd	nd	nd	nd
S	nd	nd	nd	346	523	nd	1362	nd	nd	nd	395	nd	nd
Si	513	nd	nd	500	959	nd	1356	nd	nd	nd	632	nd	nd
As	nd	nd	nd	nd	nd	nd	nd	nd	nd	nd	nd	nd	nd
V	nd	370	nd	nd	nd	nd	nd	nd	nd	nd	nd	nd	nd

Table 15 Continued.

Rock Unit	QMF-I	QMF-I	QMF-I	QMF-I	QMF-I	QMF-I	QMF-I	QMF-I	QMF-I	QMF-I	QMF-I	QMF-I
Sample ID	23	40	40	23	23	23	23	26	23	26	26	40
Grain ID	23c_ukn4	40d_ukn3	40d_ukn2	23c_ukn1	23c_ukn1	23c_ukn3	23c_ukn2	26a_ukn1	23c_20	26a_ukn4	26a_ukn3	40d_ukn2
Location	Core	Core	Rim	Rim	Core	Core	Rim	Core	Rim	Core	Core	Rim
wt. %												
Ca	39.75	39.12	39.74	39.72	39.11	39.76	39.45	38.13	39.41	39.12	39.67	39.68
P	18.18	18.06	18.23	17.99	18.16	18.30	18.15	18.02	18.17	17.71	18.40	18.33
F	3.77	3.77	3.77	3.77	3.76	3.76	3.72	3.72	3.72	3.71	3.70	3.69
Cl	0.18	0.16	0.22	0.22	0.25	0.27	0.19	1.98	0.20	1.64	0.59	0.28
O	37.71	37.30	37.76	37.44	37.41	37.85	37.57	36.47	37.57	36.54	37.90	37.88
ppm												
Sr	nd	901	557	nd	456	na	nd	nd	668	668	547	901
Ba	nd	nd	nd	nd	nd	nd	nd	nd	nd	nd	nd	nd
Na	nd	nd	nd	326	387	743	nd	1418	nd	1651	nd	nd
K	nd	nd	303	nd	nd	nd	nd	nd	nd	1387	nd	526
Mg	nd	nd	nd	nd	nd	nd	nd	nd	nd	nd	nd	nd
Ti	nd	nd	nd	nd	nd	nd	nd	nd	nd	nd	nd	nd
Mn	380	1220	1880	750	690	1250	1020	770	1000	800	nd	2930
Fe	560	340	2280	nd	nd	1100	730	2130	1720	410	nd	3050
Cu	nd	nd	nd	nd	1000	1050	nd	nd	nd	nd	790	nd
S	nd	nd	nd	375	908	1125	434	1184	513	3019	nd	nd
Si	357	nd	nd	1132	1112	1010	nd	868	1122	1240	661	nd
As	nd	nd	nd	nd	nd	nd	nd	nd	nd	nd	nd	nd
V	nd	nd	nd	nd	nd	nd	nd	nd	nd	nd	nd	nd

Table 15 Continued.

Rock Unit	QMF-I	QMF-I	QMF-I	QMF-I	QMF-I	QMF-I	QMF-I	QMF-I	QMF-I	QMF-I	QMF-I	QMF-I
Sample ID	23	23	23	23	26	23	26	26	26	26	26	26
Grain ID	23c_ukn1	23c_ukn3	23c_ukn3	23c_ukn4	26a_ukn3	23c_ukn4	26a_ukn5	26a_ukn3	26a_ukn4	26a_ukn1	26a_ukn2	26a_ukn2
Location	Rim	Rim	Rim	Rim	Rim	Rim	Core	Rim	Core	Rim	Core	Rim
wt. %												
Ca	39.38	39.48	39.47	39.55	39.71	39.25	39.20	39.06	39.10	38.52	38.60	38.30
P	18.00	17.96	18.19	18.33	18.27	18.10	17.88	18.08	18.16	18.10	17.82	17.81
F	3.68	3.67	3.66	3.66	3.66	3.64	3.64	3.64	3.63	3.63	3.62	3.59
Cl	0.24	0.24	0.26	0.16	0.35	0.17	1.26	0.36	1.70	1.98	2.07	2.08
O	37.35	37.34	37.64	37.87	37.81	37.46	36.91	37.32	37.14	36.77	36.42	36.30
ppm												
Sr	nd	790	324	nd	nd	486	1083	nd	nd	nd	729	nd
Ba	nd	nd	450	nd	nd	410	nd	nd	nd	nd	nd	nd
Na	549	580	834	nd	nd	nd	689	nd	1398	830	719	993
K	nd	nd	nd	nd	nd	nd	nd	304	1286	nd	nd	nd
Mg	nd	nd	nd	nd	nd	nd	nd	nd	nd	nd	nd	nd
Ti	nd	nd	nd	nd	nd	nd	nd	310	nd	nd	nd	320
Mn	1210	1320	1150	470	710	330	1290	460	520	1060	1480	1560
Fe	800	810	1740	700	nd	930	1070	nd	390	2880	7280	8310
Cu	nd	nd	340	nd	650	nd	nd	3410	nd	780	nd	320
S	859	1076	1046	nd	nd	810	760	700	2190	740	819	1194
Si	1152	1101	1234	857	1198	1224	992	1281	1425	527	1043	1219
As	nd	nd	nd	nd	nd	nd	nd	nd	nd	nd	nd	nd
V	nd	nd	nd	nd	nd	nd	nd	nd	nd	nd	nd	nd

Table 15 Continued.

Rock Unit	**QMF-I**	**QMF-I**	**QMF-I**	**QMF-II**	**QMF-II**	**QMF-II**	**QMF-II**	**QMF-II**	**QMF-II**	**QMF-II**	**QMF-II**	**QMF-II**
Sample ID	**26**	**26**	**26**	**38**	**38**	**38**	**38**	**38**	**38**	**38**	**41**	**41**
Grain ID	**26a_ukn1**	**26a_ukn5**	**26a_ukn2**	**38d_ukn2**	**38d_ukn2**	**38d_35**	**38d_ukn4**	**38d_ukn1**	**38d_ukn1**	**38d_35**	**41b_ukn3**	**41b_ukn2**
Location	**Rim**	**Rim**	**Rim**	**Rim**	**Core**	**Rim**	**Rim**	**Rim**	**Rim**	**Rim**	**Core**	**Rim**
wt. %												
Ca	38.82	38.74	38.67	40.62	40.51	40.30	40.15	39.71	40.19	40.16	39.38	39.29
P	18.03	17.85	17.85	18.45	18.62	18.67	18.53	18.56	18.36	18.26	17.94	18.01
F	3.58	3.55	3.54	3.83	3.83	3.81	3.81	3.80	3.80	3.77	3.76	3.75
Cl	1.76	1.69	2.04	0.12	0.14	0.18	0.10	0.21	0.15	0.07	0.49	0.44
O	36.87	36.63	36.53	38.39	38.56	38.54	38.32	38.16	38.11	38.00	37.18	37.25
ppm												
Sr	486	547	1053	638	nd	nd	779	668	840	385	1060	570
Ba	nd	nd	nd	nd	nd	nd	nd	nd	nd	nd	nd	nd
Na	1185	810	912	nd	nd	nd	nd	nd	nd	nd	304	nd
K	nd	456	nd	nd	nd	nd	nd	nd	nd	nd	nd	nd
Mg	nd	nd	nd	nd	nd	nd	nd	nd	nd	nd	nd	nd
Ti	nd	nd	nd	nd	330	nd	nd	nd	nd	nd	nd	nd
Mn	950	640	2020	nd	430	700	630	790	310	590	1760	2060
Fe	1760	380	7400	1150	840	910	1150	1180	1130	660	2990	1620
Cu	nd	nd	nd	nd	nd	nd	nd	350	nd	nd	nd	nd
S	1332	543	789	nd	nd	nd	nd	nd	nd	nd	nd	nd
Si	795	1074	992	nd	nd	nd	nd	nd	nd	nd	nd	nd
As	nd	nd	nd	nd	nd	nd	nd	nd	nd	nd	nd	nd
V	nd	nd	nd	nd	nd	nd	nd	nd	nd	nd	nd	nd

Table 15 Continued.

Rock Unit	QMF-II	QMF-II	QMF-II	QMF-II	QMF-II	QMF-II	QMF-II	QMF-II	QMF-II	QMF-II	QMF-II	QMF-II
Sample ID	38	38	38	41	41	41	41	41	41	38	41	41
Grain ID	38d_ukn1	38d_ukn4	38d_ukn1	41b_ukn1	41b_ukn4	41b_ukn2	41b_ukn5	41b_ukn5	41b_ukn3	38d_ukn4	41b_ukn1	41b_ukn5
Location	Core	Core	Core	Rim	Rim	Rim	Rim	Rim	Rim	Rim	Rim	Rim
wt. %												
Ca	39.71	40.63	40.00	39.47	39.13	38.86	39.73	39.71	39.07	40.47	39.18	39.63
P	18.44	18.45	18.77	18.15	18.31	17.84	18.44	18.17	17.90	18.53	18.14	18.00
F	3.75	3.73	3.73	3.70	3.69	3.69	3.67	3.67	3.67	3.66	3.66	3.66
Cl	0.19	0.14	0.21	0.55	0.51	0.49	0.39	0.46	0.60	0.09	0.50	0.42
O	38.03	38.43	38.58	37.50	37.59	36.88	38.03	37.66	37.02	38.51	37.40	37.42
ppm												
Sr	891	nd	nd	340	nd	520	710	nd	320	364	520	380
Ba	nd	nd	nd	nd	nd	nd	nd	nd	nd	nd	nd	nd
Na	nd	nd	nd	507	537	415	334	466	618	nd	395	nd
K	nd	nd	nd	nd	nd	nd	nd	nd	nd	nd	nd	nd
Mg	nd	nd	nd	nd	nd	nd	nd	nd	nd	nd	nd	nd
Ti	nd	nd	nd	nd	nd	nd	nd	nd	nd	nd	330	nd
Mn	620	510	530	1750	1850	1790	1920	2150	2170	450	2290	1530
Fe	1030	820	390	5010	3140	2040	2040	2170	3690	900	5580	2270
Cu	nd	nd	nd	nd	nd	nd	nd	nd	750	nd	440	nd
S	nd	nd	nd	360	nd	460	370	nd	380	nd	nd	nd
Si	nd	nd	nd	nd	400	441	nd	nd	359	nd	400	nd
As	nd	nd	nd	1000	nd	nd	nd	nd	nd	nd	nd	nd
V	nd	nd	nd	nd	nd	nd	nd	nd	nd	nd	nd	nd

Table 15 Continued.

Rock Unit	QMF-II	QMF-II	QMF-II	QMF-II	QMF-II	QMF-II	QMF-II	QMP	QMP	QMP	QMP	QMP
Sample ID	41	41	38	41	38	38	38	02	02	02	02	02
Grain ID	41b_ukn3	41b_ukn5	38d_35	41b_ukn2	38d_ukn3	38d_ukn3	38d_ukn3	02b_ukn4	02b_ukn1	02b_ukn2	02b_27	02b_ukn1
Location	Rim	Core	Core	Core	Rim	Core	Rim	Rim	Rim	Rim	Core	Rim
wt. %												
Ca	39.20	39.64	40.18	39.40	40.09	40.30	40.28	39.53	39.42	39.35	39.54	39.05
P	17.92	18.10	18.50	18.06	18.84	18.71	18.37	17.59	17.49	17.47	17.75	17.37
F	3.65	3.65	3.63	3.60	nd	nd	nd	3.73	3.72	3.63	3.61	3.60
Cl	0.54	0.42	0.25	0.43	0.17	0.18	0.11	0.17	0.24	0.31	0.21	0.24
O	37.12	37.56	38.33	37.43	40.29	40.20	39.77	36.88	36.69	36.66	37.13	36.44
ppm												
Sr	770	530	668	370	na	304	364	780	470	980	550	nd
Ba	nd	440	nd	nd	nd	nd	nd	nd	nd	nd	nd	nd
Na	669	669	nd	436	nd	nd	nd	nd	nd	nd	nd	550
K	nd	nd	nd	nd	nd	nd	nd	820	nd	340	nd	nd
Mg	nd	nd	nd	nd	nd	nd	nd	nd	nd	nd	nd	nd
Ti	nd	330	310	nd	nd	nd	nd	nd	nd	nd	nd	nd
Mn	1810	1200	650	1800	880	390	480	780	1910	2630	1020	610
Fe	4010	1990	1200	1410	1470	950	2080	660	1170	1500	1010	970
Cu	430	400	nd	nd	720	400	nd	nd	310	nd	nd	460
S	nd	nd	nd	nd	nd	nd	nd	nd	330	nd	nd	nd
Si	nd	nd	nd	nd	nd	nd	nd	310	nd	nd	nd	nd
As	nd	nd	nd	nd	nd	nd	nd	nd	nd	nd	nd	nd
V	nd	nd	nd	nd	nd	nd	nd	nd	nd	nd	nd	nd

Table 15 Continued.

Rock Unit	**QMP**	**QMP**	**QMP**	**QMP**	**QMP**	**QMP**	**QMP**	**QMP**	**QMP**	**POB**	**POB**	**POB**	**POB**
Sample ID	**02**	**02**	**02**	**02**	**02**	**02**	**02**	**02**	**02**	**47**	**47**	**42**	**34**
Grain ID	**02b_ukn1**	**02b_ukn4**	**02b_27**	**02b_27**	**02b_ukn2**	**02b_ukn2**	**02b_ukn4**	**02b_ukn3**	**02b_ukn3**	**47c_ukn4**	**47c_ukn1**	**42d_31**	**34b_12**
Location	**Core**	**Rim**	**Rim**	**Rim**	**Rim**	**Core**	**Core**	**Core**	**Rim**	**Core**	**Core**	**Core**	**Core**
wt. %													
Ca	39.37	39.76	39.17	39.54	39.10	39.11	39.56	39.24	38.98	39.63	40.07	39.57	39.75
P	17.49	17.61	17.10	17.52	17.51	17.47	17.51	17.12	17.38	18.23	18.40	18.22	17.83
F	3.59	3.58	3.58	3.51	3.48	3.44	3.39	3.36	3.27	3.98	3.84	3.81	3.76
Cl	0.23	0.20	0.30	0.21	0.34	0.32	0.24	0.28	0.26	0.36	0.28	0.29	0.21
O	36.73	37.05	36.13	36.87	36.67	36.64	36.91	36.29	36.56	37.59	38.07	37.64	37.25
ppm													
Sr	760	730	370	nd	1000	1000	1230	810	nd	nd	516	nd	500
Ba	350	nd	nd	nd	nd	nd	nd	nd	nd	nd	nd	nd	nd
Na	nd	nd	nd	nd	nd	470	nd	nd	nd	nd	304	nd	1267
K	nd	430	320	nd	nd	nd	nd	nd	400	719	nd	nd	nd
Mg	nd	nd	nd	nd	nd	nd	nd	nd	nd	370	nd	nd	nd
Ti	nd	nd	nd	420	nd	nd	nd	nd	320	nd	nd	nd	nd
Mn	860	880	1640	920	3430	3000	980	1490	1150	910	810	1550	2310
Fe	630	1180	3040	1320	1800	2040	1240	1530	2300	4130	1160	2050	2700
Cu	nd	nd	nd	nd	nd	nd	710	nd	nd	nd	nd	nd	2070
S	nd	nd	360	460	380	480	nd	nd	nd	nd	612	543	2250
Si	nd	nd	410	nd	nd	nd	nd	nd	410	372	589	551	944
As	nd	nd	nd	nd	nd	nd	nd	nd	nd	nd	nd	nd	nd
V	nd	nd	nd	nd	370	nd	nd	nd	nd	nd	nd	nd	nd

Table 15 Continued.

Rock Unit	POB	POB	POB	POB	POB	POB	POB	POB	POB	POB	POB	POB	POB	POB	POB
Sample ID	42	47	42	34	42	42	42	42	42	34	34	34	34	34	34
Grain ID	42d_01	47c_ukn1	42d_37	34b_05	42d_36	42d_31	42d_01	42d_36	42d_36	34a_15	34a_15	34b_06	34a_16	34b_06	34b_12
Location	Rim	Rim	Rim	Core	Rim	Rim	Core	Core	Rim	Rim	Rim	Rim	Core	Rim	Rim
wt. %															
Ca	39.41	39.90	39.48	39.92	39.25	39.10	40.04	39.61	39.65	40.20	40.11	39.58	40.02	39.99	39.40
P	18.05	18.36	18.17	17.87	18.67	18.50	18.16	18.42	18.36	18.09	18.15	17.79	18.20	17.96	17.94
F	3.75	3.74	3.74	3.74	3.74	3.72	3.72	3.72	3.71	3.71	3.69	3.69	3.67	3.67	3.66
Cl	nd	0.30	0.26	0.15	0.40	0.27	nd	0.28	0.22	0.08	0.09	0.16	0.13	0.13	0.36
O	37.45	37.98	37.58	37.39	38.10	37.86	37.86	37.96	37.92	37.82	37.87	37.17	37.89	37.57	37.26
ppm															
Sr	nd	nd	435	410	nd	516	nd	nd	nd	470	nd	nd	460	770	1790
Ba	nd	nd	nd	nd	nd	nd	nd	nd	nd	nd	480	nd	nd	nd	nd
Na	549	486	nd	nd	nd	nd	nd	nd	nd	nd	nd	nd	nd	nd	527
K	nd	nd	384	nd	nd	556	nd	nd	404	nd	nd	nd	nd	nd	nd
Mg	nd	330	nd	nd	550	380	nd	nd	nd	nd	nd	nd	nd	nd	650
Ti	480	nd	nd	nd	nd	nd	nd	nd	nd	nd	nd	nd	nd	nd	nd
Mn	750	720	1610	960	2640	2250	nd	1190	1210	650	310	1070	1190	1080	3250
Fe	410	1840	2280	870	4070	3230	820	2280	980	2660	510	470	1410	nd	3760
Cu	350	960	470	nd	nd	nd	nd	750	570	nd	nd	560	790	nd	990
S	2281	819	484	600	nd	622	681	444	721	nd	nd	790	420	420	970
Si	969	837	479	595	nd	744	622	347	632	nd	nd	780	595	944	472
As	1540	nd	nd	nd	nd	nd	nd	nd	nd	nd	nd	nd	nd	nd	nd
V	nd	nd	nd	nd	nd	nd	nd	nd	nd	nd	nd	nd	nd	nd	nd

Table 15 Continued.

Rock Unit	POB	POB	POB	POB	POB	POB	POB	POB	POB	POB	FP	FP	FP	FP	FP
Sample ID	42	34	47	34	42	34	47	34	34	42	13	13	13	13	13
Grain ID	42d_37	34b_05	47c_ukn3	34a_15	42d_01	34b_05	47c_ukn5	34a_16	34b_06	42d_37	13a_24	13a_24	13a_45	13a_45	13a_33
Location	Core	Rim	Rim	Core	Rim	Rim	Core	Rim	Core	Rim	Core	Rim	Rim	Core	Rim
wt. %															
Ca	39.59	40.20	39.71	40.02	39.59	40.01	39.56	39.48	39.75	39.48	39.49	39.28	39.48	39.25	39.30
P	18.34	18.02	18.51	18.02	17.89	18.19	18.25	18.05	17.98	17.79	18.47	18.47	17.97	18.08	18.55
F	3.66	3.66	3.65	3.63	3.63	3.61	3.58	3.55	3.53	3.53	3.81	3.80	3.72	3.69	3.68
Cl	0.25	0.13	0.26	0.13	nd	0.12	0.31	0.22	0.16	nd	0.27	0.28	0.32	0.31	0.27
O	37.88	37.74	38.15	37.68	37.37	37.90	37.77	37.51	37.55	37.24	37.94	37.86	37.32	37.38	38.02
ppm															
Sr	1043	620	1032	920	nd	na	810	660	660	1144	na	390	nd	440	nd
Ba	nd	nd	nd	nd	nd	420	nd	nd	nd	nd	nd	nd	nd	nd	nd
Na	nd	nd	972	nd	611	385	993	nd	nd	1893	nd	nd	770	588	557
K	nd	nd	nd	nd	799	nd	nd	1120	nd	607	460	nd	310	nd	310
Mg	nd	nd	nd	nd	nd	nd	450	nd	nd	nd	nd	nd	nd	nd	nd
Ti	nd	nd	nd	nd	nd	nd	nd	nd	nd	nd	nd	nd	nd	nd	nd
Mn	1000	540	1340	690	420	1060	1610	1570	840	nd	1860	1560	1190	1470	1490
Fe	1680	430	2360	1640	nd	730	4700	2620	640	340	1050	1460	1320	900	2050
Cu	nd	nd	470	nd	nd	310	590	nd	nd	310	nd	nd	nd	890	nd
S	464	560	1588	1020	2162	410	1460	350	520	2517	nd	470	400	350	320
Si	nd	770	878	883	948	749	857	759	564	nd	380	380	544	380	nd
As	nd	nd	nd	nd	1320	nd	nd	nd	nd	nd	nd	nd	nd	nd	nd
V	nd	nd	nd	nd	nd	nd	nd	nd	nd	340	410	nd	nd	nd	nd

Table 15 Continued.

Rock Unit	**FP**	**FP**	**FP**	**FP**	**FP**	**FP**	**FP**	**FP**	**FP**	**FP**	**FP**	**FP**	**FP**
Sample ID	**13**	**13**	**12**	**13**	**12**	**12**	**13**	**12**	**12**	**12**	**13**	**12**	**13**
Grain ID	**13a_33**	**13a_45**	**12a_ukn2**	**13a_33**	**12a_ukn2**	**12a_ukn3**	**13a_17**	**12a_ukn4**	**12a_ukn1**	**12a_ukn3**	**13a_24**	**12a_ukn3**	**13a_17**
Location	**Rim**	**Rim**	**Core**	**Core**	**Rim**	**Rim**	**Rim**	**Core**	**Core**	**Rim**	**Rim**	**Core**	**Rim**
wt. %													
Ca	39.51	39.27	39.25	39.40	39.31	39.19	39.61	39.48	38.97	39.11	39.27	39.16	38.85
P	18.30	18.31	17.56	18.41	17.36	17.56	18.15	17.13	17.58	17.41	18.12	17.09	18.15
F	3.68	3.68	3.66	3.65	3.65	3.64	3.62	3.60	3.58	3.56	3.54	3.53	3.53
Cl	0.30	0.36	0.23	0.22	0.21	0.20	0.34	0.19	0.19	0.24	0.31	0.24	0.34
O	37.78	37.68	36.74	37.91	36.52	36.73	37.64	36.31	36.70	36.53	37.51	36.15	37.37
ppm													
Sr	nd	450	480	360	570	940	710	970	550	910	na	1060	na
Ba	nd	nd	nd	nd	nd	nd	nd	nd	nd	nd	nd	nd	nd
Na	497	750	900	598	1150	840	699	1150	nd	580	nd	1350	811
K	nd	370	nd	nd	650	nd	670	nd	nd	nd	nd	nd	770
Mg	nd	nd	nd	nd	490	nd	nd	nd	nd	340	nd	nd	nd
Ti	nd	nd	nd	nd	nd	nd	nd	nd	nd	nd	nd	nd	360
Mn	2170	2230	1380	2290	1040	730	1370	1170	780	610	1830	1420	900
Fe	2490	1660	1420	1460	2840	1520	1470	1540	nd	2160	1460	1940	1210
Cu	370	nd	nd	450	nd	nd	nd	330	nd	nd	440	500	nd
S	370	410	960	320	1650	730	880	2050	400	1000	nd	1960	1460
Si	nd	421	430	nd	810	550	575	750	580	690	nd	720	883
As	nd	nd	nd	nd	nd	nd	nd	nd	nd	nd	nd	nd	nd
V	nd	nd	nd	nd	nd	nd	nd	nd	nd	nd	nd	nd	nd

Table 15 Continued.

Rock Unit	**FP**	**FP**	**FP**	**FP**	**FP**	**DLP**	**DLP**	**DLP**	**DLP**	**DLP**	**DLP**	**DLP**
Sample ID	**12**	**12**	**12**	**12**	**12**	**16**	**16**	**16**	**16**	**16**	**16**	**16**
Grain ID	**12a_ukn5**	**12a_ukn2**	**12a_ukn1**	**12a_ukn1**	**12a_ukn5**	**16a_ukn5**	**16a_ukn6**	**16a_ukn4**	**16a_ukn6**	**16a_ukn1**	**16a_ukn4**	**16a_ukn1**
Location	**Rim**	**Rim**	**Rim**	**Rim**	**Core**	**Core**	**Rim**	**Rim**	**Core**	**Core**	**Core**	**Rim**
wt. %												
Ca	39.18	39.24	39.37	38.86	39.24	40.06	39.54	39.67	39.64	39.44	39.45	39.61
P	17.04	17.16	17.54	17.18	17.06	18.43	18.03	18.40	18.30	18.36	18.16	18.34
F	3.51	3.44	3.42	3.38	3.37	3.86	3.84	3.79	3.79	3.79	3.79	3.77
Cl	0.24	0.22	0.21	0.20	0.23	0.22	0.19	0.25	0.25	0.14	0.24	0.17
O	36.10	36.32	36.87	36.22	36.21	38.11	37.40	37.93	37.79	37.82	37.54	37.86
ppm												
Sr	480	840	620	780	760	729	678	709	932	719	830	1073
Ba	nd	nd	nd	nd	nd	nd	nd	nd	nd	nd	nd	nd
Na	1460	1700	550	1330	1330	nd	458	356	509	326	845	nd
K	nd	nd	nd	370	nd	910	637	859	475	nd	506	435
Mg	nd	370	nd	nd	370	nd	nd	nd	nd	nd	nd	nd
Ti	nd	nd	nd	nd	nd	nd	nd	nd	nd	nd	nd	nd
Mn	1320	1430	1190	640	1640	840	950	990	nd	910	880	1050
Fe	3200	2000	1570	1760	3190	490	1000	850	780	540	660	1540
Cu	nd	nd	770	nd	nd	nd	nd	nd	810	nd	nd	nd
S	2140	2250	590	2140	2430	306	898	582	1096	731	958	nd
Si	790	920	880	890	670	nd	1020	377	714	nd	571	530
As	nd	nd	nd	nd	nd	nd	nd	nd	nd	nd	nd	nd
V	nd	nd	nd	nd	nd	nd	nd	nd	nd	nd	nd	nd

Table 15 Continued.

Rock Unit	DLP	DLP	DLP	DLP	DLP	DLP	DLP	DLP	DLP	DLP	DLP	DLP
Sample ID	16	16	16	16	16	17	16	16	17	17	16	17
Grain ID	16a_ukn6	16a_ukn1	16a_ukn3	16a_ukn3	16a_ukn3	17b_ukn2	16a_ukn4	16a_ukn5	17b_18	17b_ukn2	16a_ukn5	17b_ukn1
Location	Rim	Rim	Rim	Core	Rim	Core	Rim	Rim	Core	Rim	Rim	Core
wt. %												
Ca	39.81	39.37	39.73	39.70	39.72	39.34	39.42	39.68	39.46	39.32	39.86	39.40
P	18.27	18.48	18.19	18.01	18.39	17.38	18.42	18.25	17.89	17.35	18.43	17.51
F	3.77	3.75	3.74	3.72	3.71	3.70	3.67	3.66	3.65	3.65	3.62	3.58
Cl	0.23	0.25	0.26	0.31	0.27	0.25	0.25	0.21	0.18	0.21	0.21	0.21
O	37.84	37.93	37.71	37.46	37.97	36.52	37.91	37.81	37.27	36.51	38.13	36.78
ppm												
Sr	395	nd	nd	618	932	500	1053	678	nd	610	577	580
Ba	nd	nd	nd	nd	nd	nd	nd	nd	nd	nd	nd	nd
Na	nd	nd	1628	1129	nd	1900	702	nd	480	1300	nd	1620
K	404	nd	677	425	799	nd	718	1941	nd	370	768	nd
Mg	nd	nd	nd	nd	nd	nd	nd	nd	nd	nd	nd	nd
Ti	nd	nd	nd	nd	nd	nd	nd	nd	nd	nd	330	nd
Mn	720	1240	870	970	800	1030	770	610	960	1130	770	960
Fe	1240	2620	440	460	nd	800	710	880	750	nd	840	760
Cu	nd	nd	340	390	nd	nd	nd	1030	nd	400	nd	nd
S	563	592	2596	2281	642	3080	681	513	610	2300	365	2600
Si	510	540	948	816	551	920	540	1112	600	990	520	860
As	nd	nd	nd	nd	nd	nd	nd	nd	nd	nd	nd	nd
V	nd	nd	330	nd	nd	nd	nd	nd	nd	nd	470	nd

Table 15 Continued.

Rock Unit	DLP	DLP	DLP	DLP	DLP	DLP	DLP	DLP	DLP	DLP	DLP
Sample ID	17	17	17	17	17	17	17	17	17	17	17
Grain ID	17b_33	17b_33	17b_18	17b_32	17b_32	17b_ukn2	17b_33	17b_ukn1	17b_32	17b_ukn1	17b_18
Location	Rim	Core	Rim	Core	Rim	Rim	Rim	Rim	Rim	Rim	Rim
wt. %											
Ca	38.93	39.38	39.43	39.73	39.18	39.46	39.49	39.45	39.58	39.77	39.49
P	17.49	17.55	17.86	17.94	17.55	17.41	17.46	17.28	17.73	17.72	17.38
F	3.52	3.50	3.50	3.47	3.46	3.43	3.43	3.43	3.35	3.33	3.27
Cl	0.25	0.23	0.19	0.23	0.27	0.22	0.23	0.22	0.24	0.21	0.19
O	36.58	36.85	37.28	37.50	36.78	36.73	36.81	36.56	37.22	37.30	36.78
ppm											
Sr	530	600	660	nd	1040	1690	890	500	330	380	350
Ba	460	470	nd	nd	nd	nd	nd	nd	nd	nd	nd
Na	420	330	370	nd	340	340	nd	930	nd	nd	nd
K	nd	nd	nd	nd	nd	nd	nd	600	nd	540	nd
Mg	nd	nd	nd	nd	nd	nd	nd	nd	nd	nd	nd
Ti	nd	nd	nd	nd	nd	nd	nd	nd	nd	nd	nd
Mn	nd	720	1050	1160	1190	730	900	1430	1030	840	690
Fe	650	410	350	390	420	870	620	810	440	380	430
Cu	nd	920	nd	nd	nd	330	760	nd	nd	nd	nd
S	780	690	630	590	460	880	560	2050	540	990	480
Si	600	720	580	680	590	700	770	900	760	780	580
As	nd	nd	nd	nd	nd	nd	nd	nd	nd	nd	nd
V	nd	nd	nd	nd	nd	nd	nd	nd	nd	nd	nd

Table 16. Average Elemental Concentrations of Apatite Grains Determined Through LA-ICP-MS Analysis

Rock Unit	**FLA**	**FLA**	**FLA**	**FLA**	**FLA**	**FLA**	**FLA**	**FLA**	**FLA**	**FLA**	**FLA**	**FLA**	**FLA**	**FLA**
Sample ID	**21**	**21**	**21**	**21**	**21**	**21**	**21**	**21**	**21**	**21**	**21**	**21**	**21**	**21**
Grain ID	**21d_07**	**21d_ukn1**	**21d_07**	**21d_45**	**21d_ukn1**	**21d_39**	**21d_ukn1**	**21d_38**	**21d_45**	**21d_38**	**21d_07**	**21d_38**	**21d_39**	**21d_45**
Location	**Rim**	**Rim**	**Core**	**Rim**	**Rim**	**Rim**	**Core**	**Rim**	**Rim**	**Rim**	**Rim**	**Core**	**Core**	**Core**
ppm														
La	407	453	407	641	453	na	453	654	641	654	407	654	na	641
Ce	1060	1688	1060	2017	1688	2640	1688	2422	2017	2422	1060	2422	2100	2017
Pr	154	267	154	292	267	na	267	322	292	322	154	322	na	292
Nd	665	1353	665	1302	1353	na	1353	1291	1302	1291	665	1291	na	1302
Sm	157	293	157	256	293	na	293	246	256	246	157	246	na	256
Eu	15	22	15	14	22	na	22	14	14	14	15	14	na	14
Gd	139	275	139	220	275	na	275	206	220	206	139	206	na	220
Tb	17	37	17	28	37	na	37	27	28	27	17	27	na	28
Dy	88	214	88	155	214	na	214	145	155	145	88	145	na	155
Er	19	37	19	31	37	na	37	27	31	27	19	27	na	31
Yb	30	59	30	53	59	na	59	45	53	45	30	45	na	53
Lu	5	7	5	7	7	na	7	7	7	7	5	7	na	7
Hf	12	16	12	11	16	na	16	nd	11	nd	12	nd	na	11
B	45	241	45	48	241	na	241	39	48	39	45	39	na	48

nd – not detected, na – not analyzed

Table 16 Continued.

Rock Unit	QMG	QMG	QMG	QMG	QMG	QMG	QMG	QMG	QMG	QMG	QMG	QMG	QMG	QMG
Sample ID	48	48	48	48	48	48	48	48	48	48	48	48	48	48
Grain ID	48a_14g1	48a_14g2	48a_13	48a_21	48a_14g1	48a_21	48a_14g2	48a_21	48a_09	48a_14g1	48a_13	48a_09	48a_09	48a_14g2
Location	Rim	Rim	Rim	Core	Rim	Rim	Rim	Rim	Rim	Core	Rim	Core	Rim	Core
ppm														
La	na	128	187	160	na	160	128	160	143	na	187	143	143	128
Ce	380	495	727	715	1240	715	495	715	471	na	727	471	471	495
Pr	na	64	112	113	na	113	64	113	65	na	112	65	65	64
Nd	na	255	492	537	na	537	255	537	318	na	492	318	318	255
Sm	na	54	127	170	na	170	54	170	97	na	127	97	97	54
Eu	na	12	32	40	na	40	12	40	25	na	32	25	25	12
Gd	na	46	134	201	na	201	46	201	113	na	134	113	113	46
Tb	na	8	20	38	na	38	8	38	18	na	20	18	18	8
Dy	na	27	108	223	na	223	27	223	104	na	108	104	104	27
Er	na	7	22	45	na	45	7	45	21	na	22	21	21	7
Yb	na	16	50	79	na	79	16	79	45	na	50	45	45	16
Lu	na	3	9	10	na	10	3	10	7	na	9	7	7	3
Hf	na	nd	9	nd	na	nd	nd	nd	9	na	9	9	9	nd
B	na	nd	nd	41	na	41	nd	41	36	na	nd	36	36	nd

Table 16 Continued.

Rock Unit	QMG	QMF-I	QMF-I	QMF-I	QMF-I	QMF-I	QMF-I	QMF-I	QMF-I	QMF-I	QMF-I	QMF-I	QMF-I
Sample ID	48	40	40	23	23	40	23	40	40	40	23	40	40
Grain ID	48a_13	40d_ukn1	40d_ukn1	23c_ukn2	23c_20	40d_ukn3	23c_20	40d_ukn3	40d_ukn4	40d_ukn2	23c_ukn2	40d_ukn4	40d_ukn1
Location	Core	Rim	Rim	Rim	Rim	Rim	Core	Rim	Rim	Core	Core	Rim	Core
ppm													
La	187	138	138	468	na	146	na	146	145	152	468	145	138
Ce	727	423	423	761	1340	600	1150	600	447	441	761	447	423
Pr	112	50	50	81	na	98	na	98	66	59	81	66	50
Nd	492	218	218	279	na	447	na	447	280	255	279	280	218
Sm	127	61	61	54	na	102	na	102	92	69	54	92	61
Eu	32	23	23	14	na	17	na	17	29	24	14	29	23
Gd	134	73	73	57	na	83	na	83	85	67	57	85	73
Tb	20	8	8	7	na	10	na	10	12	10	7	12	8
Dy	108	47	47	37	na	46	na	46	72	48	37	72	47
Er	22	9	9	8	na	9	na	9	12	9	8	12	9
Yb	50	16	16	17	na	16	na	16	21	16	17	21	16
Lu	9	3	3	4	na	3	na	3	3	4	4	3	3
Hf	9	nd	nd	10	na	13	na	13	9	8	10	9	nd
B	nd	nd	nd	nd	na	143	na	143	42	36	nd	42	nd

Table 16 Continued.

Rock Unit	QMF-I	QMF-I	QMF-I	QMF-I	QMF-I	QMF-I	QMF-I	QMF-I	QMF-I	QMF-I	QMF-I	QMF-I
Sample ID	23	40	40	23	23	23	23	26	23	26	26	40
Grain ID	23c_ukn4	40d_ukn3	40d_ukn2	23c_ukn1	23c_ukn1	23c_ukn3	23c_ukn2	26a_ukn1	23c_20	26a_ukn4	26a_ukn3	40d_ukn2
Location	Core	Core	Rim	Rim	Core	Core	Rim	Core	Rim	Core	Core	Rim
ppm												
La	295	146	152	773	773	na	468	1274	na	911	1537	152
Ce	544	600	441	1531	1531	2420	761	2794	2230	2683	3393	441
Pr	72	98	59	184	184	na	81	358	na	354	424	59
Nd	317	447	255	747	747	na	279	1222	na	1457	1679	255
Sm	70	102	69	136	136	na	54	190	na	261	239	69
Eu	22	17	24	15	15	na	14	20	na	38	20	24
Gd	110	83	67	116	116	na	57	123	na	192	179	67
Tb	17	10	10	13	13	na	7	12	na	22	19	10
Dy	86	46	48	66	66	na	37	70	na	80	91	48
Er	20	9	9	12	12	na	8	13	na	15	16	9
Yb	30	16	16	23	23	na	17	21	na	29	24	16
Lu	5	3	4	4	4	na	4	5	na	5	4	4
Hf	nd	13	8	nd	nd	na	10	8	na	nd	nd	8
B	nd	143	36	nd	nd	na	nd	nd	na	nd	nd	36

Table 16 Continued.

Rock Unit	QMF-I	QMF-I	QMF-I	QMF-I	QMF-I	QMF-I	QMF-I	QMF-I	QMF-I	QMF-I	QMF-I	QMF-I
Sample ID	23	23	23	23	26	23	26	26	26	26	26	26
Grain ID	23c_ukn1	23c_ukn3	23c_ukn3	23c_ukn4	26a_ukn3	23c_ukn4	26a_ukn5	26a_ukn3	26a_ukn4	26a_ukn1	26a_ukn2	26a_ukn2
Location	Rim	Rim	Rim	Rim	Rim	Rim	Core	Rim	Core	Rim	Core	Rim
ppm												
La	773	na	nd	295	1537	295	1112	1537	911	1274	1391	1391
Ce	1531	2760	3050	544	3393	544	2479	3393	2683	2794	3858	3858
Pr	184	na	nd	72	424	72	298	424	354	358	414	414
Nd	747	na	nd	317	1679	317	1403	1679	1457	1222	1624	1624
Sm	136	na	nd	70	239	70	191	239	261	190	270	270
Eu	15	na	nd	22	20	22	20	20	38	20	30	30
Gd	116	na	nd	110	179	110	140	179	192	123	217	217
Tb	13	na	nd	17	19	17	15	19	22	12	21	21
Dy	66	na	nd	86	91	86	75	91	80	70	104	104
Er	12	na	nd	20	16	20	13	16	15	13	19	19
Yb	23	na	nd	30	24	30	24	24	29	21	32	32
Lu	4	na	nd	5	4	5	3	4	5	5	5	5
Hf	nd	na	nd	nd	nd	nd	15	nd	nd	8	nd	nd
B	nd	na	nd	nd	nd	nd	61	nd	nd	nd	nd	nd

Table 16 Continued.

Rock Unit	QMF-I	QMF-I	QMF-I	QMF-II	QMF-II	QMF-II	QMF-II	QMF-II	QMF-II	QMF-II	QMF-II	QMF-II
Sample ID	26	26	26	38	38	38	38	38	38	38	41	41
Grain ID	26a_ukn1	26a_ukn5	26a_ukn2	38d_ukn2	38d_ukn2	38d_35	38d_ukn4	38d_ukn1	38d_ukn1	38d_35	41b_ukn3	41b_ukn2
Location	Rim	Rim	Rim	Rim	Core	Rim	Rim	Rim	Rim	Rim	Core	Rim
ppm												
La	1274	1112	1391	na	nd	nd	154	127	127	na	587	410
Ce	2794	2479	3858	10	750	1020	661	510	510	30	1457	1118
Pr	358	298	414	na	nd	nd	102	83	83	na	235	193
Nd	1222	1403	1624	na	nd	nd	518	401	401	na	1124	941
Sm	190	191	270	na	nd	nd	137	114	114	na	278	380
Eu	20	20	30	na	nd	nd	24	20	20	na	44	77
Gd	123	140	217	na	nd	nd	119	108	108	na	251	387
Tb	12	15	21	na	nd	nd	16	14	14	na	35	35
Dy	70	75	104	na	nd	nd	94	76	76	na	185	164
Er	13	13	19	na	nd	nd	19	16	16	na	31	38
Yb	21	24	32	na	nd	nd	30	28	28	na	101	94
Lu	5	3	5	na	nd	nd	6	6	6	na	16	17
Hf	8	15	nd	na	nd	nd	12	10	10	na	nd	nd
B	nd	61	nd	na	nd	nd	61	nd	nd	na	nd	nd

Table 16 Continued.

Rock Unit	QMF-II	QMF-II	QMF-II	QMF-II	QMF-II	QMF-II	QMF-II	QMF-II	QMF-II	QMF-II	QMF-II	QMF-II
Sample ID	38	38	38	41	41	41	41	41	41	38	41	41
Grain ID	38d_ukn1	38d_ukn4	38d_ukn1	41b_ukn1	41b_ukn4	41b_ukn2	41b_ukn5	41b_ukn5	41b_ukn3	38d_ukn4	41b_ukn1	41b_ukn5
Location	Core	Core	Core	Rim	Rim	Rim	Rim	Rim	Rim	Rim	Rim	Rim
ppm												
La	127	154	127	na	nd	410	423	423	587	154	na	423
Ce	510	661	510	2180	1470	1118	1151	1151	1457	661	2800	1151
Pr	83	102	83	na	nd	193	213	213	235	102	na	213
Nd	401	518	401	na	nd	941	1030	1030	1124	518	na	1030
Sm	114	137	114	na	nd	380	406	406	278	137	na	406
Eu	20	24	20	na	nd	77	105	105	44	24	na	105
Gd	108	119	108	na	nd	387	394	394	251	119	na	394
Tb	14	16	14	na	nd	35	64	64	35	16	na	64
Dy	76	94	76	na	nd	164	357	357	185	94	na	357
Er	16	19	16	na	nd	38	57	57	31	19	na	57
Yb	28	30	28	na	nd	94	130	130	101	30	na	130
Lu	6	6	6	na	nd	17	25	25	16	6	na	25
Hf	10	12	10	na	nd	nd	49	49	nd	12	na	49
B	nd	61	nd	na	nd	nd	nd	nd	nd	61	na	nd

Table 16 Continued.

Rock Unit	QMF-II	QMF-II	QMF-II	QMF-II	QMF-II	QMF-II	QMF-II	QMP	QMP	QMP	QMP	QMP
Sample ID	41	41	38	41	38	38	38	02	02	02	02	02
Grain ID	41b_ukn3	41b_ukn5	38d_35	41b_ukn2	38d_ukn3	38d_ukn3	38d_ukn3	02b_ukn4	02b_ukn1	02b_ukn2	02b_27	02b_ukn1
Location	Rim	Core	Core	Core	Rim	Core	Rim	Rim	Rim	Rim	Core	Rim
ppm												
La	587	423	nd	410	na	nd	nd	186	211	204	274	211
Ce	1457	1151	80	1118	850	240	640	482	615	547	723	615
Pr	235	213	nd	193	na	nd	nd	76	95	77	88	95
Nd	1124	1030	nd	941	na	nd	nd	364	465	373	344	465
Sm	278	406	nd	380	na	nd	nd	93	137	74	64	137
Eu	44	105	nd	77	na	nd	nd	35	41	22	18	41
Gd	251	394	nd	387	na	nd	nd	118	139	55	71	139
Tb	35	64	nd	35	na	nd	nd	16	17	7	9	17
Dy	185	357	nd	164	na	nd	nd	100	108	31	55	108
Er	31	57	nd	38	na	nd	nd	22	21	8	11	21
Yb	101	130	nd	94	na	nd	nd	35	36	18	21	36
Lu	16	25	nd	17	na	nd	nd	5	4	3	3	4
Hf	nd	49	nd	nd	na	nd	nd	nd	8	14	12	8
B	nd	nd	nd	nd	na	nd	nd	nd	41	nd	39	41

Table 16 Continued.

Rock Unit	QMP	QMP	QMP	QMP	QMP	QMP	QMP	QMP	QMP	POB	POB	POB	POB
Sample ID	02	02	02	02	02	02	02	02	02	47	47	42	34
Grain ID	02b_ukn1	02b_ukn4	02b_27	02b_27	02b_ukn2	02b_ukn2	02b_ukn4	02b_ukn3	02b_ukn3	47c_ukn4	47c_ukn1	42d_31	34b_12
Location	Core	Rim	Rim	Rim	Rim	Core	Core	Core	Rim	Core	Core	Core	Core
ppm													
La	211	186	274	274	204	204	186	446	446	222	711	589	nd
Ce	615	482	723	723	547	547	482	1003	1003	481	1192	1504	910
Pr	95	76	88	88	77	77	76	121	121	76	115	173	nd
Nd	465	364	344	344	373	373	364	500	500	354	376	730	nd
Sm	137	93	64	64	74	74	93	85	85	114	60	163	nd
Eu	41	35	18	18	22	22	35	24	24	41	12	40	nd
Gd	139	118	71	71	55	55	118	71	71	141	49	145	nd
Tb	17	16	9	9	7	7	16	11	11	25	6	16	nd
Dy	108	100	55	55	31	31	100	63	63	139	32	81	nd
Er	21	22	11	11	8	8	22	13	13	29	7	16	nd
Yb	36	35	21	21	18	18	35	22	22	50	16	29	nd
Lu	4	5	3	3	3	3	5	4	4	6	3	6	nd
Hf	8	nd	12	12	14	14	nd	nd	nd	6	8	10	nd
B	41	nd	39	39	nd	nd	nd	47	47	51	37	27	nd

Table 16 Continued.

Rock Unit	POB	POB	POB	POB	POB	POB	POB	POB	POB	POB	POB	POB	POB	POB	POB
Sample ID	42	47	42	34	42	42	42	42	42	34	34	34	34	34	34
Grain ID	42d_01	47c_ukn1	42d_37	34b_05	42d_36	42d_31	42d_01	42d_36	42d_36	34a_15	34a_15	34b_06	34a_16	34b_06	34b_12
Location	Rim	Rim	Rim	Core	Rim	Rim	Core	Core	Rim	Rim	Rim	Rim	Core	Rim	Rim
ppm															
La	939	711	518	nd	545	589	939	545	545	na	nd	nd	nd	nd	nd
Ce	2692	1192	1429	1810	1096	1504	2692	1096	1096	600	520	2470	2590	1750	1690
Pr	373	115	203	nd	103	173	373	103	103	na	nd	nd	nd	nd	nd
Nd	1571	376	778	nd	333	730	1571	333	333	na	nd	nd	nd	nd	nd
Sm	321	60	201	nd	58	163	321	58	58	na	nd	nd	nd	nd	nd
Eu	36	12	48	nd	13	40	36	13	13	na	nd	nd	nd	nd	nd
Gd	347	49	186	nd	53	145	347	53	53	na	nd	nd	nd	nd	nd
Tb	54	6	25	nd	8	16	54	8	8	na	nd	nd	nd	nd	nd
Dy	346	32	116	nd	42	81	346	42	42	na	nd	nd	nd	nd	nd
Er	75	7	22	nd	10	16	75	10	10	na	nd	nd	nd	nd	nd
Yb	141	16	37	nd	22	29	141	22	22	na	nd	nd	nd	nd	nd
Lu	20	3	5	nd	4	6	20	4	4	na	nd	nd	nd	nd	nd
Hf	nd	8	nd	nd	9	10	nd	9	9	na	nd	nd	nd	nd	nd
B	36	37	nd	nd	nd	27	36	nd	nd	na	nd	nd	nd	nd	nd

Table 16 Continued.

Rock Unit	POB	POB	POB	POB	POB	POB	POB	POB	POB	POB	FP	FP	FP	FP	FP
Sample ID	42	34	47	34	42	34	47	34	34	42	13	13	13	13	13
Grain ID	42d_37	34b_05	47c_ukn3	34a_15	42d_01	34b_05	47c_ukn5	34a_16	34b_06	42d_37	13a_24	13a_24	13a_45	13a_45	13a_33
Location	Core	Rim	Rim	Core	Rim	Rim	Core	Rim	Core	Rim	Core	Rim	Rim	Core	Rim
ppm															
La	518	na	480	na	939	na	93	na	nd	518	na	nd	nd	nd	346
Ce	1429	2670	872	3460	2692	2160	187	2110	2270	1429	620	930	850	2710	995
Pr	203	na	97	na	373	na	24	na	nd	203	na	nd	nd	nd	193
Nd	778	na	361	na	1571	na	106	na	nd	778	na	nd	nd	nd	872
Sm	201	na	71	na	321	na	65	na	nd	201	na	nd	nd	nd	287
Eu	48	na	17	na	36	na	25	na	nd	48	na	nd	nd	nd	49
Gd	186	na	61	na	347	na	60	na	nd	186	na	nd	nd	nd	214
Tb	25	na	12	na	54	na	8	na	nd	25	na	nd	nd	nd	30
Dy	116	na	45	na	346	na	55	na	nd	116	na	nd	nd	nd	163
Er	22	na	11	na	75	na	14	na	nd	22	na	nd	nd	nd	37
Yb	37	na	21	na	141	na	20	na	nd	37	na	nd	nd	nd	83
Lu	5	na	4	na	20	na	4	na	nd	5	na	nd	nd	nd	17
Hf	nd	na	nd	na	nd	na	nd	na	nd	nd	na	nd	nd	nd	nd
B	nd	na	50	na	36	na	nd	na	nd	nd	na	nd	nd	nd	nd

Table 16 Continued.

Rock Unit	FP	FP	FP	FP	FP	FP	FP	FP	FP	FP	FP	FP	FP
Sample ID	13	13	12	13	12	12	13	12	12	12	13	12	13
Grain ID	13a_33	13a_45	12a_ukn2	13a_33	12a_ukn2	12a_ukn3	13a_17	12a_ukn4	12a_ukn1	12a_ukn3	13a_24	12a_ukn3	13a_17
Location	Rim	Rim	Core	Core	Rim	Rim	Rim	Core	Core	Rim	Rim	Core	Rim
ppm													
La	346	na	616	346	616	669	na	568	786	669	na	669	na
Ce	995	980	1408	995	1408	1804	1860	1241	1525	1804	850	1804	1660
Pr	193	na	208	193	208	254	na	135	184	254	na	254	na
Nd	872	na	992	872	992	1049	na	516	736	1049	na	1049	na
Sm	287	na	230	287	230	205	na	102	123	205	na	205	na
Eu	49	na	35	49	35	28	na	16	nd	28	na	28	na
Gd	214	na	205	214	205	147	na	94	102	147	na	147	na
Tb	30	na	28	30	28	17	na	9	nd	17	na	17	na
Dy	163	na	146	163	146	85	na	45	54	85	na	85	na
Er	37	na	29	37	29	16	na	12	nd	16	na	16	na
Yb	83	na	59	83	59	56	na	29	30	56	na	56	na
Lu	17	na	9	17	9	12	na	6	6	12	na	12	na
Hf	nd	na	nd	nd	nd	1173	na	nd	14	1173	na	1173	na
B	nd	na	51	nd	51	157	na	nd	nd	157	na	157	na

Table 16 Continued.

Rock Unit	FP	FP	FP	FP	FP	DLP	DLP	DLP	DLP	DLP	DLP	DLP
Sample ID	12	12	12	12	12	16	16	16	16	16	16	16
Grain ID	12a_ukn5	12a_ukn2	12a_ukn1	12a_ukn1	12a_ukn5	16a_ukn5	16a_ukn6	16a_ukn4	16a_ukn6	16a_ukn1	16a_ukn4	16a_ukn1
Location	Rim	Rim	Rim	Rim	Core	Core	Rim	Rim	Core	Core	Core	Rim
ppm												
La	677	616	786	786	677	na	680	464	680	588	464	588
Ce	1278	1408	1525	1525	1278	110	1262	1502	1262	1164	1502	1164
Pr	161	208	184	184	161	na	157	188	157	121	188	121
Nd	615	992	736	736	615	na	643	832	643	429	832	429
Sm	91	230	123	123	91	na	111	193	111	73	193	73
Eu	22	35	nd	nd	22	na	35	26	35	14	26	14
Gd	66	205	102	102	66	na	89	142	89	66	142	66
Tb	9	28	nd	nd	9	na	9	15	9	7	15	7
Dy	40	146	54	54	40	na	36	59	36	36	59	36
Er	9	29	nd	nd	9	na	13	10	13	7	10	7
Yb	26	59	30	30	26	na	15	22	15	16	22	16
Lu	6	9	6	6	6	na	4	4	4	3	4	3
Hf	17	nd	14	14	17	na	19	223	19	17	223	17
B	52	51	nd	nd	52	na	93	nd	93	51	nd	51

Table 16 Continued.

Rock Unit	DLP	DLP	DLP	DLP	DLP	DLP	DLP	DLP	DLP	DLP	DLP	DLP
Sample ID	16	16	16	16	16	17	16	16	17	17	16	17
Grain ID	16a_ukn6	16a_ukn1	16a_ukn3	16a_ukn3	16a_ukn3	17b_ukn2	16a_ukn4	16a_ukn5	17b_18	17b_ukn2	16a_ukn5	17b_ukn1
Location	Rim	Rim	Rim	Core	Rim	Core	Rim	Rim	Core	Rim	Rim	Core
ppm												
La	680	588	641	641	641	719	464	na	707	719	na	785
Ce	1262	1164	1304	1304	1304	1203	1502	1300	1254	1203	640	1237
Pr	157	121	120	120	120	142	188	na	142	142	na	129
Nd	643	429	376	376	376	578	832	na	564	578	na	485
Sm	111	73	61	61	61	85	193	na	91	85	na	78
Eu	35	14	14	14	14	20	26	na	19	20	na	17
Gd	89	66	47	47	47	74	142	na	78	74	na	63
Tb	9	7	6	6	6	8	15	na	9	8	na	10
Dy	36	36	25	25	25	40	59	na	41	40	na	28
Er	13	7	6	6	6	8	10	na	10	8	na	7
Yb	15	16	15	15	15	23	22	na	27	23	na	29
Lu	4	3	3	3	3	5	4	na	7	5	na	11
Hf	19	17	nd	nd	nd	18	223	na	nd	18	na	nd
B	93	51	35	35	35	49	nd	na	50	49	na	55

Table 16 Continued.

Rock Unit	DLP	DLP	DLP	DLP	DLP	DLP	DLP	DLP	DLP	DLP	DLP
Sample ID	17	17	17	17	17	17	17	17	17	17	17
Grain ID	17b_33	17b_33	17b_18	17b_32	17b_32	17b_ukn2	17b_33	17b_ukn1	17b_32	17b_ukn1	17b_18
Location	Rim	Core	Rim	Core	Rim	Rim	Rim	Rim	Rim	Rim	Rim
ppm											
La	801	801	707	815	815	719	801	785	815	785	707
Ce	1538	1538	1254	1405	1405	1203	1538	1237	1405	1237	1254
Pr	171	171	142	149	149	142	171	129	149	129	142
Nd	665	665	564	545	545	578	665	485	545	485	564
Sm	97	97	91	87	87	85	97	78	87	78	91
Eu	22	22	19	19	19	20	22	17	19	17	19
Gd	90	90	78	75	75	74	90	63	75	63	78
Tb	11	11	9	8	8	8	11	10	8	10	9
Dy	43	43	41	36	36	40	43	28	36	28	41
Er	11	11	10	9	9	8	11	7	9	7	10
Yb	36	36	27	22	22	23	36	29	22	29	27
Lu	7	7	7	8	8	5	7	11	8	11	7
Hf	22	22	nd	109	109	18	22	nd	109	nd	nd
B	54	54	50	48	48	49	54	55	48	55	50

APPENDIX D

RELATIVE STANDARD ERROR AND LIMITS OF DETECTION FOR LA-ICP-MS ANALYSES

This appendix contains the relative standard error and limits of detection for LA-ICP-MS analyses (Table 17).

Table 17. Relative Standard Error and Limits of Detection for LA-ICP-MS Analysis of Individual Apatite Grains.

Grain ID	02b_27	02b_ukn1	02b_ukn2	02b_ukn3	02b_ukn4	12a_ukn1	12a_ukn2	12a_ukn3	12a_ukn4	12a_ukn5	13a_33	16a_ukn1
1σ												
La	15.4	12.7	10.6	15.8	8.1	16.2	32.9	31.2	43.2	15.4	34.0	35.1
Ce	51.0	42.5	33.5	59.7	23.9	36.0	59.1	120.7	107.7	29.5	71.0	64.2
Pr	5.1	5.9	3.9	7.9	4.6	6.3	9.3	15.3	11.7	5.3	15.7	8.0
Nd	21.7	37.1	27.6	34.2	20.8	35.9	62.0	66.5	47.2	26.9	53.1	29.5
Sm	5.8	16.7	7.7	6.1	7.3	9.7	19.0	18.6	12.3	7.4	28.3	5.4
Eu	1.7	4.2	2.6	1.9	2.2	nd	3.7	2.6	1.3	1.7	6.4	1.3
Gd	8.6	14.0	4.8	7.0	6.6	8.9	17.9	15.6	10.0	4.6	19.8	5.1
Tb	0.8	1.7	0.8	1.2	1.0	nd	2.4	2.2	1.2	0.8	3.0	0.5
Dy	6.9	10.9	2.8	7.6	5.9	6.7	14.7	10.9	4.6	3.2	16.1	3.6
Yb	1.9	2.6	2.3	1.4	2.9	2.2	5.8	11.1	3.8	1.6	0.6	0.9
Lu	0.3	0.2	0.4	0.4	0.4	0.6	0.8	3.6	0.3	0.6	nd	0.4
Hf	nd	nd	3.5	nd	nd	1.3	nd	525.3	nd	nd	nd	7.5
B	5.6	3.2	nd	nd	nd	nd	nd	nd	nd	6.8	nd	5.5
LOD												
La	4	3	5	4	4	167	8	8	7	6	19	5
Ce	3	2	3	3	3	4	6	6	7	5	17	2
Pr	3	3	3	3	4	116	4	4	5	4	14	3
Nd	16	15	21	20	18	31	28	32	25	37	78	11
Sm	19	23	19	18	18	28	40	26	25	33	124	26
Eu	4	4	4	7	6	222	9	8	8	8	21	4
Gd	22	18	17	22	23	38	34	27	37	37	83	26
Tb	3	2	3	3	4	141	4	4	4	5	13	3
Dy	13	13	11	7	13	21	22	26	18	19	53	10
Yb	8	11	9	9	9	19	20	22	20	17	67	11
Lu	2	2	2	2	2	4	4	5	5	4	14	2
Hf	7	7	6	5	8	10	15	14	12	16	47	7
B	31	34	30	36	30	75	50	59	48	40	103	33

nd – not detected, na – not analyzed.

Table 17 Continued.

Grain ID	16a_ukn2	16a_ukn3	16a_ukn4	16a_ukn6	17b_18	17b_32	17b_33	17b_ukn1	17b_ukn2	21d_07	21d_38	21d_45
1σ												
La	40.5	24.3	22.6	38.4	14.2	21.3	19.9	17.8	29.5	23.3	20.6	19.2
Ce	105.9	70.3	91.0	119.5	33.4	50.2	38.6	38.6	61.9	72.5	86.4	67.0
Pr	16.6	5.7	13.1	21.8	4.4	7.6	5.1	4.7	7.4	12.3	10.0	11.1
Nd	86.3	20.7	66.4	95.0	21.8	29.4	18.9	23.0	34.1	56.9	38.6	48.9
Sm	23.2	5.1	14.2	23.2	4.9	4.7	6.2	8.9	7.3	16.9	9.3	8.7
Eu	4.2	1.5	2.2	7.2	1.2	1.2	1.3	1.9	1.7	0.9	0.9	0.5
Gd	11.0	3.5	10.4	14.0	5.1	4.2	5.2	5.6	6.5	11.5	8.1	6.9
Tb	1.5	0.6	1.5	1.5	0.6	0.6	0.9	1.4	0.8	1.7	1.1	1.0
Dy	6.8	2.3	5.4	5.3	2.9	2.5	2.9	2.4	4.2	7.6	5.9	5.0
Yb	1.6	1.6	4.2	1.9	0.3	1.3	3.2	3.2	2.1	2.1	1.9	1.9
Lu	3.7	nd	0.5	0.5	0.5	1.0	0.5	nd	0.5	0.4	0.3	0.3
Hf	8.8	nd	80.6	nd	nd	26.8	1.9	nd	nd	nd	nd	3.0
B	1.5	nd	nd	14.3	2.1	1.9	2.6	nd	5.8	7.6	3.8	nd
LOD												
La	4	3	5	5	8	6	6	9	8	4	6	5
Ce	5	2	3	2	5	4	5	6	5	4	7	3
Pr	2	2	3	3	5	4	4	5	4	4	4	3
Nd	15	18	22	29	29	29	30	25	25	25	28	20
Sm	23	28	21	20	31	26	32	40	34	36	25	18
Eu	5	5	5	5	8	8	10	9	8	9	7	7
Gd	22	30	23	17	31	45	29	32	35	30	27	24
Tb	3	3	4	3	6	4	4	5	4	4	3	3
Dy	12	10	12	11	21	15	16	17	21	16	15	12
Yb	8	9	11	10	26	15	17	23	15	13	9	14
Lu	2	3	3	2	5	5	5	5	4	3	3	3
Hf	7	10	6	6	15	16	13	14	17	11	9	8
B	32	32	36	28	42	43	44	55	42	34	31	41

Table 17 Continued.

Grain ID	21d_ukn1	23c_ukn1	23c_ukn2	23c_ukn4	26a_ukn1	26a_ukn2	26a_ukn3	26a_ukn4	26a_ukn5	38d_ukn1	38d_ukn4	40d_ukn1
1σ												
La	24.3	22.4	20.0	59.3	52.7	68.4	258.6	88.1	46.4	5.7	10.2	9.9
Ce	99.6	46.4	40.9	67.4	153.4	182.9	474.3	646.7	126.4	27.2	59.7	27.6
Pr	18.7	7.7	4.4	14.2	23.8	26.8	55.1	98.4	15.8	3.9	11.0	3.4
Nd	127.6	27.4	16.0	55.0	91.1	89.6	208.1	331.5	128.9	22.8	56.8	17.6
Sm	23.3	5.4	4.1	10.4	19.6	20.0	25.1	72.0	14.6	9.5	18.0	7.8
Eu	1.9	1.1	0.9	4.6	1.7	2.7	1.4	8.4	2.4	1.2	3.1	2.2
Gd	22.5	7.2	4.5	25.4	13.0	25.7	13.8	40.5	12.4	7.8	17.4	9.2
Tb	2.9	0.7	0.5	2.9	1.1	1.4	1.8	5.4	1.5	1.0	2.0	0.8
Dy	18.1	4.5	2.4	12.3	7.8	14.1	6.6	15.5	6.6	5.0	10.1	4.4
Yb	3.5	1.4	1.4	2.6	1.2	3.1	1.7	4.4	2.5	1.7	2.4	1.1
Lu	0.3	0.3	0.4	0.5	0.4	0.6	0.4	0.8	0.4	0.6	0.4	0.4
Hf	4.6	nd	2.6	nd	0.6	nd	nd	nd	1.6	0.8	0.4	nd
B	149.9	nd	nd	nd	nd	nd	nd	nd	1.1	nd	nd	nd
LOD												
La	7	4	5	5	5	4	5	7	6	5	6	4
Ce	3	2	3	3	3	3	4	3	4	4	4	3
Pr	4	2	2	2	4	3	3	3	2	3	4	2
Nd	26	14	15	17	16	20	22	20	19	23	20	22
Sm	33	15	18	20	21	25	24	29	29	27	26	10
Eu	6	4	6	5	6	4	5	6	6	5	6	4
Gd	23	25	14	20	30	24	28	28	37	38	20	15
Tb	4	2	3	3	3	4	4	4	4	3	4	3
Dy	13	9	10	10	14	14	15	15	12	19	14	10
Yb	13	7	6	8	13	10	10	10	12	12	14	8
Lu	3	2	2	1	3	2	3	2	2	3	3	2
Hf	8	8	6	6	7	7	11	9	9	8	9	7
B	39	25	25	26	69	68	52	66	55	68	59	31

Table 17 Continued.

Grain ID	40d_ukn2	40d_ukn3	40d_ukn4	41b_ukn2	41b_ukn3	41b_ukn5	42d_01	42d_31	42d_36	42d_37	47c_ukn1	47c_ukn2
1σ												
La	6.5	6.8	15.1	24.4	21.9	23.1	59.6	22.6	28.0	21.2	16.8	34.8
Ce	17.5	22.1	74.9	107.9	68.5	101.6	174.0	89.0	49.3	107.5	36.7	86.6
Pr	2.8	3.6	12.3	23.5	9.6	27.2	18.5	15.1	3.6	19.8	3.7	11. 0
Nd	11.4	16.7	41.3	108.2	59.5	133.5	76.1	92.3	9.5	95. 7	14.6	52.5
Sm	3.5	3.8	14.0	61.8	15.0	58.3	18.2	21.4	2.8	28.7	3.7	13.6
Eu	1.3	0.8	4.6	13.0	2.5	12.2	2.1	8.6	0.7	6.8	0.8	3.4
Gd	4.8	3.9	11.5	52.8	14.9	39.2	21.1	21.6	3.1	27.2	3.6	13.1
Tb	0.6	0.4	1.4	3.3	2.2	8.1	3.4	1.9	0.6	3.3	0.4	2.6
Dy	2.6	2.0	8.1	17.5	12.5	38.5	26.7	9.4	3.4	15.1	2.8	16.4
Yb	0.9	0.7	1.8	15.1	8.0	15.7	11.2	3.2	1.6	5.1	1.4	5.1
Lu	0.5	0.2	0.2	1.4	1.4	4.5	1.6	0.6	0.3	0.4	0.2	0.8
Hf	nd	nd	0.2	nd	nd	nd	nd	nd	0.4	nd	nd	nd
B	3.9	66.6	1.8	nd	nd	nd	2.1	nd	nd	nd	1.4	6.4
LOD												
La	4	3	5	16	17	19	3	3	4	5	4	4
Ce	3	4	3	15	15	17	3	3	3	3	2	3
Pr	4	2	2	14	13	13	2	2	3	3	2	3
Nd	23	19	18	107	91	110	16	15	17	15	14	21
Sm	19	21	19	97	74	91	18	17	17	23	15	15
Eu	5	6	4	21	22	25	3	3	5	5	6	4
Gd	27	24	27	117	104	117	18	21	20	28	20	15
Tb	3	3	3	15	17	15	3	3	3	3	2	2
Dy	15	14	16	49	62	55	13	10	11	13	9	10
Yb	7	8	10	68	71	76	8	9	12	7	8	7
Lu	3	2	2	14	13	13	2	2	2	2	2	2
Hf	7	9	7	40	45	48	9	8	7	7	6	7
B	29	33	32	82	99	101	28	23	22	24	34	45

Table 17 Continued.

Grain ID	47c_ukn3	47c_ukn4	47c_ukn5	47c_ukn6	48a_09	48a_13	48a_14g2	48a_21
1σ								
La	27.1	19.5	8.6	4.5	10.5	7.7	5.5	7. 7
Ce	58.9	51.7	20.1	12.1	35.9	33.2	22.2	64.3
Pr	7.0	10.0	3.1	2.9	6.1	5.3	2.4	10.6
Nd	25.0	66.5	14.4	14.0	29.7	27.0	9.7	62.2
Sm	8.3	24.9	9.8	7.6	9.8	7.6	4.0	20.7
Eu	2.6	7.2	2.8	3.3	2.8	1.9	0.6	5.0
Gd	8.0	31.5	10.6	5.6	12.9	9.0	2.9	23.6
Tb	2.6	3.9	1.1	1.9	2.1	1.2	0.6	4.9
Dy	6.0	20.9	11.5	9.5	12.0	7.3	1.6	26.8
Yb	3.0	7.8	2.1	3.8	4.4	2.7	0.5	6.1
Lu	0.4	0.8	0.9	0.7	0.5	0.5	0.2	0.6
Hf	nd	nd	nd	nd	0.6	nd	nd	nd
B	4.4	10.0	nd	nd	nd	nd	nd	5.1
LOD								
La	4	4	4	4	3	5	4	4
Ce	4	3	3	3	4	4	4	5
Pr	3	3	2	3	3	4	5	4
Nd	16	16	21	19	26	24	24	23
Sm	21	21	22	17	26	30	29	22
Eu	4	4	4	4	7	6	7	5
Gd	19	24	18	22	18	30	24	30
Tb	4	3	3	4	4	4	6	4
Dy	10	9	15	11	15	20	14	14
Yb	7	8	10	9	11	11	14	13
Lu	2	2	2	2	3	2	3	3
Hf	7	5	6	6	7	8	8	10
B	44	36	36	37	33	39	40	35

APPENDIX E

APATITE FORMULA UNIT

This appendix contains calculated atoms per apatite formula unit for analyses of apatite grains (Table 18). Atoms per formula unit are based on 16 cation M + Z site occupancy. One hundred ninety two analyses from 71 apatite grains are included.

Table 18. Atoms per Formula Unit for Analyses of Apatite Grains.

Rock Unit	FLA	FLA	FLA	FLA	FLA	FLA	FLA	FLA	FLA	FLA	FLA	FLA	FLA	FLA
Sample ID	21	21	21	21	21	21	21	21	21	21	21	21	21	21
Grain ID	21d_07	21d_38	21d_07	21d_45	21d_ukn1	21d_45	21d_07	21d_38	21d_ukn1	21d_45	21d_38	21d_39	21d_39	21d_ukn1
Anal. Location	Rim	Core	Rim	Rim	Rim	Rim	Core	Rim	Core	Core	Rim	Rim	Core	Rim
Ca	9.971	10.024	10.019	10.032	10.070	10.064	10.011	10.030	9.958	10.138	9.950	10.063	10.027	10.072
P	5.937	5.857	5.851	5.824	5.822	5.837	5.917	5.869	5.919	5.763	5.885	5.849	5.896	5.805
Sr	nd	nd	0.007	0.004	nd	nd	nd	nd	0.006	nd	0.007	0.007	0.007	nd
Ba	0.003	nd	nd	nd	nd		nd	nd	nd	nd	nd	nd	nd	nd
Na	nd	nd	0.018	0.023	nd	nd	nd	nd	nd	0.014	nd	nd	nd	nd
K	nd	nd	nd	nd	nd	nd	0.010	nd	nd	nd	nd	nd	nd	nd
Mg	nd	nd	nd	nd	nd	nd	nd	nd	nd	nd	nd	nd	nd	nd
Ti	nd	nd	nd	nd	nd	nd	nd	nd	nd	nd	nd	nd	nd	nd
Mn	0.016	0.009	0.021	0.019	0.014	0.011	0.015	nd	0.016	0.015	0.018	0.009	0.015	0.015
Fe	0.021	0.013	0.025	0.011	0.016	0.007	0.023	0.015	0.008	nd	0.013	0.010	nd	0.009
Cu	nd	0.011	nd	nd	nd	0.005	nd	0.007	nd	nd	0.006	nd	0.009	0.010
S	0.010	nd	0.012	0.014	nd	nd	nd	nd	nd	nd	nd	nd	nd	nd
B	0.004	0.004	0.004	0.005	0.023	0.005	0.004	0.004	0.023	0.005	0.004	nd	na	0.023
Si	0.017	0.043	0.017	0.032	0.022	0.034	nd	0.037	0.022	0.029	0.073	0.037	0.030	0.032
As	nd	nd	0.006	nd	nd	nd	nd	nd	0.008	nd	0.004	0.005	nd	nd
V	nd	nd	nd	nd	nd	nd	nd	nd	0.007	nd	nd	nd	nd	nd
F	1.97	1.91	1.92	1.91	1.97	1.95	1.97	1.92	1.94	1.89	1.94	1.96	1.91	1.97
Cl	0.27	0.13	0.29	0.17	0.15	0.14	0.29	0.13	0.18	0.15	0.14	0.13	0.15	0.13
O	23.81	23.80	23.69	23.73	23.66	23.73	23.73	23.81	23.79	23.63	23.85	23.77	23.85	23.65

nd – not detected, na – not analyzed.

Table 18 Continued.

Rock Unit	FLA	FLA	FLA	FLA	FLA	FLA	FLA	FLA	FLA	FLA	FLA	FLA	FLA	FLA
Sample ID	21	21	21	21	21	21	21	21	21	21	21	21	21	21
Grain ID	21d_07	21d_38	21d_07	21d_45	21d_ukn1	21d_45	21d_07	21d_38	21d_ukn1	21d_45	21d_38	21d_39	21d_39	21d_ukn1
Anal. Location	Rim	Core	Rim	Rim	Rim	Rim	Core	Rim	Core	Core	Rim	Rim	Core	Rim
La	0.003	0.005	0.003	0.005	0.003	0.005	0.003	0.005	0.003	0.005	0.005	na	na	0.003
Ce	0.008	0.018	0.008	0.015	0.012	0.015	0.008	0.018	0.012	0.015	0.018	0.019	0.015	0.012
Pr	0.0011	0.0023	0.0011	0.0021	0.0019	0.0021	0.0011	0.0023	0.0019	0.0021	0.0023	na	na	0.0020
Nd	0.0047	0.0091	0.0047	0.0092	0.0095	0.0092	0.0047	0.0091	0.0096	0.0092	0.0092	na	na	0.0096
Sm	0.0011	0.0017	0.0011	0.0017	0.0020	0.0017	0.0011	0.0017	0.0020	0.0017	0.0017	na	na	0.0020
Eu	0.0001	0.0001	0.0001	0.0001	0.0001	0.0001	0.0001	0.0001	0.0001	0.0001	0.0001	na	na	0.0001
Gd	0.0009	0.0013	0.0009	0.0014	0.0018	0.0014	0.0009	0.0013	0.0018	0.0014	0.0013	na	na	0.0018
Tb	0.0001	0.0002	0.0001	0.0002	0.0002	0.0002	0.0001	0.0002	0.0002	0.0002	0.0002	na	na	0.0002
Dy	0.0005	0.0009	0.0006	0.0010	0.0013	0.0010	0.0006	0.0009	0.0013	0.0010	0.0009	na	na	0.0014
Er	0.0001	0.0002	0.0001	0.0002	0.0002	0.0002	0.0001	0.0002	0.0002	0.0002	0.0002	na	na	0.0002
Ho	0.0003	0.0004	0.0003	0.0005	0.0006	0.0005	0.0003	0.0004	0.0006	0.0005	0.0004	na	na	0.0006
Yb	0.0002	0.0003	0.0002	0.0003	0.0003	0.0003	0.0002	0.0003	0.0003	0.0003	0.0003	na	na	0.0003
Lu	0.0000	0.0000	0.0000	0.0000	0.0000	0.0000	0.0000	0.0000	0.0000	0.0000	0.0000	na	na	0.0000
Hf	0.0001	nd	0.0001	0.0001	0.0001	0.0001	0.0001	nd	0.0001	0.0001	nd	na	na	0.0001
Total (+)	49.92	49.72	49.66	49.63	49.58	49.64	49.78	49.74	49.89	49.39	49.87	49.65	49.76	49.55
Total (-)	-49.87	-49.64	-49.59	-49.54	-49.44	-49.55	-49.72	-49.66	-49.70	-49.31	-49.77	-49.63	-49.76	-49.41
Charge Diff.	0.06	0.08	0.07	0.09	0.14	0.09	0.06	0.08	0.19	0.09	0.10	0.02	0.00	0.14
X Site Total	2.24	2.03	2.21	2.08	2.12	2.10	2.26	2.05	2.12	2.04	2.07	2.09	2.06	2.10

Table 18 Continued.

Rock Unit	FLA	FLA	QMG	QMG	QMG	QMG	QMG	QMG	QMG	QMG	QMG	QMG
Sample ID	21	21	48	48	48	48	48	48	48	48	48	48
Grain ID	21d_39	21d_ukn1	48a_13	48a_14g1	48a_09	48a_21	48a_13	48a_14g1	48a_21	48a_09	48a_09	48a_21
Anal. Location	Core	Rim	Rim	Rim	Rim	Core	Core	Core	Rim	Rim	Core	Rim
Ca	10.027	10.072	10.006	10.105	10.091	10.007	10.025	10.130	10.038	10.006	10.031	10.018
P	5.896	5.805	5.911	5.846	5.818	5.889	5.886	5.844	5.835	5.884	5.878	5.822
Sr	0.007	nd	nd	nd	nd	nd	0.009	nd	0.010	nd	nd	nd
Ba	nd	nd	nd	nd	nd	nd	nd	nd	nd	nd	nd	nd
Na	nd	nd	nd	nd	nd	nd	nd	nd	nd	nd	nd	nd
K	nd	nd	nd	nd	nd	nd	nd	nd	nd	nd	nd	nd
Mg	nd	nd	nd	nd	nd	nd	nd	nd	nd	nd	nd	nd
Ti	nd	nd	nd	nd	0.009	0.007	nd	nd	nd	0.030	nd	0.022
Mn	0.015	0.015	0.018	0.012	0.014	0.028	0.016	nd	0.026	0.017	0.013	0.022
Fe	nd	0.009	0.051	0.034	0.055	0.038	0.030	0.026	0.049	0.037	0.035	0.065
Cu	0.009	0.010	nd	nd	nd	nd	nd	nd	0.008	nd	0.014	0.007
S	nd	nd	nd	nd	nd	nd	nd	nd	nd	nd	nd	nd
B	na	0.023	nd	na	0.003	0.004	nd	na	0.004	0.003	0.003	0.004
Si	0.030	0.032	nd	nd	nd	0.011	0.018	nd	0.014	0.013	0.015	0.013
As	nd	nd	nd	nd	nd	nd	nd	nd	nd	nd	nd	0.011
V	nd	nd	nd	nd	nd	nd	nd	nd	nd	nd	nd	nd
F	1.91	1.97	2.00	2.06	1.94	2.02	1.89	1.97	2.01	1.99	1.95	2.02
Cl	0.15	0.13	0.03	0.02	0.03	0.06	0.05	0.02	0.07	0.04	0.03	0.10
O	23.85	23.65	23.84	23.73	23.74	23.80	23.87	23.77	23.71	23.84	23.83	23.69

Table 18 Continued.

Rock Unit	FLA	FLA	QMG	QMG	QMG	QMG	QMG	QMG	QMG	QMG	QMG	QMG
Sample ID	21	21	48	48	48	48	48	48	48	48	48	48
Grain ID	21d_39	21d_ukn1	48a_13	48a_14g1	48a_09	48a_21	48a_13	48a_14g1	48a_21	48a_09	48a_09	48a_21
Anal. Location	Core	Rim	Rim	Rim	Rim	Core	Core	Core	Rim	Rim	Core	Rim
La	na	0.003	0.001	na	0.001	0.001	0.001	na	0.001	0.001	0.001	0.001
Ce	0.015	0.012	0.005	0.003	0.003	0.005	0.005	na	0.005	0.003	0.003	0.005
Pr	na	0.0020	0.0008	na	0.0005	0.0008	0.0008	na	0.0008	0.0005	0.0005	0.0008
Nd	na	0.0096	0.0034	na	0.0022	0.0038	0.0034	na	0.0038	0.0022	0.0022	0.0038
Sm	na	0.0020	0.0008	na	0.0007	0.0011	0.0009	na	0.0011	0.0007	0.0007	0.0012
Eu	na	0.0001	0.0002	na	0.0002	0.0003	0.0002	na	0.0003	0.0002	0.0002	0.0003
Gd	na	0.0018	0.0009	na	0.0007	0.0013	0.0009	na	0.0013	0.0007	0.0007	0.0013
Tb	na	0.0002	0.0001	na	0.0001	0.0002	0.0001	na	0.0002	0.0001	0.0001	0.0002
Dy	na	0.0014	0.0007	na	0.0006	0.0014	0.0007	na	0.0014	0.0006	0.0006	0.0014
Er	na	0.0002	0.0001	na	0.0001	0.0003	0.0001	na	0.0003	0.0001	0.0001	0.0003
Ho	na	0.0006	0.0004	na	0.0004	0.0006	0.0004	na	0.0006	0.0004	0.0004	0.0006
Yb	na	0.0003	0.0003	na	0.0003	0.0005	0.0003	na	0.0005	0.0003	0.0003	0.0005
Lu	na	0.0000	0.0000	na	0.0000	0.0001	0.0000	na	0.0001	0.0000	0.0000	0.0001
Hf	na	0.0001	0.0001	na	0.0001	nd	0.0001	na	nd	0.0001	0.0001	nd
Total (+)	49.76	49.55	49.75	49.54	49.49	49.73	49.72	49.53	49.56	49.76	49.68	49.57
Total (-)	-49.76	-49.41	-49.72	-49.54	-49.45	-49.68	-49.68	-49.53	-49.51	-49.72	-49.64	-49.49
Charge Diff.	0.00	0.14	0.03	0.00	0.04	0.05	0.03	0.00	0.05	0.04	0.04	0.09
X Site Total	2.06	2.10	2.04	2.08	1.97	2.08	1.94	2.00	2.08	2.03	1.98	2.11

Table 18 Continued.

Rock Unit	QMG	QMG	QMG	QMG	QMF-I	QMF-I	QMF-I	QMF-I	QMF-I	QMF-I	QMF-I	QMF-I
Sample ID	48	48	48	48	40	26	40	26	40	26	40	23
Grain ID	48a_14g1	48a_14g2	48a_14g2	48a_14g2	40d_ukn1	26a_ukn4	40d_ukn1	26a_ukn3	40d_ukn3	26a_ukn2	40d_ukn2	23c_ukn3
Anal. Location	Rim	Rim	Core	Rim	Rim	Core	Core	Core	Rim	Rim	Core	Core
Ca	10.160	10.073	10.141	10.216	9.933	9.823	9.947	9.939	9.901	9.802	9.983	9.916
P	5.778	5.881	5.817	5.709	6.005	5.904	5.947	5.965	6.003	5.856	5.932	5.904
Sr	nd	nd	0.005	0.005	0.007	nd	0.015	0.006	0.006	0.012	0.006	nd
Ba	nd	nd	0.003	nd	nd	nd	nd	nd	nd	nd	nd	nd
Na	nd	nd	nd	nd	nd	0.061	nd	nd	nd	0.040	nd	0.032
K	nd	nd	nd	nd	nd	0.033	nd	nd	nd	nd	nd	nd
Mg	nd	nd	nd	nd	nd	nd	nd	nd	nd	nd	nd	nd
Ti	nd	nd	nd	nd	nd	nd	nd	nd	nd	nd	nd	nd
Mn	0.008	0.008	0.009	0.013	0.022	0.010	0.045	nd	0.029	0.037	0.030	0.023
Fe	0.031	0.023	0.017	0.036	0.018	0.007	0.040	nd	0.038	0.135	0.037	0.020
Cu	nd	nd	nd	nd	0.008	nd	nd	0.012	nd	nd	nd	0.017
S	nd	nd	nd	nd	nd	0.069	nd	nd	nd	0.025	nd	0.035
B	na	nd	nd	nd	nd	nd	nd	nd	0.013	nd	0.003	na
Si	0.014	nd	nd	0.012	nd	0.051	nd	0.024	nd	0.036	nd	0.036
As	nd	nd	nd	nd	nd	nd	nd	nd	nd	nd	nd	nd
V	nd	0.007	nd	nd	nd	nd	nd	nd	nd	nd	nd	nd
F	2.01	2.05	1.94	2.02	2.04	1.92	1.98	1.95	2.01	1.89	1.99	1.98
Cl	0.04	0.02	0.03	0.04	0.04	0.48	0.08	0.17	0.04	0.58	0.06	0.08
O	23.66	23.78	23.74	23.54	23.96	23.79	23.88	23.91	23.96	23.61	23.86	23.93

Table 18 Continued.

Rock Unit	QMG	QMG	QMG	QMG	QMF-I	QMF-I	QMF-I	QMF-I	QMF-I	QMF-I	QMF-I	QMF-I
Sample ID	48	48	48	48	40	26	40	26	40	26	40	23
Grain ID	48a_14g1	48a_14g2	48a_14g2	48a_14g2	40d_ukn1	26a_ukn4	40d_ukn1	26a_ukn3	40d_ukn3	26a_ukn2	40d_ukn2	23c_ukn3
Anal. Location	Rim	Rim	Core	Rim	Rim	Core	Core	Core	Rim	Rim	Core	Core
La	na	0.001	0.001	0.001	0.001	0.007	0.001	0.011	0.001	0.010	0.001	na
Ce	0.009	0.004	0.004	0.004	0.003	0.019	0.003	0.024	0.004	0.028	0.003	0.017
Pr	na	0.0005	0.0005	0.0005	0.0004	0.0025	0.0004	0.0030	0.0007	0.0030	0.0004	na
Nd	na	0.0018	0.0018	0.0018	0.0015	0.0102	0.0015	0.0117	0.0031	0.0114	0.0018	na
Sm	na	0.0004	0.0004	0.0004	0.0004	0.0017	0.0004	0.0016	0.0007	0.0018	0.0005	na
Eu	na	0.0001	0.0001	0.0001	0.0001	0.0003	0.0001	0.0001	0.0001	0.0002	0.0002	na
Gd	na	0.0003	0.0003	0.0003	0.0005	0.0012	0.0005	0.0011	0.0005	0.0014	0.0004	na
Tb	na	0.0000	0.0000	0.0000	0.0001	0.0001	0.0001	0.0001	0.0001	0.0001	0.0001	na
Dy	na	0.0002	0.0002	0.0002	0.0003	0.0005	0.0003	0.0006	0.0003	0.0006	0.0003	na
Er	na	0.0000	0.0000	0.0000	0.0001	0.0001	0.0001	0.0001	0.0001	0.0001	0.0001	na
Ho	na	0.0001	0.0001	0.0001	0.0001	0.0002	0.0001	0.0002	0.0001	0.0003	0.0001	na
Yb	na	0.0001	0.0001	0.0001	0.0001	0.0002	0.0001	0.0001	0.0001	0.0002	0.0001	na
Lu	na	0.0000	0.0000	0.0000	0.0000	0.0000	0.0000	0.0000	0.0000	0.0000	0.0000	na
Hf	na	nd	nd	nd	nd	nd	nd	nd	0.0001	nd	0.0000	na
Total (+)	49.37	49.66	49.46	49.16	50.03	50.06	49.85	50.04	50.04	49.80	49.81	49.91
Total (-)	-49.37	-49.62	-49.44	-49.14	-50.01	-49.98	-49.83	-49.93	-49.97	-49.69	-49.78	-49.91
Charge Diff.	0.00	0.04	0.02	0.02	0.02	0.08	0.02	0.11	0.07	0.10	0.03	0.00
X Site Total	2.05	2.07	1.96	2.06	2.08	2.41	2.07	2.12	2.06	2.48	2.05	2.05

Table 18 Continued.

Rock Unit	QMF-I	QMF-I	QMF-I	QMF-I	QMF-I	QMF-I	QMF-I	QMF-I	QMF-I	QMF-I	QMF-I
Sample ID	23	26	26	26	40	40	26	40	23	26	40
Grain ID	23c_20	26a_ukn2	26a_ukn3	26a_ukn4	40d_ukn2	40d_ukn4	26a_ukn1	40d_ukn4	23c_ukn3	26a_ukn1	40d_ukn1
Anal. Location	Rim	Core	Rim	Core	Rim	Rim	Rim	Rim	Rim	Rim	Rim
Ca	9.969	9.816	9.954	9.886	9.925	9.902	9.855	9.943	9.898	9.820	9.967
P	5.936	5.862	5.926	5.792	5.932	5.980	5.922	5.965	5.902	5.971	5.977
Sr	0.007	0.008	nd	0.008	0.010	0.011	0.006	0.008	0.004	nd	0.010
Ba	nd	nd	nd	nd	nd	nd	nd	nd	0.003	nd	nd
Na	nd	0.032	nd	0.073	nd	nd	0.052	nd	0.036	0.037	nd
K	nd	nd	nd	0.036	0.013	nd	nd	nd	nd	nd	nd
Mg	nd	nd	nd	nd	nd	nd	nd	nd	nd	nd	nd
Ti	nd	nd	nd	nd	nd	nd	nd	nd	nd	nd	nd
Mn	0.010	0.027	0.013	0.015	0.053	0.046	0.018	0.030	0.021	0.020	0.012
Fe	0.017	0.133	nd	0.007	0.055	0.049	0.032	0.031	0.031	0.053	0.020
Cu	nd	nd	0.010	nd	nd	nd	nd	0.011	0.005	0.013	nd
S	0.016	0.026	nd	0.095	nd	nd	0.042	nd	0.033	0.024	nd
B	na	nd	nd	nd	0.003	0.004	nd	0.004	na	nd	nd
Si	0.034	0.038	0.043	0.045	nd	nd	0.029	nd	0.044	0.019	nd
As	nd	nd	nd	nd	nd	nd	nd	nd	nd	nd	nd
V	nd	nd	nd	nd	nd	nd	nd	nd	nd	nd	0.007
F	2.03	1.94	1.93	1.98	1.94	2.00	1.92	2.01	1.94	1.95	2.07
Cl	0.08	0.60	0.10	0.47	0.08	0.08	0.51	0.06	0.07	0.57	0.04
O	23.92	23.60	23.91	23.64	23.87	23.92	23.76	23.90	23.95	23.74	23.90

Table 18 Continued.

Rock Unit	**QMF-I**	**QMF-I**	**QMF-I**	**QMF-I**	**QMF-I**	**QMF-I**	**QMF-I**	**QMF-I**	**QMF-I**	**QMF-I**	**QMF-I**
Sample ID	**23**	**26**	**26**	**26**	**40**	**40**	**26**	**40**	**23**	**26**	**40**
Grain ID	**23c_20**	**26a_ukn2**	**26a_ukn3**	**26a_ukn4**	**40d_ukn2**	**40d_ukn4**	**26a_ukn1**	**40d_ukn4**	**23c_ukn3**	**26a_ukn1**	**40d_ukn1**
Anal. Location	**Rim**	**Core**	**Rim**	**Core**	**Rim**	**Rim**	**Rim**	**Rim**	**Rim**	**Rim**	**Rim**
La	na	0.010	0.011	0.007	0.001	0.001	0.009	0.001	na	0.009	0.001
Ce	0.010	0.028	0.024	0.019	0.003	0.003	0.020	0.003	0.022	0.020	0.003
Pr	na	0.0030	0.0030	0.0025	0.0004	0.0005	0.0026	0.0005	na	0.0026	0.0004
Nd	na	0.0115	0.0117	0.0102	0.0018	0.0020	0.0086	0.0020	na	0.0087	0.0015
Sm	na	0.0018	0.0016	0.0018	0.0005	0.0006	0.0013	0.0006	na	0.0013	0.0004
Eu	na	0.0002	0.0001	0.0003	0.0002	0.0002	0.0001	0.0002	na	0.0001	0.0002
Gd	na	0.0014	0.0011	0.0012	0.0004	0.0005	0.0008	0.0005	na	0.0008	0.0005
Tb	na	0.0001	0.0001	0.0001	0.0001	0.0001	0.0001	0.0001	na	0.0001	0.0001
Dy	na	0.0007	0.0006	0.0005	0.0003	0.0004	0.0004	0.0004	na	0.0004	0.0003
Er	na	0.0001	0.0001	0.0001	0.0001	0.0001	0.0001	0.0001	na	0.0001	0.0001
Ho	na	0.0003	0.0002	0.0002	0.0001	0.0002	0.0002	0.0002	na	0.0002	0.0001
Yb	na	0.0002	0.0001	0.0002	0.0001	0.0001	0.0001	0.0001	na	0.0001	0.0001
Lu	na	0.0000	0.0000	0.0000	0.0000	0.0000	0.0000	0.0000	na	0.0000	0.0000
Hf	na	nd	nd	nd	0.0000	0.0000	0.0000	0.0000	na	0.0000	nd
Total (+)	49.95	49.83	49.96	49.81	49.80	49.96	50.02	49.91	49.91	50.09	49.95
Total (-)	-49.95	-49.73	-49.86	-49.73	-49.77	-49.92	-49.94	-49.88	-49.91	-50.00	-49.91
Charge Diff.	0.00	0.10	0.11	0.08	0.03	0.04	0.09	0.04	0.00	0.09	0.04
X Site Total	2.11	2.54	2.03	2.44	2.02	2.07	2.42	2.08	2.01	2.52	2.11

Table 18 Continued.

Rock Unit	QMF-I	QMF-I	QMF-I	QMF-I	QMF-I	QMF-I	QMF-I	QMF-I	QMF-I	QMF-I	QMF-I	QMF-I
Sample ID	40	26	40	26	23	23	23	26	23	23	23	23
Grain ID	40d_ukn2	26a_ukn5	40d_ukn3	26a_ukn3	23c_ukn2	23c_20	23c_ukn4	26a_ukn1	23c_ukn1	23c_ukn3	23c_ukn4	23c_ukn1
Anal. Location	Rim	Core	Rim	Rim	Core	Rim	Rim	Core	Rim	Rim	Core	Core
Ca	9.976	9.940	9.812	9.882	9.990	9.940	9.963	9.784	10.020	9.967	10.026	9.904
P	5.922	5.866	5.989	5.918	5.924	5.930	5.974	5.985	5.873	5.866	5.933	5.950
Sr	0.006	0.013	nd	nd	nd	0.008	nd	nd	nd	0.009	nd	0.005
Ba	nd	nd	nd	nd	nd	nd	nd	nd	nd	nd	nd	nd
Na	nd	0.030	nd	nd	nd	nd	nd	0.063	0.014	0.026	nd	0.017
K	0.008	nd	nd	0.008	nd	nd	nd	nd	nd	nd	nd	nd
Mg	nd	nd	0.030	nd	nd	nd	nd	nd	nd	nd	nd	nd
Ti	nd	nd	nd	0.007	nd	nd	nd	nd	nd	nd	nd	nd
Mn	0.034	0.024	0.070	0.008	0.020	0.018	0.009	0.014	0.014	0.024	0.007	0.013
Fe	0.041	0.019	0.074	nd	0.018	0.031	0.013	0.039	nd	0.015	0.010	nd
Cu	nd	nd	nd	0.054	nd	nd	nd	nd	nd	nd	nd	0.016
S	nd	0.024	nd	0.022	0.012	0.016	nd	0.038	0.012	0.034	nd	0.029
B	0.003	0.006	0.013	nd	nd	na	nd	nd	nd	na	nd	nd
Si	nd	0.036	nd	0.046	0.023	0.040	0.031	0.032	0.041	0.040	0.013	0.040
As	nd	nd	nd	nd	nd	nd	nd	nd	nd	nd	nd	nd
V	nd	nd	nd	nd	nd	nd	nd	nd	nd	nd	nd	nd
F	2.00	1.95	2.03	1.94	2.01	1.98	1.94	2.01	2.01	1.95	2.01	2.01
Cl	0.06	0.36	0.15	0.10	0.06	0.06	0.05	0.57	0.06	0.07	0.05	0.07
O	23.84	23.70	23.88	23.94	23.89	23.96	23.99	23.76	23.83	23.89	23.88	23.97

Table 18 Continued.

Rock Unit	QMF-I	QMF-I	QMF-I	QMF-I	QMF-I	QMF-I	QMF-I	QMF-I	QMF-I	QMF-I	QMF-I	QMF-I
Sample ID	40	26	40	26	23	23	23	26	23	23	23	23
Grain ID	40d_ukn2	26a_ukn5	40d_ukn3	26a_ukn3	23c_ukn2	23c_20	23c_ukn4	26a_ukn1	23c_ukn1	23c_ukn3	23c_ukn4	23c_ukn1
Anal. Location	Rim	Core	Rim	Rim	Core	Rim	Rim	Core	Rim	Rim	Core	Core
La	0.001	0.008	0.001	0.011	0.003	na	0.002	0.009	0.006	na	0.002	0.006
Ce	0.003	0.018	0.004	0.025	0.005	0.016	0.004	0.021	0.011	0.020	0.004	0.011
Pr	0.0004	0.0021	0.0007	0.0031	0.0006	na	0.0005	0.0026	0.0013	na	0.0005	0.0013
Nd	0.0018	0.0099	0.0031	0.0118	0.0020	na	0.0022	0.0087	0.0052	na	0.0022	0.0053
Sm	0.0005	0.0013	0.0007	0.0016	0.0004	na	0.0005	0.0013	0.0009	na	0.0005	0.0009
Eu	0.0002	0.0001	0.0001	0.0001	0.0001	na	0.0001	0.0001	0.0001	na	0.0001	0.0001
Gd	0.0004	0.0009	0.0005	0.0012	0.0004	na	0.0007	0.0008	0.0007	na	0.0007	0.0007
Tb	0.0001	0.0001	0.0001	0.0001	0.0000	na	0.0001	0.0001	0.0001	na	0.0001	0.0001
Dy	0.0003	0.0005	0.0003	0.0006	0.0002	na	0.0005	0.0004	0.0004	na	0.0005	0.0004
Er	0.0001	0.0001	0.0001	0.0001	0.0000	na	0.0001	0.0001	0.0001	na	0.0001	0.0001
Ho	0.0001	0.0002	0.0001	0.0002	0.0001	na	0.0003	0.0002	0.0002	na	0.0003	0.0002
Yb	0.0001	0.0001	0.0001	0.0001	0.0001	na	0.0002	0.0001	0.0001	na	0.0002	0.0001
Lu	0.0000	0.0000	0.0000	0.0000	0.0000	na	0.0000	0.0000	0.0000	na	0.0000	0.0000
Hf	0.0000	0.0001	0.0001	nd	0.0001	na	nd	0.0000	nd	na	nd	nd
Total (+)	49.78	49.82	50.00	50.04	49.89	49.95	50.00	50.19	49.78	49.81	49.85	50.08
Total (-)	-49.74	-49.71	-49.93	-49.93	-49.86	-49.95	-49.97	-50.10	-49.73	-49.80	-49.82	-50.02
Charge Diff.	0.03	0.10	0.07	0.11	0.03	0.00	0.03	0.09	0.06	0.00	0.03	0.06
X Site Total	2.06	2.31	2.18	2.04	2.08	2.03	1.99	2.59	2.07	2.02	2.06	2.08

Table 18 Continued.

Rock Unit	QMF-I	QMF-I	QMF-I	QMF-I	QMF-I	QMF-I	QMF-I	QMF-II	QMF-II	QMF-II	QMF-II	QMF-II
Sample ID	23	26	23	23	23	23	40	38	38	38	38	38
Grain ID	23c_ukn1	26a_ukn5	23c_ukn2	23c_ukn2	23c_20	23c_ukn4	40d_ukn3	38d_ukn2	38d_35	38d_ukn4	38d_ukn4	38d_ukn2
Anal. Location	Rim	Rim	Rim	Rim	Core	Rim	Core	Core	Rim	Core	Rim	Rim
Ca	9.957	9.913	9.966	9.993	10.000	9.950	9.976	10.012	9.980	10.051	10.018	10.060
P	5.888	5.909	5.952	5.948	5.840	5.937	5.960	5.954	5.984	5.907	5.935	5.912
Sr	nd	0.006	nd	nd	0.008	0.006	0.011	nd	nd	nd	0.004	0.007
Ba	nd	nd	nd	nd	nd	0.003	nd	nd	nd	nd	nd	nd
Na	0.024	0.036	nd	nd	0.028	nd	nd	nd	nd	nd	nd	nd
K	nd	0.012	nd	nd	nd	nd	nd	nd	nd	nd	nd	nd
Mg	nd	nd	nd	nd	nd	nd	nd	nd	nd	nd	nd	nd
Ti	nd	nd	nd	nd	nd	nd	nd	0.007	nd	nd	nd	nd
Mn	0.022	0.012	0.019	0.019	0.015	0.006	0.023	0.008	0.013	0.009	0.008	nd
Fe	0.015	0.007	0.011	0.013	0.009	0.017	0.006	0.015	0.016	0.015	0.016	0.020
Cu	nd	nd	0.010	nd	nd	nd	nd	nd	nd	nd	nd	nd
S	0.027	0.017	0.011	0.014	0.043	0.026	nd	nd	nd	nd	nd	nd
B	nd	0.006	nd	nd	na	nd	0.014	na	na	0.006	0.006	na
Si	0.042	0.039	0.018	nd	0.049	0.044	nd	nd	nd	nd	nd	nd
As	nd	nd	nd	nd	nd	nd	nd	nd	nd	nd	nd	nd
V	nd	nd	nd	nd	nd	nd	nd	nd	nd	nd	nd	nd
F	1.96	1.92	2.06	1.99	2.04	1.95	2.03	2.00	1.99	1.95	1.91	2.00
Cl	0.07	0.49	0.06	0.05	0.10	0.05	0.05	0.04	0.05	0.04	0.03	0.03
O	23.90	23.70	23.91	23.93	23.81	24.00	23.88	23.92	23.96	23.85	23.92	23.85

Table 18 Continued.

Rock Unit	**QMF-I**	**QMF-I**	**QMF-I**	**QMF-I**	**QMF-I**	**QMF-I**	**QMF-I**	**QMF-II**	**QMF-II**	**QMF-II**	**QMF-II**	**QMF-II**
Sample ID	**23**	**26**	**23**	**23**	**23**	**23**	**40**	**38**	**38**	**38**	**38**	**38**
Grain ID	**23c_ukn1**	**26a_ukn5**	**23c_ukn2**	**23c_ukn2**	**23c_20**	**23c_ukn4**	**40d_ukn3**	**38d_ukn2**	**38d_35**	**38d_ukn4**	**38d_ukn4**	**38d_ukn2**
Anal. Location	**Rim**	**Rim**	**Rim**	**Rim**	**Core**	**Rim**	**Core**	**Core**	**Rim**	**Core**	**Rim**	**Rim**
La	0.006	0.008	0.003	0.003	na	0.002	0.001	na	na	0.001	0.001	na
Ce	0.011	0.018	0.006	0.006	0.008	0.004	0.004	0.005	0.007	0.005	0.005	0.000
Pr	0.0013	0.0022	0.0006	0.0006	na	0.0005	0.0007	na	na	0.0007	0.0007	na
Nd	0.0052	0.0100	0.0020	0.0020	na	0.0022	0.0032	na	na	0.0036	0.0036	na
Sm	0.0009	0.0013	0.0004	0.0004	na	0.0005	0.0007	na	na	0.0009	0.0009	na
Eu	0.0001	0.0001	0.0001	0.0001	na	0.0001	0.0001	na	na	0.0002	0.0002	na
Gd	0.0007	0.0009	0.0004	0.0004	na	0.0007	0.0005	na	na	0.0008	0.0008	na
Tb	0.0001	0.0001	0.0000	0.0000	na	0.0001	0.0001	na	na	0.0001	0.0001	na
Dy	0.0004	0.0005	0.0002	0.0002	na	0.0005	0.0003	na	na	0.0006	0.0006	na
Er	0.0001	0.0001	0.0000	0.0000	na	0.0001	0.0001	na	na	0.0001	0.0001	na
Ho	0.0002	0.0002	0.0001	0.0001	na	0.0003	0.0001	na	na	0.0002	0.0002	na
Yb	0.0001	0.0001	0.0001	0.0001	na	0.0002	0.0001	na	na	0.0002	0.0002	na
Lu	0.0000	0.0000	0.0000	0.0000	na	0.0000	0.0000	na	na	0.0000	0.0000	na
Hf	nd	0.0001	0.0001	0.0001	na	nd	0.0001	na	na	0.0001	0.0001	na
Total (+)	49.88	49.91	49.96	49.93	49.77	50.02	49.91	49.88	49.96	49.74	49.83	49.74
Total (-)	-49.82	-49.81	-49.93	-49.90	-49.76	-49.99	-49.84	-49.87	-49.95	-49.69	-49.78	-49.73
Charge Diff.	0.06	0.10	0.03	0.03	0.00	0.03	0.07	0.00	0.00	0.05	0.05	0.00
X Site Total	2.03	2.41	2.12	2.04	2.14	2.00	2.07	2.03	2.04	1.99	1.94	2.04

Table 18 Continued.

Rock Unit	QMF-II	QMF-II	QMF-II	QMF-II	QMF-II	QMF-II	QMF-II	QMF-II	QMF-II	QMF-II	QMF-II	QMF-II
Sample ID	38	41	38	38	38	38	41	41	38	41	41	38
Grain ID	38d_ukn1	41b_ukn5	38d_ukn4	38d_35	38d_ukn1	38d_ukn1	41b_ukn1	41b_ukn5	38d_ukn1	41b_ukn5	41b_ukn1	38d_35
Anal. Location	Core	Rim	Rim	Core	Rim	Rim	Rim	Rim	Core	Core	Rim	Rim
Ca	9.939	9.911	9.980	9.996	10.027	9.933	9.913	9.968	9.964	9.969	9.872	10.056
P	6.034	5.952	5.961	5.956	5.927	6.008	5.898	5.902	5.985	5.890	5.913	5.917
Sr	nd	0.008	0.009	0.008	0.010	0.008	0.004	nd	0.010	0.006	0.006	0.004
Ba	nd	nd	nd	nd	nd	nd	nd	nd	nd	0.003	nd	nd
Na	nd	0.015	nd	nd	nd	nd	0.022	0.020	nd	0.029	0.017	nd
K	nd	nd	nd	nd	nd	nd	nd	nd	nd	nd	nd	nd
Mg	nd	nd	nd	nd	nd	nd	nd	nd	nd	nd	nd	nd
Ti	nd	nd	nd	0.006	nd	nd	nd	nd	nd	0.007	0.007	nd
Mn	0.010	0.035	0.011	0.012	0.006	0.014	0.032	0.039	0.011	0.022	0.042	0.011
Fe	0.007	0.037	0.021	0.021	0.020	0.021	0.090	0.039	0.019	0.036	0.101	0.012
Cu	nd	nd	nd	nd	nd	0.006	nd	nd	nd	0.006	0.007	nd
S	nd	0.012	nd	nd	nd	nd	0.011	nd	nd	nd	nd	nd
B	nd	nd	0.006	na	nd	nd	na	nd	nd	nd	na	nd
Si	nd	nd	nd	nd	nd	nd	nd	nd	nd	nd	0.014	nd
As	nd	nd	nd	nd	nd	nd	0.013	nd	nd	nd	nd	nd
V	nd	nd	nd	nd	nd	nd	nd	nd	nd	nd	nd	nd
F	1.96	1.93	2.00	1.91	2.00	2.01	1.96	1.94	1.98	1.93	1.95	1.99
Cl	0.06	0.11	0.03	0.07	0.04	0.06	0.16	0.13	0.05	0.12	0.14	0.02
O	24.04	23.91	23.91	23.95	23.87	23.97	23.79	23.79	23.95	23.78	23.85	23.87

Table 18 Continued.

Rock Unit	QMF-II	QMF-II	QMF-II	QMF-II	QMF-II	QMF-II	QMF-II	QMF-II	QMF-II	QMF-II	QMF-II	QMF-II
Sample ID	38	41	38	38	38	38	41	41	38	41	41	38
Grain ID	38d_ukn1	41b_ukn5	38d_ukn4	38d_35	38d_ukn1	38d_ukn1	41b_ukn1	41b_ukn5	38d_ukn1	41b_ukn5	41b_ukn1	38d_35
Anal. Location	Core	Rim	Rim	Core	Rim	Rim	Rim	Rim	Core	Core	Rim	Rim
La	0.001	0.003	0.001	na	0.001	0.001	na	0.003	0.001	0.003	na	nd
Ce	0.004	0.008	0.005	0.001	0.004	0.004	0.016	0.008	0.004	0.008	0.020	0.000
Pr	0.0006	0.0015	0.0007	na	0.0006	0.0006	na	0.0015	0.0006	0.0015	na	nd
Nd	0.0028	0.0071	0.0036	na	0.0028	0.0028	na	0.0072	0.0028	0.0072	na	nd
Sm	0.0008	0.0027	0.0009	na	0.0008	0.0008	na	0.0027	0.0008	0.0027	na	nd
Eu	0.0001	0.0007	0.0002	na	0.0001	0.0001	na	0.0007	0.0001	0.0007	na	nd
Gd	0.0007	0.0025	0.0008	na	0.0007	0.0007	na	0.0025	0.0007	0.0025	na	nd
Tb	0.0001	0.0004	0.0001	na	0.0001	0.0001	na	0.0004	0.0001	0.0004	na	nd
Dy	0.0005	0.0022	0.0006	na	0.0005	0.0005	na	0.0022	0.0005	0.0022	na	nd
Er	0.0001	0.0003	0.0001	na	0.0001	0.0001	na	0.0003	0.0001	0.0003	na	nd
Ho	0.0002	0.0011	0.0002	na	0.0002	0.0002	na	0.0011	0.0002	0.0011	na	nd
Yb	0.0002	0.0007	0.0002	na	0.0002	0.0002	na	0.0008	0.0002	0.0008	na	nd
Lu	0.0000	0.0001	0.0000	na	0.0000	0.0000	na	0.0001	0.0000	0.0001	na	nd
Hf	0.0001	0.0003	0.0001	na	0.0001	0.0001	na	0.0003	0.0001	0.0003	na	nd
Total (+)	50.12	49.93	49.91	49.88	49.80	50.04	49.75	49.73	49.97	49.70	49.79	49.75
Total (-)	-50.09	-49.86	-49.86	-49.88	-49.77	-50.01	-49.70	-49.65	-49.94	-49.62	-49.78	-49.75
Charge Diff.	0.03	0.08	0.05	0.00	0.03	0.03	0.05	0.08	0.03	0.08	0.00	0.00
X Site Total	2.02	2.04	2.03	1.98	2.04	2.07	2.12	2.07	2.04	2.05	2.09	2.01

Table 18 Continued.

Rock Unit	QMF-II	QMF-II	QMF-II	QMF-II	QMF-II	QMF-II	QMF-II	QMF-II	QMF-II	QMF-II	QMF-II	QMP
Sample ID	41	41	41	41	41	38	41	41	38	41	38	02
Grain ID	41b_ukn4	41b_ukn5	41b_ukn3	41b_ukn3	41b_ukn3	38d_ukn3	41b_ukn2	41b_ukn2	38d_ukn3	41b_ukn2	38d_ukn3	02b_ukn4
Anal. Location	Rim	Rim	Core	Rim	Rim	Rim	Core	Rim	Core	Rim	Rim	Rim
Ca	9.880	10.011	9.975	9.939	9.915	9.913	9.974	9.979	9.974	9.941	10.027	10.126
P	5.980	5.883	5.881	5.878	5.879	6.028	5.917	5.920	5.991	5.905	5.919	5.805
Sr	nd	0.004	0.012	0.009	0.004	nd	0.004	0.007	0.003	0.006	0.004	0.009
Ba	nd	nd	nd	nd	nd	nd	nd	nd	nd	nd	nd	nd
Na	0.024	nd	0.013	0.030	0.027	nd	0.019	nd	nd	0.019	nd	nd
K	nd	nd	nd	nd	nd	nd	nd	nd	nd	nd	nd	0.011
Mg	nd	nd	nd	nd	nd	nd	nd	nd	nd	nd	nd	nd
Ti	nd	nd	nd	nd	nd	nd	nd	nd	nd	nd	nd	nd
Mn	0.034	0.028	0.033	0.033	0.040	0.016	0.033	0.038	0.007	0.033	0.009	0.016
Fe	0.057	0.041	0.054	0.073	0.067	0.026	0.026	0.030	0.017	0.037	0.037	0.022
Cu	nd	nd	nd	0.007	0.012	0.011	nd	nd	0.006	nd	nd	nd
S	nd	nd	nd	nd	0.012	nd	nd	nd	nd	0.015	nd	nd
B	na	nd	nd	nd	nd	na	nd	nd	na	nd	na	nd
Si	0.014	nd	nd	nd	0.013	nd	nd	nd	nd	0.016	nd	nd
As	nd	nd	nd	nd	nd	nd	nd	nd	nd	nd	nd	nd
V	nd	nd	nd	nd	nd	nd	nd	nd	nd	nd	nd	nd
F	1.97	1.95	2.01	1.95	1.96		1.92	2.01		1.99		1.93
Cl	0.15	0.12	0.14	0.15	0.17	0.05	0.12	0.13	0.05	0.14	0.03	0.06
O	23.92	23.77	23.73	23.74	23.76	25.02	23.83	23.80	24.96	23.81	24.87	23.70

Table 18 Continued.

Rock Unit	QMF-II	QMF-II	QMF-II	QMF-II	QMF-II	QMF-II	QMF-II	QMF-II	QMF-II	QMF-II	QMF-II	QMP
Sample ID	41	41	41	41	41	38	41	41	38	41	38	02
Grain ID	41b_ukn4	41b_ukn5	41b_ukn3	41b_ukn3	41b_ukn3	38d_ukn3	41b_ukn2	41b_ukn2	38d_ukn3	41b_ukn2	38d_ukn3	02b_ukn4
Anal. Location	Rim	Rim	Core	Rim	Rim	Rim	Core	Rim	Core	Rim	Rim	Rim
La	na	0.003	0.004	0.004	0.004	na	0.003	0.003	na	0.003	na	0.001
Ce	0.011	0.008	0.011	0.011	0.011	0.006	0.008	0.008	0.002	0.008	0.005	0.004
Pr	na	0.0015	0.0017	0.0017	0.0017	na	0.0014	0.0014	na	0.0014	na	0.0006
Nd	na	0.0072	0.0079	0.0079	0.0079	na	0.0066	0.0066	na	0.0067	na	0.0026
Sm	na	0.0027	0.0019	0.0019	0.0019	na	0.0026	0.0026	na	0.0026	na	0.0006
Eu	na	0.0007	0.0003	0.0003	0.0003	na	0.0005	0.0005	na	0.0005	na	0.0002
Gd	na	0.0025	0.0016	0.0016	0.0016	na	0.0025	0.0025	na	0.0025	na	0.0008
Tb	na	0.0004	0.0002	0.0002	0.0002	na	0.0002	0.0002	na	0.0002	na	0.0001
Dy	na	0.0022	0.0012	0.0012	0.0012	na	0.0010	0.0010	na	0.0010	na	0.0006
Er	na	0.0003	0.0002	0.0002	0.0002	na	0.0002	0.0002	na	0.0002	na	0.0001
Ho	na	0.0011	0.0005	0.0005	0.0005	na	0.0007	0.0007	na	0.0007	na	0.0003
Yb	na	0.0008	0.0006	0.0006	0.0006	na	0.0006	0.0006	na	0.0006	na	0.0002
Lu	na	0.0001	0.0001	0.0001	0.0001	na	0.0001	0.0001	na	0.0001	na	0.0000
Hf	na	0.0003	nd	nd	nd	na	nd	nd	na	nd	na	nd
Total (+)	49.96	49.70	49.68	49.65	49.73	50.09	49.77	49.80	49.97	49.83	49.76	49.42
Total (-)	-49.95	-49.62	-49.61	-49.58	-49.66	-50.09	-49.70	-49.73	-49.97	-49.76	-49.76	-49.39
Charge Diff.	0.00	0.08	0.07	0.07	0.07	0.00	0.07	0.07	0.00	0.07	0.00	0.03
X Site Total	2.11	2.07	2.15	2.11	2.13	0.05	2.05	2.14	0.05	2.13	0.03	1.98

Table 18 Continued.

Rock Unit	QMP	QMP	QMP	QMP	QMP	QMP	QMP	QMP	QMP	QMP	QMP	QMP
Sample ID	02	02	02	02	02	02	02	02	02	02	02	02
Grain ID	02b_27	02b_ukn4	02b_ukn1	02b_27	02b_ukn4	02b_ukn2	02b_ukn2	02b_ukn2	02b_ukn1	02b_ukn3	02b_27	02b_ukn1
Anal. Location	Core	Rim	Rim	Rim	Core	Rim	Rim	Core	Core	Rim	Rim	Rim
Ca	10.083	10.103	10.103	10.118	10.124	10.093	10.042	10.043	10.123	10.070	10.133	10.103
P	5.857	5.818	5.801	5.801	5.798	5.799	5.819	5.805	5.820	5.811	5.724	5.817
Sr	0.006	0.009	0.006	nd	0.014	0.011	0.012	0.012	0.009	nd	0.004	nd
Ba	nd	nd	nd	nd	nd	nd	nd	nd	0.003	nd	nd	nd
Na	nd	nd	nd	nd	nd	nd	nd	0.021	nd	nd	nd	0.025
K	nd	0.021	nd	nd	nd	0.009	nd	nd	nd	0.011	0.008	nd
Mg	nd	nd	nd	nd	nd	nd	nd	nd	nd	nd	nd	nd
Ti	nd	nd	nd	0.009	nd	nd	nd	nd	nd	0.007	nd	nd
Mn	0.019	0.015	0.036	0.017	0.018	0.049	0.064	0.056	0.016	0.022	0.031	0.012
Fe	0.018	0.012	0.022	0.024	0.023	0.028	0.033	0.038	0.012	0.043	0.056	0.018
Cu	nd	nd	0.005	nd	0.011	nd	nd	nd	nd	nd	nd	0.008
S	nd	nd	0.011	0.015	nd	nd	0.012	0.015	nd	nd	0.012	nd
B	0.004	nd	0.004	0.004	nd	nd	nd	nd	0.004	0.004	0.004	0.004
Si	nd	0.011	nd	nd	nd	nd	nd	nd	nd	0.015	0.015	nd
As	nd	nd	nd	nd	nd	nd	nd	nd	nd	nd	nd	nd
V	nd	nd	nd	nd	nd	nd	0.007	nd	nd	nd	nd	nd
F	1.94	2.01	2.01	1.90	1.83	1.96	1.89	1.86	1.95	1.78	1.96	1.97
Cl	0.06	0.05	0.07	0.06	0.07	0.09	0.10	0.09	0.07	0.08	0.09	0.07
O	23.78	23.69	23.67	23.75	23.74	23.66	23.75	23.75	23.71	23.80	23.59	23.68

Table 18 Continued.

Rock Unit	QMP	QMP	QMP	QMP	QMP	QMP	QMP	QMP	QMP	QMP	QMP	QMP
Sample ID	02	02	02	02	02	02	02	02	02	02	02	02
Grain ID	02b_27	02b_ukn4	02b_ukn1	02b_27	02b_ukn4	02b_ukn2	02b_ukn2	02b_ukn2	02b_ukn1	02b_ukn3	02b_27	02b_ukn1
Anal. Location	Core	Rim	Rim	Rim	Core	Rim	Rim	Core	Core	Rim	Rim	Rim
La	0.002	0.001	0.002	0.002	0.001	0.002	0.002	0.002	0.002	0.003	0.002	0.002
Ce	0.005	0.004	0.005	0.005	0.004	0.004	0.004	0.004	0.005	0.007	0.005	0.005
Pr	0.0006	0.0006	0.0007	0.0006	0.0006	0.0006	0.0006	0.0006	0.0007	0.0009	0.0006	0.0007
Nd	0.0024	0.0026	0.0033	0.0024	0.0026	0.0027	0.0027	0.0027	0.0033	0.0036	0.0025	0.0033
Sm	0.0004	0.0006	0.0009	0.0004	0.0006	0.0005	0.0005	0.0005	0.0009	0.0006	0.0004	0.0009
Eu	0.0001	0.0002	0.0003	0.0001	0.0002	0.0001	0.0001	0.0001	0.0003	0.0002	0.0001	0.0003
Gd	0.0005	0.0008	0.0009	0.0005	0.0008	0.0004	0.0004	0.0004	0.0009	0.0005	0.0005	0.0009
Tb	0.0001	0.0001	0.0001	0.0001	0.0001	0.0000	0.0000	0.0000	0.0001	0.0001	0.0001	0.0001
Dy	0.0003	0.0006	0.0007	0.0003	0.0006	0.0002	0.0002	0.0002	0.0007	0.0004	0.0004	0.0007
Er	0.0001	0.0001	0.0001	0.0001	0.0001	0.0000	0.0000	0.0000	0.0001	0.0001	0.0001	0.0001
Ho	0.0002	0.0003	0.0004	0.0002	0.0003	0.0001	0.0001	0.0001	0.0004	0.0002	0.0002	0.0004
Yb	0.0001	0.0002	0.0002	0.0001	0.0002	0.0001	0.0001	0.0001	0.0002	0.0001	0.0001	0.0002
Lu	0.0000	0.0000	0.0000	0.0000	0.0000	0.0000	0.0000	0.0000	0.0000	0.0000	0.0000	0.0000
Hf	0.0001	nd	0.0000	0.0001	nd	0.0001	0.0001	0.0001	0.0000	nd	0.0001	0.0000
Total (+)	49.59	49.47	49.47	49.50	49.41	49.41	49.53	49.47	49.49	49.50	49.27	49.45
Total (-)	-49.56	-49.44	-49.42	-49.47	-49.38	-49.38	-49.48	-49.45	-49.44	-49.45	-49.23	-49.40
Charge Diff.	0.04	0.03	0.05	0.04	0.03	0.03	0.05	0.03	0.05	0.05	0.04	0.05
X Site Total	2.00	2.06	2.08	1.96	1.90	2.05	1.99	1.95	2.02	1.86	2.04	2.04

Table 18 Continued.

Rock Unit	QMP	POB	POB	POB	POB	POB	POB	POB	POB	POB	POB	POB
Sample ID	02	47	47	47	42	47	42	42	42	34	47	42
Grain ID	02b_ukn3	47c_ukn3	47c_ukn1	47c_ukn1	42d_36	47c_ukn5	42d_31	42d_01	42d_36	34a_16	47c_ukn4	42d_36
Anal. Location	Core	Rim	Core	Rim	Rim	Core	Rim	Core	Core	Core	Core	Rim
Ca	10.171	9.839	9.963	9.920	9.805	9.849	9.794	10.012	9.917	9.999	9.933	9.930
P	5.741	5.935	5.921	5.907	6.035	5.877	5.997	5.877	5.966	5.884	5.912	5.950
Sr	0.010	0.012	0.006	nd	nd	0.009	0.006	nd	nd	0.005	nd	nd
Ba	nd	nd	nd	nd	nd	nd	nd	nd	nd	nd	nd	nd
Na	nd	0.042	0.013	0.021	nd	0.043	nd	nd	nd	nd	nd	nd
K	nd	nd	nd	nd	nd	nd	0.014	nd	nd	nd	0.018	0.010
Mg	nd	nd	nd	0.014	0.023	0.018	0.016	nd	nd	nd	0.015	nd
Ti	nd	nd	nd	nd	nd	nd	nd	nd	nd	nd	nd	nd
Mn	0.028	0.024	0.015	0.013	0.048	0.029	0.041	nd	0.022	0.022	0.017	0.022
Fe	0.028	0.042	0.021	0.033	0.073	0.084	0.058	0.015	0.041	0.025	0.074	0.018
Cu	nd	0.007	nd	0.015	nd	0.009	nd	nd	0.012	0.012	nd	0.009
S	nd	0.049	0.019	0.025	nd	0.045	0.019	0.021	0.014	0.013	nd	0.023
B	0.004	0.005	0.003	0.003	nd	nd	0.003	0.003	nd	na	0.005	nd
Si	nd	0.031	0.021	0.030	nd	0.030	0.027	0.022	0.012	0.021	0.013	0.023
As	nd	nd	nd	nd	nd	nd	nd	nd	nd	nd	nd	nd
V	nd	nd	nd	nd	nd	nd	nd	nd	nd	nd	nd	nd
F	1.84	1.91	2.01	1.96	1.97	1.88	1.97	1.96	1.96	1.94	2.10	1.96
Cl	0.08	0.07	0.08	0.09	0.11	0.09	0.08		0.08	0.04	0.10	0.06
O	23.65	24.01	23.88	23.90	24.01	23.93	24.03	23.88	23.97	23.89	23.76	23.97

Table 18 Continued.

Rock Unit	QMP	POB	POB	POB	POB	POB	POB	POB	POB	POB	POB	POB
Sample ID	02	47	47	47	42	47	42	42	42	34	47	42
Grain ID	02b_ukn3	47c_ukn3	47c_ukn1	47c_ukn1	42d_36	47c_ukn5	42d_31	42d_01	42d_36	34a_16	47c_ukn4	42d_36
Anal. Location	Core	Rim	Core	Rim	Rim	Core	Rim	Core	Core	Core	Core	Rim
La	0.003	0.003	0.005	0.005	0.004	0.001	0.004	0.007	0.004	na	0.002	0.004
Ce	0.007	0.006	0.008	0.008	0.008	0.001	0.011	0.019	0.008	0.019	0.003	0.008
Pr	0.0009	0.0007	0.0008	0.0008	0.0007	0.0002	0.0012	0.0027	0.0007	na	0.0005	0.0007
Nd	0.0036	0.0025	0.0026	0.0026	0.0023	0.0007	0.0051	0.0109	0.0023	na	0.0025	0.0023
Sm	0.0006	0.0005	0.0004	0.0004	0.0004	0.0004	0.0011	0.0021	0.0004	na	0.0008	0.0004
Eu	0.0002	0.0001	0.0001	0.0001	0.0001	0.0002	0.0003	0.0002	0.0001	na	0.0003	0.0001
Gd	0.0005	0.0004	0.0003	0.0003	0.0003	0.0004	0.0009	0.0022	0.0003	na	0.0009	0.0003
Tb	0.0001	0.0001	0.0000	0.0000	0.0001	0.0001	0.0001	0.0003	0.0001	na	0.0002	0.0001
Dy	0.0004	0.0003	0.0002	0.0002	0.0003	0.0003	0.0005	0.0021	0.0003	na	0.0009	0.0003
Er	0.0001	0.0001	0.0000	0.0000	0.0001	0.0001	0.0001	0.0005	0.0001	na	0.0002	0.0001
Ho	0.0002	0.0001	0.0001	0.0001	0.0001	0.0002	0.0002	0.0013	0.0001	na	0.0004	0.0001
Yb	0.0001	0.0001	0.0001	0.0001	0.0001	0.0001	0.0002	0.0008	0.0001	na	0.0003	0.0001
Lu	0.0000	0.0000	0.0000	0.0000	0.0000	0.0000	0.0000	0.0001	0.0000	na	0.0000	0.0000
Hf	nd	nd	0.0000	0.0000	0.0001	nd	0.0001	nd	0.0001	na	0.0000	0.0001
Total (+)	49.26	50.05	49.91	49.90	50.14	49.84	50.15	49.84	50.01	49.76	49.77	50.01
Total (-)	-49.21	-50.01	-49.86	-49.85	-50.10	-49.82	-50.09	-49.73	-49.98	-49.76	-49.72	-49.97
Charge Diff.	0.05	0.05	0.05	0.05	0.03	0.02	0.06	0.11	0.03	0.00	0.05	0.03
X Site Total	1.92	1.98	2.09	2.05	2.08	1.97	2.04	1.96	2.04	1.97	2.20	2.03

Table 18 Continued.

Rock Unit	POB	POB	POB	POB	POB	POB	POB	POB	POB	POB	POB	POB
Sample ID	34	34	34	42	42	42	34	34	42	34	42	34
Grain ID	34b_12	34b_05	34a_15	42d_01	42d_37	42d_31	34b_12	34b_05	42d_37	34a_15	42d_01	34a_15
Anal. Location	Core	Rim	Core	Rim	Core	Core	Rim	Rim	Rim	Rim	Rim	Rim
Ca	9.937	10.002	10.021	9.895	9.942	9.945	9.896	10.071	9.934	10.067	9.953	10.078
P	5.768	5.885	5.838	5.864	5.958	5.925	5.830	5.840	5.915	5.863	5.819	5.900
Sr	0.006	nd	0.011	nd	0.012	nd	0.021	0.007	0.005	0.005	nd	nd
Ba	nd	0.003	nd	nd	nd	nd	nd	nd	nd	nd	nd	0.004
Na	0.055	0.017	nd	0.024	nd	nd	0.023	nd	nd	nd	0.027	nd
K	nd	nd	nd	nd	nd	nd	nd	nd	0.010	nd	0.021	nd
Mg	nd	nd	nd	nd	nd	nd	0.027	nd	nd	nd	nd	nd
Ti	nd	nd	nd	0.010	nd	nd	nd	nd	nd	nd	nd	nd
Mn	0.042	0.019	0.013	0.014	0.018	0.028	0.060	0.010	0.030	0.012	0.008	0.006
Fe	0.048	0.013	0.029	0.007	0.030	0.037	0.068	0.008	0.041	0.048	nd	0.009
Cu	0.033	0.005	nd	0.006	nd	nd	0.016	nd	0.007	nd	nd	nd
S	0.070	0.013	0.032	0.072	0.015	0.017	0.030	0.018	0.015	nd	0.068	nd
B	na	na	na	0.003	nd	0.003	na	na	nd	na	0.003	na
Si	0.034	0.027	0.032	0.035	nd	0.020	0.017	0.028	0.017	nd	0.034	nd
As	nd	nd	nd	0.021	nd	nd	nd	nd	nd	nd	0.018	nd
V	nd	nd	nd	nd	nd	nd	nd	nd	nd	nd	nd	nd
F	1.98	1.90	1.92	1.98	1.94	2.02	1.94	1.93	1.99	1.96	1.92	1.96
Cl	0.06	0.03	0.04		0.07	0.08	0.10	0.04	0.07	0.02		0.03
O	23.78	23.91	23.89	23.94	23.95	23.88	23.79	23.85	23.88	23.81	23.88	23.86

Table 18 Continued.

Rock Unit	**POB**	**POB**	**POB**	**POB**	**POB**	**POB**	**POB**	**POB**	**POB**	**POB**	**POB**	**POB**
Sample ID	**34**	**34**	**34**	**42**	**42**	**42**	**34**	**34**	**42**	**34**	**42**	**34**
Grain ID	**34b_12**	**34b_05**	**34a_15**	**42d_01**	**42d_37**	**42d_31**	**34b_12**	**34b_05**	**42d_37**	**34a_15**	**42d_01**	**34a_15**
Anal. Location	**Core**	**Rim**	**Core**	**Rim**	**Core**	**Core**	**Rim**	**Rim**	**Rim**	**Rim**	**Rim**	**Rim**
La	na	na	na	0.007	0.004	0.004	na	na	0.004	na	0.007	na
Ce	0.007	0.015	0.025	0.019	0.010	0.011	0.012	0.019	0.010	0.004	0.019	0.004
Pr	na	na	na	0.0027	0.0015	0.0012	na	na	0.0015	na	0.0027	na
Nd	na	na	na	0.0110	0.0054	0.0051	na	na	0.0054	na	0.0110	na
Sm	na	na	na	0.0021	0.0013	0.0011	na	na	0.0014	na	0.0022	na
Eu	na	na	na	0.0002	0.0003	0.0003	na	na	0.0003	na	0.0002	na
Gd	na	na	na	0.0022	0.0012	0.0009	na	na	0.0012	na	0.0022	na
Tb	na	na	na	0.0003	0.0002	0.0001	na	na	0.0002	na	0.0003	na
Dy	na	na	na	0.0021	0.0007	0.0005	na	na	0.0007	na	0.0021	na
Er	na	na	na	0.0005	0.0001	0.0001	na	na	0.0001	na	0.0005	na
Ho	na	na	na	0.0013	0.0003	0.0002	na	na	0.0003	na	0.0013	na
Yb	na	na	na	0.0008	0.0002	0.0002	na	na	0.0002	na	0.0008	na
Lu	na	na	na	0.0001	0.0000	0.0000	na	na	0.0000	na	0.0001	na
Hf	na	na	na	nd	nd	0.0001	na	na	nd	na	nd	na
Total (+)	49.60	49.76	49.73	50.05	49.97	49.93	49.64	49.66	49.87	49.59	49.85	49.70
Total (-)	-49.60	-49.76	-49.73	-49.87	-49.92	-49.87	-49.63	-49.66	-49.82	-49.59	-49.68	-49.70
Charge Diff.	0.00	0.00	0.00	0.18	0.05	0.06	0.00	0.00	0.05	0.00	0.17	0.00
X Site Total	2.04	1.94	1.95	1.98	2.01	2.10	2.04	1.97	2.06	1.98	1.92	1.98

Table 18 Continued.

Rock Unit	POB	POB	POB	POB	POB	POB	FP	FP	FP	FP	FP	FP
Sample ID	34	34	34	34	42	34	13	13	13	13	13	13
Grain ID	34b_06	34a_16	34b_05	34b_06	42d_37	34b_06	13a_33	13a_33	13a_33	13a_24	13a_17	13a_24
Anal. Location	Rim	Rim	Core	Core	Rim	Rim	Rim	Rim	Core	Core	Rim	Rim
Ca	10.063	9.948	10.073	10.036	9.959	10.048	9.852	9.912	9.885	9.911	9.939	9.888
P	5.849	5.885	5.836	5.876	5.807	5.844	6.019	5.941	5.976	5.998	5.892	6.017
Sr	0.009	0.008	0.005	0.008	0.013	nd	nd	nd	0.004	nd	0.008	0.004
Ba	nd	nd	nd	nd	nd	nd	nd	nd	nd	nd	nd	nd
Na	nd	nd	nd	nd	0.083	nd	0.024	0.022	0.026	nd	0.031	nd
K	nd	0.029	nd	nd	0.016	nd	0.008	nd	nd	0.012	0.017	nd
Mg	nd	nd	nd	nd	nd	nd	nd	nd	nd	nd	nd	nd
Ti	nd	nd	nd	nd	nd	nd	nd	nd	nd	nd	nd	nd
Mn	0.020	0.029	0.018	0.015	nd	0.020	0.027	0.040	0.042	0.034	0.025	0.029
Fe	nd	0.047	0.016	0.012	0.006	0.009	0.037	0.045	0.026	0.019	0.026	0.026
Cu	nd	nd	nd	nd	0.005	0.009	nd	0.006	0.007	nd	nd	nd
S	0.013	0.011	0.019	0.016	0.079	0.025	0.010	0.012	0.010	nd	0.028	0.015
B	na	na	na	na	nd	na	nd	nd	nd	na	na	na
Si	0.034	0.027	0.021	0.020	nd	0.028	nd	nd	nd	0.014	0.021	0.014
As	nd	nd	nd	nd	nd	nd	nd	nd	nd	nd	nd	nd
V	nd	nd	nd	nd	0.007	nd	nd	nd	nd	0.008	nd	nd
F	1.95	1.89	1.99	1.88	1.88	1.98	1.95	1.95	1.93	2.02	1.92	2.02
Cl	0.04	0.06	0.04	0.05		0.05	0.08	0.09	0.06	0.08	0.10	0.08
O	23.85	23.89	23.80	23.91	23.87	23.84	24.01	23.90	23.96	23.95	23.89	24.02

Table 18 Continued.

Rock Unit	POB	POB	POB	POB	POB	POB	FP	FP	FP	FP	FP	FP
Sample ID	34	34	34	34	42	34	13	13	13	13	13	13
Grain ID	34b_06	34a_16	34b_05	34b_06	42d_37	34b_06	13a_33	13a_33	13a_33	13a_24	13a_17	13a_24
Anal. Location	Rim	Rim	Core	Core	Rim	Rim	Rim	Rim	Core	Core	Rim	Rim
La	na	na	na	na	0.004	na	0.003	0.003	0.003	na	na	na
Ce	0.013	0.015	0.013	0.016	0.010	0.018	0.007	0.007	0.007	0.004	0.013	0.007
Pr	na	na	na	na	0.0015	na	0.0014	0.0014	0.0014	na	na	na
Nd	na	na	na	na	0.0055	na	0.0061	0.0061	0.0061	na	na	na
Sm	na	na	na	na	0.0014	na	0.0019	0.0019	0.0019	na	na	na
Eu	na	na	na	na	0.0003	na	0.0003	0.0003	0.0003	na	na	na
Gd	na	na	na	na	0.0012	na	0.0014	0.0014	0.0014	na	na	na
Tb	na	na	na	na	0.0002	na	0.0002	0.0002	0.0002	na	na	na
Dy	na	na	na	na	0.0007	na	0.0010	0.0010	0.0010	na	na	na
Er	na	na	na	na	0.0001	na	0.0002	0.0002	0.0002	na	na	na
Ho	na	na	na	na	0.0003	na	0.0005	0.0005	0.0005	na	na	na
Yb	na	na	na	na	0.0002	na	0.0005	0.0005	0.0005	na	na	na
Lu	na	na	na	na	0.0000	na	0.0001	0.0001	0.0001	na	na	na
Hf	na	na	na	na	nd	na	nd	nd	nd	na	na	na
Total (+)	49.68	49.74	49.64	49.75	49.69	49.71	50.10	49.88	49.98	50.02	49.79	50.14
Total (-)	-49.68	-49.74	-49.63	-49.75	-49.61	-49.70	-50.04	-49.83	-49.92	-49.99	-49.79	-50.14
Charge Diff.	0.00	0.00	0.00	0.00	0.08	0.00	0.06	0.06	0.06	0.03	0.00	0.00
X Site Total	1.98	1.95	2.03	1.93	1.88	2.02	2.02	2.03	2.00	2.10	2.01	2.10

Table 18 Continued.

Rock Unit	FP	FP	FP	FP	FP	FP	FP	FP	FP	FP	FP	FP
Sample ID	13	13	13	13	13	12	12	12	12	12	12	12
Grain ID	13a_45	13a_45	13a_45	13a_17	13a_24	12a_ukn2	12a_ukn2	12a_ukn3	12a_ukn1	12a_ukn3	12a_ukn2	12a_ukn4
Anal. Location	Rim	Core	Rim	Rim	Rim	Rim	Core	Rim	Rim	Rim	Rim	Core
Ca	9.884	9.942	9.990	9.851	9.971	10.002	10.022	10.011	10.040	10.017	10.025	10.099
P	5.963	5.925	5.883	5.957	5.955	5.716	5.801	5.803	5.789	5.771	5.672	5.670
Sr	0.005	0.005	nd	nd	nd	0.007	0.006	0.011	0.007	0.011	0.010	0.011
Ba	nd	nd	nd	nd	nd	nd	nd	nd	nd	nd	nd	nd
Na	0.033	0.026	0.034	0.036	nd	0.051	0.040	0.037	0.024	0.026	0.076	0.051
K	0.010	nd	0.008	0.020	nd	0.017	nd	nd	nd	nd	nd	nd
Mg	nd	nd	nd	nd	nd	0.021	nd	nd	nd	0.014	0.016	nd
Ti	nd	nd	nd	0.008	nd	nd	nd	nd	nd	nd	nd	nd
Mn	0.041	0.027	0.022	0.017	0.034	0.019	0.026	0.014	0.022	0.011	0.027	0.022
Fe	0.030	0.016	0.024	0.022	0.027	0.052	0.026	0.028	0.029	0.040	0.037	0.028
Cu	nd	0.014	nd	nd	0.007	nd	nd	nd	0.012	nd	nd	0.005
S	0.013	0.011	0.013	0.046	nd	0.052	0.031	0.023	0.019	0.032	0.072	0.066
B	na	na	na	na	na	0.005	0.005	0.015	nd	0.015	0.005	nd
Si	0.015	0.014	0.020	0.032	nd	0.029	0.016	0.020	0.032	0.025	0.034	0.027
As	nd	nd	nd	nd	nd	nd	nd	nd	nd	nd	nd	nd
V	nd	nd	nd	nd	nd	nd	nd	nd	nd	nd	nd	nd
F	1.95	1.97	1.98	1.89	1.90	1.96	1.97	1.96	1.84	1.92	1.85	1.94
Cl	0.10	0.09	0.09	0.10	0.09	0.06	0.06	0.06	0.06	0.07	0.06	0.06
O	23.94	23.89	23.81	24.05	23.94	23.65	23.73	23.71	23.79	23.71	23.68	23.64

Table 18 Continued.

Rock Unit	FP	FP	FP	FP	FP	FP	FP	FP	FP	FP	FP	FP
Sample ID	13	13	13	13	13	12	12	12	12	12	12	12
Grain ID	13a_45	13a_45	13a_45	13a_17	13a_24	12a_ukn2	12a_ukn2	12a_ukn3	12a_ukn1	12a_ukn3	12a_ukn2	12a_ukn4
Anal. Location	Rim	Core	Rim	Rim	Rim	Rim	Core	Rim	Rim	Rim	Rim	Core
La	na	na	na	na	na	0.005	0.005	0.005	0.006	0.005	0.005	0.004
Ce	0.007	0.020	0.006	0.012	0.006	0.010	0.010	0.013	0.011	0.013	0.010	0.009
Pr	na	na	na	na	na	0.0015	0.0015	0.0018	0.0013	0.0019	0.0015	0.0010
Nd	na	na	na	na	na	0.0070	0.0070	0.0074	0.0052	0.0075	0.0070	0.0037
Sm	na	na	na	na	na	0.0016	0.0016	0.0014	0.0008	0.0014	0.0016	0.0007
Eu	na	na	na	na	na	0.0002	0.0002	0.0002	nd	0.0002	0.0002	0.0001
Gd	na	na	na	na	na	0.0013	0.0013	0.0010	0.0007	0.0010	0.0013	0.0006
Tb	na	na	na	na	na	0.0002	0.0002	0.0001	nd	0.0001	0.0002	0.0001
Dy	na	na	na	na	na	0.0009	0.0009	0.0005	0.0003	0.0005	0.0009	0.0003
Er	na	na	na	na	na	0.0002	0.0002	0.0001	nd	0.0001	0.0002	0.0001
Ho	na	na	na	na	na	0.0005	0.0005	0.0003	nd	0.0003	0.0005	0.0001
Yb	na	na	na	na	na	0.0003	0.0003	0.0003	0.0002	0.0003	0.0003	0.0002
Lu	na	na	na	na	na	0.0001	0.0001	0.0001	0.0000	0.0001	0.0001	0.0000
Hf	na	na	na	na	na	nd	nd	0.0067	0.0001	0.0067	nd	nd
Total (+)	49.93	49.84	49.70	50.09	49.87	49.40	49.57	49.58	49.53	49.54	49.35	49.31
Total (-)	-49.93	-49.84	-49.70	-50.09	-49.87	-49.32	-49.49	-49.45	-49.48	-49.41	-49.27	-49.27
Charge Diff.	0.00	0.00	0.00	0.00	0.00	0.08	0.08	0.13	0.05	0.13	0.08	0.04
X Site Total	2.05	2.06	2.08	1.99	1.98	2.02	2.03	2.02	1.90	1.99	1.92	2.00

Table 18 Continued.

Rock Unit	FP	FP	FP	FP	FP	DLP	DLP	DLP	DLP	DLP	DLP	DLP
Sample ID	12	12	12	12	12	16	16	16	16	16	16	16
Grain ID	12a_ukn3	12a_ukn5	12a_ukn5	12a_ukn1	12a_ukn1	16a_ukn3	16a_ukn5	16a_ukn4	16a_ukn6	16a_ukn5	16a_ukn3	16a_ukn6
Anal. Location	Core	Core	Rim	Core	Rim	Rim	Core	Rim	Core	Rim	Rim	Rim
Ca	10.043	10.046	10.059	10.053	10.018	9.884	9.987	9.914	9.915	9.944	9.938	9.966
P	5.672	5.652	5.662	5.866	5.731	5.856	5.947	5.950	5.923	5.950	5.955	5.917
Sr	0.012	0.009	0.006	0.006	0.009	nd	0.008	0.008	0.011	0.007	0.011	0.005
Ba	nd	nd	nd	nd	nd	nd	nd	nd	nd	nd	nd	nd
Na	0.060	0.059	0.065	nd	0.060	0.071	nd	0.016	0.022	nd	nd	nd
K	nd	nd	nd	nd	0.010	0.017	0.023	0.022	0.012	0.020	0.020	0.010
Mg	nd	0.016	nd	nd	nd	nd	nd	nd	nd	nd	nd	nd
Ti	nd	nd	nd	nd	nd	nd	nd	nd	nd	0.007	nd	nd
Mn	0.027	0.031	0.025	0.015	0.012	0.016	0.015	0.018	nd	0.014	0.015	0.013
Fe	0.036	0.059	0.059	nd	0.033	0.008	0.009	0.015	0.014	0.015	nd	0.022
Cu	0.008	nd	nd	nd	nd	0.005	nd	nd	0.013	nd	nd	nd
S	0.063	0.078	0.069	0.013	0.069	0.081	0.010	0.018	0.034	0.011	0.020	0.018
B	0.015	0.005	0.005	nd	nd	0.003	na	nd	0.009	na	0.003	0.009
Si	0.026	0.024	0.029	0.021	0.033	0.034	nd	0.013	0.025	0.019	0.020	0.018
As	nd	nd	nd	nd	nd	nd	nd	nd	nd	nd	nd	nd
V	nd	nd	nd	nd	nd	0.006	nd	nd	nd	0.009	nd	nd
F	1.91	1.82	1.90	1.95	1.84	1.96	2.03	2.00	2.00	1.91	1.96	1.99
Cl	0.07	0.07	0.07	0.05	0.06	0.07	0.06	0.07	0.07	0.06	0.07	0.07
O	23.61	23.68	23.63	23.84	23.78	23.91	23.88	23.91	23.92	23.97	23.96	23.88

Table 18 Continued.

Rock Unit	FP	FP	FP	FP	FP	DLP	DLP	DLP	DLP	DLP	DLP	DLP
Sample ID	12	12	12	12	12	16	16	16	16	16	16	16
Grain ID	12a_ukn3	12a_ukn5	12a_ukn5	12a_ukn1	12a_ukn1	16a_ukn3	16a_ukn5	16a_ukn4	16a_ukn6	16a_ukn5	16a_ukn3	16a_ukn6
Anal. Location	Core	Core	Rim	Core	Rim	Rim	Core	Rim	Core	Rim	Rim	Rim
La	0.005	0.005	0.005	0.006	0.006	0.005	na	0.003	0.005	na	0.005	0.005
Ce	0.013	0.009	0.009	0.011	0.011	0.009	0.001	0.011	0.009	0.005	0.009	0.009
Pr	0.0019	0.0012	0.0012	0.0013	0.0013	0.0008	na	0.0013	0.0011	na	0.0009	0.0011
Nd	0.0075	0.0044	0.0044	0.0053	0.0053	0.0026	na	0.0058	0.0045	na	0.0026	0.0045
Sm	0.0014	0.0006	0.0006	0.0008	0.0008	0.0004	na	0.0013	0.0007	na	0.0004	0.0007
Eu	0.0002	0.0002	0.0002	nd	nd	0.0001	na	0.0002	0.0002	na	0.0001	0.0002
Gd	0.0010	0.0004	0.0004	0.0007	0.0007	0.0003	na	0.0009	0.0006	na	0.0003	0.0006
Tb	0.0001	0.0001	0.0001	nd	nd	0.0000	na	0.0001	0.0001	na	0.0000	0.0001
Dy	0.0005	0.0003	0.0003	0.0003	0.0003	0.0002	na	0.0004	0.0002	na	0.0002	0.0002
Er	0.0001	0.0001	0.0001	nd	nd	0.0000	na	0.0001	0.0001	na	0.0000	0.0001
Ho	0.0003	0.0001	0.0001	nd	nd	0.0001	na	0.0001	0.0001	na	0.0001	0.0001
Yb	0.0003	0.0002	0.0002	0.0002	0.0002	0.0001	na	0.0001	0.0001	na	0.0001	0.0001
Lu	0.0001	0.0000	0.0000	0.0000	0.0000	0.0000	na	0.0000	0.0000	na	0.0000	0.0000
Hf	0.0068	0.0001	0.0001	0.0001	0.0001	nd	na	0.0013	0.0001	na	nd	0.0001
Total (+)	49.33	49.30	49.30	49.74	49.51	49.92	49.86	49.95	49.97	49.94	50.01	49.90
Total (-)	-49.20	-49.24	-49.24	-49.69	-49.46	-49.85	-49.85	-49.90	-49.90	-49.91	-49.96	-49.82
Charge Diff.	0.13	0.06	0.06	0.05	0.05	0.07	0.00	0.05	0.07	0.03	0.05	0.07
X Site Total	1.98	1.88	1.97	2.00	1.89	2.03	2.09	2.07	2.07	1.96	2.03	2.06

Table 18 Continued.

Rock Unit	DLP	DLP	DLP	DLP	DLP	DLP	DLP	DLP	DLP	DLP	DLP	DLP
Sample ID	16	16	16	16	16	16	16	16	17	17	17	17
Grain ID	16a_ukn4	16a_ukn1	16a_ukn3	16a_ukn5	16a_ukn1	16a_ukn4	16a_ukn1	16a_ukn6	17b_32	17b_ukn1	17b_18	17b_18
Anal. Location	Rim	Rim	Core	Rim	Rim	Core	Core	Rim	Core	Rim	Core	Rim
Ca	9.875	9.874	9.942	9.927	9.935	9.924	9.925	9.952	10.036	10.068	10.009	10.014
P	5.971	5.996	5.837	5.907	5.953	5.912	5.980	5.873	5.864	5.805	5.872	5.870
Sr	0.012	nd	0.007	0.008	0.012	0.010	0.008	0.008	nd	0.004	nd	0.008
Ba	nd	nd	nd	nd	nd	nd	nd	nd	nd	nd	nd	nd
Na	0.031	nd	0.049	nd	nd	0.037	0.014	0.020	nd	nd	0.021	0.016
K	0.018	nd	0.011	0.050	0.011	0.013	nd	0.016	nd	0.014	nd	nd
Mg	nd	nd	nd	nd	nd	nd	nd	nd	nd	nd	nd	nd
Ti	nd	nd	nd	nd	nd	nd	nd	nd	nd	nd	nd	nd
Mn	0.014	0.023	0.018	0.011	0.019	0.016	0.017	0.017	0.021	0.016	0.018	0.019
Fe	0.013	0.047	0.008	0.016	0.028	0.012	0.010	0.018	0.007	0.007	0.014	0.006
Cu	nd	nd	0.006	0.016	nd	nd	nd	nd	nd	nd	nd	nd
S	0.021	0.019	0.071	0.016	nd	0.030	0.023	0.028	0.019	0.031	0.019	0.020
B	nd	0.005	0.003	na	0.005	nd	0.005	0.009	0.005	0.005	0.005	0.005
Si	0.019	0.019	0.029	0.040	0.019	0.021	nd	0.037	0.025	0.028	0.022	0.021
As	nd	nd	nd	nd	nd	nd	nd	nd	nd	nd	nd	nd
V	nd	nd	nd	nd	nd	nd	nd	nd	nd	nd	nd	nd
F	1.94	1.98	1.97	1.93	2.00	2.01	2.01	2.04	1.85	1.78	1.96	1.87
Cl	0.07	0.07	0.09	0.06	0.05	0.07	0.04	0.05	0.06	0.06	0.05	0.06
O	23.98	24.02	23.87	23.91	23.91	23.88	23.98	23.83	23.90	23.87	23.85	23.89

Table 18 Continued.

Rock Unit	DLP	DLP	DLP	DLP	DLP	DLP	DLP	DLP	DLP	DLP	DLP	DLP
Sample ID	16	16	16	16	16	16	16	16	17	17	17	17
Grain ID	16a_ukn4	16a_ukn1	16a_ukn3	16a_ukn5	16a_ukn1	16a_ukn4	16a_ukn1	16a_ukn6	17b_32	17b_ukn1	17b_18	17b_18
Anal. Location	Rim	Rim	Core	Rim	Rim	Core	Core	Rim	Core	Rim	Core	Rim
La	0.003	0.004	0.005	na	0.004	0.003	0.004	0.005	0.006	0.006	0.005	0.005
Ce	0.011	0.008	0.009	0.009	0.008	0.011	0.008	0.009	0.010	0.009	0.009	0.009
Pr	0.0013	0.0009	0.0009	na	0.0009	0.0013	0.0009	0.0011	0.0011	0.0009	0.0010	0.0010
Nd	0.0058	0.0030	0.0026	na	0.0030	0.0058	0.0030	0.0045	0.0038	0.0034	0.0040	0.0040
Sm	0.0013	0.0005	0.0004	na	0.0005	0.0013	0.0005	0.0007	0.0006	0.0005	0.0006	0.0006
Eu	0.0002	0.0001	0.0001	na	0.0001	0.0002	0.0001	0.0002	0.0001	0.0001	0.0001	0.0001
Gd	0.0009	0.0004	0.0003	na	0.0004	0.0009	0.0004	0.0006	0.0005	0.0004	0.0005	0.0005
Tb	0.0001	0.0000	0.0000	na	0.0000	0.0001	0.0000	0.0001	0.0001	0.0001	0.0001	0.0001
Dy	0.0004	0.0002	0.0002	na	0.0002	0.0004	0.0002	0.0002	0.0002	0.0002	0.0003	0.0003
Er	0.0001	0.0000	0.0000	na	0.0000	0.0001	0.0000	0.0001	0.0001	0.0000	0.0001	0.0001
Ho	0.0001	0.0001	0.0001	na	0.0001	0.0001	0.0001	0.0001	0.0002	0.0001	0.0002	0.0002
Yb	0.0001	0.0001	0.0001	na	0.0001	0.0001	0.0001	0.0001	0.0001	0.0002	0.0002	0.0002
Lu	0.0000	0.0000	0.0000	na	0.0000	0.0000	0.0000	0.0000	0.0000	0.0001	0.0000	0.0000
Hf	0.0013	0.0001	nd	na	0.0001	0.0013	0.0001	0.0001	0.0006	nd	nd	nd
Total (+)	50.03	50.14	49.83	49.82	49.92	49.89	50.06	49.82	49.77	49.63	49.76	49.76
Total (-)	-49.97	-50.09	-49.79	-49.82	-49.87	-49.83	-50.00	-49.74	-49.70	-49.57	-49.70	-49.70
Charge Diff.	0.05	0.05	0.05	0.00	0.05	0.05	0.05	0.08	0.06	0.06	0.06	0.06
X Site Total	2.01	2.06	2.05	1.99	2.05	2.08	2.05	2.09	1.91	1.84	2.01	1.93

Table 18 Continued.

Rock Unit	DLP	DLP	DLP	DLP	DLP	DLP	DLP	DLP	DLP	DLP	DLP
Sample ID	17	17	17	17	17	17	17	17	17	17	17
Grain ID	17b_ukn1	17b_ukn2	17b_32	17b_33	17b_ukn2	17b_33	17b_ukn1	17b_ukn2	17b_32	17b_18	17b_33
Anal. Location	Core	Core	Rim	Core	Rim	Rim	Rim	Rim	Rim	Rim	Rim
Ca	10.000	10.003	10.064	10.059	10.034	10.096	10.066	10.090	10.052	10.139	10.042
P	5.751	5.716	5.832	5.801	5.729	5.777	5.706	5.761	5.826	5.773	5.839
Sr	0.007	0.006	0.004	0.007	0.007	0.010	0.006	0.020	0.012	0.004	0.006
Ba	nd	nd	nd	0.004	nd	nd	nd	nd	nd	nd	0.003
Na	0.072	0.084	nd	0.015	0.058	nd	0.041	0.015	0.015	nd	0.019
K	nd	nd	nd	nd	0.010	nd	0.016	nd	nd	nd	nd
Mg	nd	nd	nd	nd	nd	nd	nd	nd	nd	nd	nd
Ti	nd	nd	nd	nd	nd	nd	nd	nd	nd	nd	nd
Mn	0.018	0.019	0.019	0.013	0.021	0.017	0.027	0.014	0.022	0.013	nd
Fe	0.014	0.015	0.008	0.008	nd	0.011	0.015	0.016	0.008	0.008	0.012
Cu	nd	nd	nd	0.015	0.006	0.012	nd	0.005	nd	nd	nd
S	0.082	0.098	0.017	0.022	0.073	0.018	0.065	0.028	0.015	0.015	0.025
B	0.005	0.005	0.005	0.005	0.005	0.005	0.005	0.005	0.005	0.005	0.005
Si	0.031	0.033	0.028	0.026	0.036	0.028	0.033	0.026	0.022	0.021	0.022
As	nd	nd	nd	nd	nd	nd	nd	nd	nd	nd	nd
V	nd	nd	nd	nd	nd	nd	nd	nd	nd	nd	nd
F	1.92	1.98	1.80	1.89	1.97	1.85	1.84	1.85	1.87	1.77	1.92
Cl	0.06	0.07	0.07	0.07	0.06	0.07	0.06	0.06	0.08	0.06	0.07
O	23.79	23.73	23.87	23.78	23.72	23.76	23.73	23.75	23.80	23.79	23.82

Table 18 Continued.

Rock Unit	**DLP**	**DLP**	**DLP**	**DLP**	**DLP**	**DLP**	**DLP**	**DLP**	**DLP**	**DLP**	**DLP**
Sample ID	**17**	**17**	**17**	**17**	**17**	**17**	**17**	**17**	**17**	**17**	**17**
Grain ID	**17b_ukn1**	**17b_ukn2**	**17b_32**	**17b_33**	**17b_ukn2**	**17b_33**	**17b_ukn1**	**17b_ukn2**	**17b_32**	**17b_18**	**17b_33**
Anal. Location	**Core**	**Core**	**Rim**	**Core**	**Rim**	**Rim**	**Rim**	**Rim**	**Rim**	**Rim**	**Rim**
La	0.006	0.005	0.006	0.006	0.005	0.006	0.006	0.005	0.006	0.005	0.006
Ce	0.009	0.009	0.010	0.011	0.009	0.011	0.009	0.009	0.010	0.009	0.011
Pr	0.0009	0.0010	0.0011	0.0012	0.0010	0.0012	0.0009	0.0010	0.0011	0.0010	0.0013
Nd	0.0034	0.0041	0.0038	0.0047	0.0041	0.0047	0.0034	0.0041	0.0039	0.0040	0.0048
Sm	0.0005	0.0006	0.0006	0.0007	0.0006	0.0007	0.0005	0.0006	0.0006	0.0006	0.0007
Eu	0.0001	0.0001	0.0001	0.0001	0.0001	0.0001	0.0001	0.0001	0.0001	0.0001	0.0002
Gd	0.0004	0.0005	0.0005	0.0006	0.0005	0.0006	0.0004	0.0005	0.0005	0.0005	0.0006
Tb	0.0001	0.0001	0.0001	0.0001	0.0001	0.0001	0.0001	0.0001	0.0001	0.0001	0.0001
Dy	0.0002	0.0002	0.0002	0.0003	0.0002	0.0003	0.0002	0.0002	0.0002	0.0003	0.0003
Er	0.0000	0.0001	0.0001	0.0001	0.0001	0.0001	0.0000	0.0001	0.0001	0.0001	0.0001
Ho	0.0001	0.0001	0.0002	0.0002	0.0001	0.0002	0.0001	0.0001	0.0002	0.0002	0.0002
Yb	0.0002	0.0001	0.0001	0.0002	0.0001	0.0002	0.0002	0.0001	0.0001	0.0002	0.0002
Lu	0.0001	0.0000	0.0000	0.0000	0.0000	0.0000	0.0001	0.0000	0.0000	0.0000	0.0000
Hf	nd	0.0001	0.0006	0.0001	0.0001	0.0001	nd	0.0001	0.0006	nd	0.0001
Total (+)	49.62	49.57	49.67	49.58	49.53	49.51	49.44	49.48	49.62	49.47	49.70
Total (-)	-49.56	-49.51	-49.61	-49.51	-49.47	-49.44	-49.37	-49.42	-49.55	-49.41	-49.63
Charge Diff.	0.06	0.06	0.06	0.07	0.06	0.07	0.06	0.06	0.07	0.06	0.07
X Site Total	1.98	2.05	1.86	1.95	2.02	1.92	1.91	1.91	1.95	1.82	1.99

APPENDIX F

APATITE ELEMENTAL ZONATION

This appendix contains zonation patterns calculated for elements measured in each grain by electron microprobe (Table 19). Three spots located along a traverse across the grain, or in a fashion so that change in concentrations from core to rim could be evaluated were attributed as core or rim based on their location. Zonation of S was evaluated using the following seven categories: decreasing rim to rim, core high irregular, rim high irregular, core high concentric, rim high concentric, high asymmetric plateau (indicating a core and one rim high with one rim low), low asymmetric plateau (indicating a core and one rim low with one rim high) and no zonation. Only grains with three or more spots having above detection levels (>300 ppm) and at least one of the three above 500 ppm were included for evaluation and attributed. Distinction of one category from another was based on a difference in value of greater or less than an estimated 1 sigma (est.1σ). The est.1σ was extrapolated as a best fit line for combined residuals of all elements determined for analyses of the Fap apatite standard analyzed as an unknown. This line is described by Equation 5 where x = measured concentration and y = calculated est.1σ.

$$y = 62.905 \ln(x) - 348.12 \quad (5)$$

Table 19. Zonation Patterns in Apatite Grains for Microprobe Analyses.

Sample ID	**48**	**48**	**48**	**48**	**48**	**47**
Grain ID	**48a_21**	**48a_14g2**	**48a_14g1**	**48a_13**	**48a_09**	**47c_ukn1**
Ca	rim to rim	rim to rim	core high irregular	low asymmetric plateau	rim to rim	core high irregular
P	core high irregular	rim to rim	high asymmetric plateau	rim to rim	high asymmetric plateau	low asymmetric plateau
F	high asymmetric plateau	rim high irregular	rim high irregular	rim high irregular	low asymmetric plateau	high asymmetric plateau
Cl	rim high irregular	rim to rim	rim to rim	high asymmetric plateau	rim high irregular	rim high concentric
Sr	low asymmetric plateau	low asymmetric plateau		core high concentric		core high concentric
Ba						
Na				low asymmetric plateau		low asymmetric plateau
K						
Mg						
Ti	low asymmetric plateau				low asymmetric plateau	
Mn	core high irregular	rim to rim	low asymmetric plateau	low asymmetric plateau	low asymmetric plateau	rim to rim
Fe	rim high irregular	rim high irregular	rim high irregular	rim to rim	low asymmetric plateau	rim high irregular
Cu					core high concentric	low asymmetric plateau
S						rim to rim
Si	rim high concentric			core high irregular	low asymmetric plateau	rim to rim
As	low asymmetric plateau					

Table 19 Continued.

Sample ID	**42**	**42**	**42**	**41**	**41**	**41**
Grain ID	**42d_37**	**42d_36**	**42d_01**	**41b_ukn5**	**41b_ukn3**	**41b_ukn2**
Ca	core high concentric	high asymmetric plateau	core high irregular	rim high concentric	core high irregular	core high irregular
P	core high irregular	rim to rim	core high irregular	rim high irregular	no zonation	core high irregular
F	rim to rim	no zonation	high asymmetric plateau	no zonation	core high concentric	rim high irregular
Cl	high asymmetric plateau	rim to rim		rim to rim	rim high irregular	low asymmetric plateau
Sr	rim to rim			rim to rim	core high irregular	rim high irregular
Ba						
Na	low asymmetric plateau		rim high irregular	core high irregular	rim high irregular	low asymmetric plateau
K	low asymmetric plateau		low asymmetric plateau			
Mg		low asymmetric plateau				
Ti						
Mn	rim to rim	low asymmetric plateau	low asymmetric plateau	rim high irregular	low asymmetric plateau	low asymmetric plateau
Fe	rim to rim	rim to rim	core high irregular	low asymmetric plateau	rim high irregular	rim high irregular
Cu		core high irregular			low asymmetric plateau	
S	low asymmetric plateau	low asymmetric plateau	rim high irregular			
Si		low asymmetric plateau	rim high concentric			
As			rim high irregular			

Table 19 Continued.

Sample ID	**40**	**40**	**40**	**38**	**38**	**38**
Grain ID	**40d_ukn3**	**40d_ukn2**	**40d_ukn1**	**38d_ukn4**	**38d_ukn3**	**38d_ukn1**
Ca	rim to rim	core high irregular	rim to rim	core high irregular	high asymmetric plateau	low asymmetric plateau
P	rim high irregular	core high irregular	rim to rim	rim high concentric	rim to rim	rim to rim
F	rim high concentric	high asymmetric plateau	rim high concentric	rim to rim		rim high concentric
Cl	low asymmetric plateau	rim high irregular	core high concentric	core high irregular	high asymmetric plateau	rim to rim
Sr	core high irregular	rim high irregular	core high irregular	low asymmetric plateau	low asymmetric plateau	high asymmetric plateau
Ba						
Na						
K		low asymmetric plateau				
Mg	low asymmetric plateau					
Ti						
Mn	rim high irregular	rim high irregular	core high irregular	rim to rim	rim high irregular	rim to rim
Fe	rim high irregular	rim high irregular	core high concentric	rim high irregular	rim high irregular	rim high concentric
Cu			low asymmetric plateau		low asymmetric plateau	
S						
Si						
As						

Table 19 Continued.

Sample ID	**38**	**34**	**34**	**34**	**26**	**26**
Grain ID	**38d_35**	**34b_06**	**34b_05**	**34a_15**	**26a_ukn3**	**26a_ukn2**
Ca	low asymmetric plateau	rim to rim	rim high irregular	rim high irregular	rim to rim	rim to rim
P	rim to rim	high asymmetric plateau	rim high irregular	rim high irregular	core high irregular	no zonation
F	rim high irregular	rim high concentric	core high irregular	rim high concentric	core high concentric	core high irregular
Cl	core high irregular	high asymmetric plateau	core high concentric	core high irregular	core high concentric	high asymmetric plateau
Sr	core high irregular	rim to rim	low asymmetric plateau	core high irregular	core high concentric	rim to rim
Ba						
Na						rim high irregular
K						
Mg						
Ti						
Mn	high asymmetric plateau	rim high concentric	rim to rim	high asymmetric plateau	low asymmetric plateau	low asymmetric plateau
Fe	core high irregular	core high irregular	core high irregular	rim to rim		low asymmetric plateau
Cu		low asymmetric plateau			rim to rim	
S		rim to rim	high asymmetric plateau	core high concentric	low asymmetric plateau	low asymmetric plateau
Si		rim high irregular	rim high concentric	core high concentric	rim high irregular	low asymmetric plateau
As						

Table 19 Continued.

Sample ID	**26**	**23**	**23**	**23**	**23**	**23**
Grain ID	**26a_ukn1**	**23c_ukn4**	**23c_ukn3**	**23c_ukn2**	**23c_ukn1**	**23c_20**
Ca	rim high irregular	core high irregular	core high concentric	core high irregular	rim high irregular	low asymmetric plateau
P	low asymmetric plateau	rim to rim	core high irregular	no zonation	core high concentric	rim high irregular
F	core high irregular	core high concentric	core high concentric	rim to rim	high asymmetric plateau	rim to rim
Cl	high asymmetric plateau	high asymmetric plateau	high asymmetric plateau	core high concentric	high asymmetric plateau	core high irregular
Sr			low asymmetric plateau			no zonation
Ba						
Na	core high irregular		rim to rim		rim to rim	core high concentric
K						
Mg						
Ti						
Mn	rim high irregular	rim to rim	no zonation	no zonation	low asymmetric plateau	rim to rim
Fe	rim to rim	rim high irregular	rim to rim	core high irregular	low asymmetric plateau	rim high irregular
Cu	low asymmetric plateau		core high concentric	low asymmetric plateau	core high concentric	
S	rim to rim	low asymmetric plateau	no zonation	rim to rim	high asymmetric plateau	core high concentric
Si	high asymmetric plateau	rim high irregular	rim high irregular	core high irregular	no zonation	core high irregular
As						

Table 19 Continued.

Sample ID	**21**	**21**	**21**	**21**	**17**	**17**
Grain ID	**21d_ukn1**	**21d_45**	**21d_38**	**21d_07**	**17b_ukn2**	**17b_ukn1**
Ca	rim high irregular	core high irregular	core high irregular	rim high concentric	low asymmetric plateau	rim high irregular
P	core high irregular	rim high concentric	high asymmetric plateau	rim to rim	no zonation	rim to rim
F	low asymmetric plateau	rim high irregular	low asymmetric plateau	rim to rim	core high irregular	core high irregular
Cl	core high irregular	rim to rim	low asymmetric plateau	high asymmetric plateau	core high irregular	no zonation
Sr	core high concentric		low asymmetric plateau	low asymmetric plateau	rim high irregular	core high irregular
Ba						
Na		low asymmetric plateau			core high irregular	core high irregular
K						rim high irregular
Mg						
Ti						
Mn	high asymmetric plateau	rim to rim	low asymmetric plateau	low asymmetric plateau	rim to rim	rim to rim
Fe	rim high irregular	low asymmetric plateau	low asymmetric plateau	low asymmetric plateau	high asymmetric plateau	high asymmetric plateau
Cu	low asymmetric plateau		core high concentric			
S					core high irregular	core high irregular
Si	low asymmetric plateau	rim high concentric	rim to rim		high asymmetric plateau	high asymmetric plateau
As	core high concentric					

Table 19 Continued.

Sample ID	**17**	**17**	**17**	**16**	**16**	**16**
Grain ID	**17b_33**	**17b_32**	**17b_18**	**16a_ukn6**	**16a_ukn5**	**16a_ukn4**
Ca	rim to rim	core high irregular	no zonation	rim to rim	core high irregular	low asymmetric plateau
P	core high concentric	core high irregular	high asymmetric plateau	high asymmetric plateau	high asymmetric plateau	rim high concentric
F	high asymmetric plateau	high asymmetric plateau	core high irregular	low asymmetric plateau	core high irregular	high asymmetric plateau
Cl	low asymmetric plateau	low asymmetric plateau	no zonation	core high irregular	core high concentric	no zonation
Sr	rim to rim	low asymmetric plateau	low asymmetric plateau	core high irregular	high asymmetric plateau	rim to rim
Ba	low asymmetric plateau					
Na	low asymmetric plateau		low asymmetric plateau	core high irregular		core high irregular
K				rim to rim	rim to rim	rim high irregular
Mg						
Ti						
Mn	rim to rim	high asymmetric plateau	rim to rim	rim high irregular	high asymmetric plateau	rim to rim
Fe	rim high concentric	rim high concentric	core high irregular	rim high irregular	rim high concentric	low asymmetric plateau
Cu	core high irregular			core high concentric	low asymmetric plateau	
S	rim to rim	high asymmetric plateau	high asymmetric plateau	core high irregular	rim high irregular	core high irregular
Si	high asymmetric plateau	rim to rim	no zonation	rim to rim	rim high irregular	high asymmetric plateau
As						

Table 19 Continued.

Sample ID	**16**	**16**	**13**	**13**	**13**	**12**
Grain ID	**16a_ukn3**	**16a_ukn1**	**13a_45**	**13a_33**	**13a_24**	**12a_ukn3**
Ca	no zonation	rim to rim	low asymmetric plateau	rim to rim	core high concentric	high asymmetric plateau
P	rim high irregular	low asymmetric plateau	rim to rim	rim to rim	high asymmetric plateau	rim high irregular
F	no zonation	high asymmetric plateau	no zonation	no zonation	high asymmetric plateau	rim high irregular
Cl	core high concentric	rim high irregular	low asymmetric plateau	rim high irregular	low asymmetric plateau	high asymmetric plateau
Sr	rim to rim	rim to rim	low asymmetric plateau			core high concentric
Ba						
Na	rim to rim		rim high concentric	high asymmetric plateau		core high irregular
K	rim high irregular					
Mg						
Ti						
Mn	core high concentric	rim high irregular	rim to rim	high asymmetric plateau	high asymmetric plateau	core high irregular
Fe	low asymmetric plateau	rim high irregular	rim high irregular	rim high irregular	rim high concentric	rim to rim
Cu	low asymmetric plateau		core high concentric	low asymmetric plateau		
S	rim to rim	core high irregular	rim high concentric	low asymmetric plateau		core high irregular
Si	rim to rim	rim high concentric	rim high irregular		low asymmetric plateau	high asymmetric plateau
As						

Table 19 Continued.

Sample ID	**12**	**12**	**02**	**02**	**02**	**02**
Grain ID	**12a_ukn2**	**12a_ukn1**	**02b_ukn4**	**02b_ukn2**	**02b_ukn1**	**02b_27**
Ca	low asymmetric plateau	rim to rim	low asymmetric plateau	low asymmetric plateau	high asymmetric plateau	high asymmetric plateau
P	core high irregular	high asymmetric plateau	rim high concentric	no zonation	high asymmetric plateau	core high irregular
F	high asymmetric plateau	core high irregular	rim high irregular	rim high irregular	low asymmetric plateau	high asymmetric plateau
Cl	high asymmetric plateau	low asymmetric plateau	core high irregular	low asymmetric plateau	no zonation	low asymmetric plateau
Sr	rim high irregular	rim high irregular	core high concentric	no zonation	core high irregular	core high irregular
Ba						
Na	rim high irregular	rim high irregular			low asymmetric plateau	
K	low asymmetric plateau		low asymmetric plateau			
Mg						
Ti						
Mn	high asymmetric plateau	rim to rim	core high irregular	rim to rim	rim to rim	rim to rim
Fe	rim high irregular	rim high irregular	high asymmetric plateau	core high irregular	rim high irregular	rim high irregular
Cu		low asymmetric plateau	core high concentric			
S	rim high irregular	rim high irregular		low asymmetric plateau		
Si	rim high irregular	rim high concentric				
As						

REFERENCES

Banks, N.G., 1982, Sulfur and copper in magma and rocks, *in* S. R Titley, *ed.*, Advances in Geology of the Porphyry Copper Deposits: Southwestern North America, University of Arizona Press, Tucson, Arizona, p. 227-258.

Bauer, M., and Klee, W.E., 1993, The monoclinic-hexagonal phase transition in chlorapatite: European Journal of Mineralogy, v. 5, p. 307-316.

Belousava, E.A., Griffin, W.L., Oreilly, Suzanne Y., and Fisher, N.I., 2002, Apatite as an indicator mineral for exploration: Trace-element compositions and their relationship to host rock type: Journal of Geochemical Exploration, v. 76, p. 45-69.

Carroll, M.R., and Rutherford, M.J., 1987, The stability of igneous anhydrite: Experimental results and implications for sulfur behavior in the 1982 El Chichón trachyandesite and other evolved magmas: Journal of Petrology, v. 28, p. 781-801.

Chu, M., Wang, K., Griffin, W.L., Chung, S., O'Reilly, S.Y., Pearson, N.J., and Iisuka, Y., 2009, Apatite composition: Trace petrogenetic processes in Transhimalayan Granitoids: Journal of Petrology, v. 50, n. 10, p. 1829-1855.

Cline, J.S. and Bodnar, R.J., 1991, Can economic porphyry copper mineralization be generated by a typical calc-alkalic melt? Journal of Geophysical Research, v. 96, p. 8113-8126.

Cooke, D.R., Hollings, P., and Walshe, J.L., 2005, Giant porphyry deposits: Characteristics, distribution, and tectonic controls: Economic Geology, v. 100, p. 801-819.

Core, D.P., 2004, Oxygen and sulfur fugacities of granitoids: Implications for ore-forming processes: Unpublished Ph.D. dissertation, Michigan, United States, University of Michigan, p. 245.

Davidson, P, Kamenetsky, V., Cooke, D.R., and Frikken, P., 2005, Magmatic precursors of hydrothermal fluid at the Río Blanco Cu-Mo deposit, Chile: Links to silicate magma and metal transport: Economic Geology, v. 100, p. 963-978.

Deckart, K., Clark, A.H., Aguilar, C., Vargas, R., Bertens, A.N., Mortensen, J.K., and Fanning, M., 2005, Magmatic and hydrothermal chronology of the giant Río Blanco porphyry copper deposit, central Chile: Implications of an integrated U-Pb and $^{40}Ar/^{39}Ar$ database: Economic Geology, v. 100, p. 905-934.

Deckart, K., Clark, A.H., Cuadra, P., and Fanning, M., 2012, Refinement of the time-space evolution of the giant Mio-Pliocene Río Blanco-Los Bronces porphyry Cu-Mo cluster, Central Chile: New U-Pb (SHRIMP II) and Re-Os geochronology and $^{40}Ar/^{39}Ar$ thermochronology data: Mineralium Deposita, v. 48, no. 1, p. 57-79.

Fleet, M.E., Liu, X.Y., and Pan, Y., 2000, Site preference of rare-earth elements in hydroxyapatite [$Ca_{10}(PO_4)_6(OH)_2$]: Journal of Solid State Chemistry, v. 149, p. 391–398.

Frei, R., 1996, Sulfur in bulk rock and igneous apatite; tracing mineralized and barren trends in intrusions: Schweizerische Mineralogische und Petrographische Mitteilungen, v. 57-73.

Frikken, P.H., 2004, Breccia-hosted copper-molybdenum mineralization at Río Blanco, Chile: Unpublished Ph.D. thesis, Hobart, Tasmania, University of Tasmania, 290 p.

Gow, P.A., and Walshe, J.L., 2005, The role of pre-existing geologic architecture in the formation of giant porphyry-related Cu +/- Au deposits—Examples from New Guinea and Chile: Economic Geology, v. 100, p. 819-833.

Harrison, T.M. and Watson, E.B., 1984, The behavior of apatite during crustal anatexis: Equilibrium and kinetic considerations: Geochimica et Cosmochimica Acta, v. 48, p. 1467-1477.

Hattori, K.H., and Keith, J.D., 2001, Contribution of mafic melt to porphyry copper mineralization: Evidence from Mount Pinatubo, Philippines and Bingham Canyon, Utah, USA: Mineralium Deposita, v. 36, p. 799-806.

Hollings, P., Cooke, D., and Clarke, A., 2005, Regional geochemistry of Tertiary igneous rocks in central Chile: Implications for the geodynamic environment of giant porphyry copper and epithermal gold mineralization: Economic Geology, v. 100, p. 887-904.

Hughes, J.M., Rakovan, J., 2002. The crystal structure of apatite, $Ca_5(PO_4)_3(F,OH,Cl)$. In: Kohn, M.J., Rakovan, J., Hughes, J.M., eds., Phosphates: Geochemical, geobiological, and materials importance. Reviews of Mineralogy and Geochemistry, v. 48, p.1-12.

Imai, A., 2004. Variation of Cl and SO_3 contents of microphenocrysic apatite in intermediate to silicic igneous rocks of cenozoic Japanese island arcs: Implications for porphyry Cu metallogenesis in the western Pacific island arcs: Resource Geology v. 54, no. 3, p 357-372.

Keith, J.D., Whitney, J.A., Hattori, K., Ballantyne, G.H., Christensen, E.H., Barr, D.L., Cannan, T.M. and Hook, C.J., 1997, The role of magmatic sulfides and mafic alkaline magmas in the Bingham and Tintic mining districts, Utah: Journal of Petrology v. 38, p. 1679-1690.

Mackie, P.E., and Young, R.A., 1974. Fluorine-chlorine interaction in fluor-chlorapatite. Journal of Solid State Chemistry, v. ll, p. 319-329.

Pankhurst, R.J., and Hervé, F., 2007, Introduction and overview, In: Moreno T, Gibbons W, Editors. The Geology of Chile: London, Geological Society, p. 1-4.

Pan, Y., Fleet, M.E., 2002, Compositions of the apatite-group minerals: Substitution mechanisms and controlling factors. In: Kohn, M.J., Rakovan, J., Hughes, J.M., Eds., Phosphates Geochemical, Geobilogical and Materials Importance, Mineralogical Society of America, v. 48. p. 13-49.

Parat, F. and Holtz, F., 2004, Sulfur partitioning between apatite and melt and effect of sulfur on apatite solubility at oxidizing conditions: Contributions to Mineralogy and Petrology, v. 147, p. 201-212.

Pearce, J.A., 1996, A users guide to basalt discrimination diagrAm. In Wyman, D. A., ed. Trace element geochemistry of volcanic rocks: Applications for massive sulphide exploration: Geological Association of Canada. Short Course Notes 12, p.79-113.

Piccoli, P. and Candela, P., 1994, Apatite in felsic rocks: A model for the estimation of initial halogen concentrations in the Bishop Tuff (Long Valley) and the Tuolumne Intrusive Suite (Sierra Nevada Batholith) magmas: American Journal of Science, v. 294, p. 92-135.

Porter, J.P. and Titley, S.R., 2004, Sulfur evolution of the Ertsberg Intrusion and sulfur isotopes of the Ertsberg stock work zone, Ertsberg Mining District, West Papau, Indonesia: Unpublished M.S. thesis, Arizona, United States, Arizona State University, 116 p.

Sillitoe, R.H., 2010, Porphyry copper systems: Economic Geology, v. 105, p. 3-41.

Skewes, M.A. and Stern, C.R., 1994, Tectonic trigger for the formation of late Miocene Cu-rich breccia pipes in the Andes of central Chile: Geology, v. 22, p. 551-554.

Skewes, M.A. and Stern, C.R., 1996, Late Miocene mineralized breccias in the Andes of central Chile: Sr- and Nd-isotopic evidence for multiple magmatic sources. In: Camus, F., Sillitoe, R. H. and Petersen, R., eds., Andean Copper Deposits: Society of Economic Geologists Special Publications 5, p. 119-130.

Skewes, M.A., Arévalo, A., Floody, R., Zuñiga, P.H., and Stern, C.R., 2002, The giant El Teniente breccia deposit: Hypogene copper distribution and emplacement: Society of Economic Geologists Special Publication 9, p. 299-332.

Streck, M.J. and Dilles, J.H., 1998, Sulfur evolution of oxidized arc magmas as recorded in apatite from a porphyry copper batholith: Geology, v. 26, p. 523-526.

Sun, S. and McDonough, W.F., 1989, Chemical and isotopic systematics of oceanic basalts: Implications for mantle composition and processes, in A.D. Saunders and M.J. Norry, eds., Magmatism in the Ocean Basins, Special Publication Volume. Geological Society of London, v. 42, p. 313-345.

Toro, J.C., Ortuzar, J., Zamorano, J., Cuadra, P., Hermosilla, J., and Sprohnle, C., 2012, Protracted magmatic-hydrothermal history of the Río Blanco-Los Bronces district, central Chile: Development of world's greatest known concentration of copper: Society of Economic Geologists Special Publication 16.

Vargas, R., Gustafson, L.B., Vukasovic, M., Tidy, E., and Skewes, M.A., 1999, Ore breccias in the Río Blanco-Los Bronces porphyry copper deposit, Chile: Society of Economic Geologists Special Publication 7, p. 281-297.

Warnaars, F.W., Holmgren, C., and Barassi, S., 1985, Porphyry copper and tourmaline breccias at Los Bronces-Río Blanco, Chile: Economic Geology, v. 80, p. 1544-1565.

White, W.M., 2013, Geochemistry: Hoboken, New Jersey, Wiley & Blackwell, 672 p.

Whitney, J.A., 1988, The origin of granite: The role and source of water in the evolution of granitic magmas: Geolgical Society of America Bulletin, v. 100, p. 1886-1897.

Winter, J.D., 2001, An introduction to igneous and metamorphic petrology: Upper Saddle River, Prince Hall, New Jersey, Prentice Hall, 702 p.